PEOPLE's DEMOCRATIC REPUBLIC OF ALGERIA
MINISTRY OF HIGHER EDUCATION AND SCIENTIFIC RESEARCH
UNIVERSITY OF CONSTANTINE 1
FACULTY OF EXACT SCIENCES
DEPARTMENT OF PHYSICS

N° : .....
Series : .....

THESIS

TO OBTAIN THE DEGREE OF DOCTOR OF SCIENCE

DISCIPLINE : THEORETICAL PHYSICS

THEME :

CONTINUOUS VARIABLE CLUSTER STATES IN OPTOMECHANICAL SYSTEMS

PRESENTED BY :

OUSSAMA HOUHOU

On : 03/05/2016

Jury members:

Chairman:

Mr. Noureddine Mebarki	Prof.	University of Constantine

Supervisor:

Mr. Habib Aissaoui	Prof.	University of Constantine

Examiners:

Mr. Achour Benslama	Prof.	University of Constantine
Mr. Smain Kouadik	Prof.	University of Médéa
Mr. Mahmoud Hachemane	Prof.	Houari Boumedienne university (USTHB), Algiers
Mr. Mounir Boussahal	MCA.	University of M'sila

Dedication

I dedicate this thesis to my beloved father and mother for their help and support during all stages of preparation of this work.

Also, I dedicate this thesis to my wife for her support and patience.

Acknowledgements

I take this opportunity to thank Prof. Habib Aissaoui for having accepted the supervision of this work and for his guidance, advices and support provided throughout my doctorate project. Also I thank Dr. Alessandro Ferraro for his help, comments and collaboration in part of this work.

I am very glad to Prof. Noureddine Mebarki for accepting to be the chairman of the jury for my thesis defence, and also I thank the other members Prof. Achour Benslama, Prof. Smain Kouadik, Prof. Mahmoud Hachemane and Dr. Mounir Boussahal.

I thank Prof. Mauro Paternaustro and Dr. Alessandro Ferraro for inviting me to Queen's University Belfast, and I thank the people at *QTEQ* group[1] and *The school of Mathematics and Physics, Queen's University Belfast* for collaboration, support and hospitality for hosting me in their institution for the last year of this work.

This work was supported by *the Algerian ministry of higher education and scientific research* (Grant 235/PNE/ENS/GB/2014-2015), *LPMS*[2], *LPTEAM*[3], and *university of Médéa*.

[1] *Quantum Technology at Queen's, School of mathematics and physics, Queen's university Belfast, United Kingdom.*

[2] Laboratoire de Physique Mathématique et Subatomique LPMS, University of Constantine 1

[3] Laboratoire de Physique des Techniques Expérimentales et Applications de Médéa, University of Médéa

Notation and Abbreviations

Abbreviations

Abbreviations used in the manuscript, given in alphabetical order:

CV	Continuous variables
dB	deci Bell
DFS	Decoherence free sub-spaces
DV	Discrete varaiables
EPR	Einstein–Podolsky–Rosen
GNFS	General Number Field Sieve
QIP	Quantum Information Processing
QND	Quantum Non–Demolition
Qubit	Quantum bit
RSA	Rivest-Shamir-Adleman
RWA	Rotating wave approximation
TMSS	Two–modes squeezed state
TO-QCT	Time Optimal Quantum Control Theory

Notation

$\mathbb{1}_m$	$m \times m$ identity matrix
0_m	$m \times m$ zero matrix
$0_{m\times n}$	$m \times n$ zero matrix
$\Re z$	real part of complex number z
$\Im z$	imaginary part of complex number z
$\log x$	the natural logarithm of x
$\log_{10} x$	logarithm base 10 of x

Contents

List of Figures

List of Tables

Chapter 1

Introduction

During the past two decades, quantum information and quantum computation have attracted much attention as a new mode of information processing, and it was the subject of many scientific research supported by different organizations (universities, governments, military, banks, ...)

In this chapter we review briefly the subject of quantum information and quantum computation and namely we discuss the problem of decoherence in quantum computers.

1.1 Quantum Computation

Quantum information processing (QIP) is based on the use of the laws and properties[1] of quantum mechanics where the information is encoded in the different states of a quantum system, and the computation is accomplished by applying a series of (unitary) transformations of these states. The result of computation (output) is obtained by appropriate measurements done on the system. The device that performs QIP is called *quantum computer*.

The idea of quantum computers goes back to the early 80's [1–3]. R. Feynman suggested [2] that building computers obeying the laws of quantum mechanics would allow us to simulate quantum mechanical systems, because it is very difficult to do that in classical computers[2]. The idea of Feynman was raised earlier by R. Poplavskii [4], who showed that, due to the superposition of states present in quantum systems, one can not simmulate the dynamics of the system using a classical computer.

Quantum computers can efficiently solve problems that are believed to be hard to solve in classical computers. The solution of a problem is obtained by using an algorithm. An algorithm is said to be efficient if it gives a solution using resources (time, memory[3] , energy) scaling as a polynomial function of the size of the (input of) problem. There are problems that are believed to have no efficient classical[4] algorithm in a classical computer, but have an efficient quantum algorithm in a quantum computer. The most famous example is the problem of finding the prime factors of an integer number. The best classical algorithm, up-to-date, is the *general*

[1] quantum mechanical properties such as *entanglement* and *superposition*

[2] A classical computer is a device performing computation using the laws of classical physics. The computers that we use today are classical computers.

[3] Some times it is called *space*.

[4] All algorithms that do not use quantum mechanics are called classical algorithm.

number field sieve (GNFS) that finds a solution in a time scaling sub-exponentially with the number of bits of the (input) integer [5]. On the other hand, in a quantum computer, this problem can be solved by a quantum algorithm proposed by P. Shor [6]. Shor's algorithm solves the prime factoring problem in time exponentially faster than its classical counterpart. Other problems where quantum computers have advantage over classical computers are: discrete logarithm [6], searching in a database [7, 8], linear system of equations [9].

Quantum computers gained much interest because they can solve many problems encountered in classical computers. Also, they can be used to verify some fundamental theories in quantum mechanics. There are many reasons and advantages to consider a quantum computer:

- Simulating physical systems: Simulating physical systems in a classical computer is a difficult task, even for small systems with few degrees of freedom, because the dimension of Hilbert space increases exponentially with the size of the system [4]. Simulating physical systems in a quantum computer is the natural choice as stated by R. Feynman [2], and investigated further by D. Deutsch [3] and S. Lloyd [10].

- Improving communications security: Ciphering information is in the heart of protecting information during communication process from eavesdropping, and it is the subject of cryptography. Many cryptographic systems depend on the difficulty of solving some problems on a classical computer [11]. For example, the *RSA* cryptosystem [12] depends on the difficulty of solving the problem of finding prime factors of (big) integers[5], but this problem has an efficient quantum algorithm in a quantum computer (Shor's algorithm [6]). Therefore, the RSA cryptosystem can be broken using a quantum computer. On the other hand, one can use quantum computers to build (quantum) cryptosystems that are more secure than their classical counterparts [15–17].

- Quantum effects issues in classical computers: Classical computers are becoming more powerful and smaller, where an increasing number of electric devices is put together in a very small area [18], which will make (in the near future) quantum effects interfere with the normal functioning of computers [19–22]. Quantum computers, on the other hand, will not suffer from this issue, because quantum effects are an essential part in their functioning.

1.2 Models of quantum computation

Quantum computation relies on encoding information in a physical system and applying a set of (unitary) operations that constitutes the computation. Physical systems that encode information can be classified into two categories : *discrete variables* (DV) and *continuous variables* (CV) systems.

In DV systems, the information is encoded in the different levels of the system. A system of d–levels is sometimes referred to as *qudit* [23]. The very common systems

[5] In 2009, researchers from many institutions collaborated to factorize 768 bit number with 232 decimal digits [13]. The two years needed to finish calculations were equivalent to approximately 2000 years of calculations if it was performed on 2.2 GHz single-core AMD-Opteron [14]

used in DV quantum computation are *qubits*. A qubit is a two–level quantum system and information in encoded as $|0\rangle$ and $|1\rangle$ which is in analogy to (classical) bits 0 and 1. On the other hand, information in CV systems is encoded in an infinite–dimensional systems [24]. Since CV quantum computation uses less complex realizations compared to its DV version, it is easier to encode information and to process it using CV systems [25].

In both modes of computation (DV and CV), there are many models of quantum computation such as the circuit model [26, 27], *measurement–based* (or *one–way*) model [28], *quantum walks* [29], and *quantum Turing machines* [3, 30]. These models are equivalent *i.e.,* they perform computations with the same efficiency.

In particular, the one–way model of quantum computation consists of performing a series of measurements on a particular quantum state called *cluster state* (more details on cluster states are given in **Section 2.5**). In this thesis, we are interested in preparing this quantum state over CV.

1.3 Decoherence in quantum computers

Many physical implementations of quantum computer devices were proposed and fabricated during the last decades: Ion traps [31–36], Nuclear magnetic resonance [37–41], high-Q optical cavities [42–44], ...

To be able to build a quantum computer, one needs to be able to:

1. **represent quantum information as the states of a quantum system:** There are two approaches of QIP: discrete and continuous. In the discrete case, the information is encoded in the state of two level systems: the *qubit*. The qubit's two states are denoted $|0\rangle$ and $|1\rangle$ [45, 46].

   In contrast, the CV approach of QIP consists of encoding information in the state of a bosonic system: each boson[6] has a *mode* described by the quadratures $\hat{q}$ and $\hat{p}$ ($[\hat{q}, \hat{p}] = i\hbar$). CV QIP uses the quadratures $\hat{q}$ and $\hat{p}$ to represent information [24, 47–49].

2. **prepare the system in a desired initial state:** Quantum computation is the evolution of the state of the system (quantum computer) from an initial state (input) to some final state that represents the outcome of the computation (output). Therefore, to do computation, one must be able to to prepare the input state of the quantum computer in some predefined state. The process of preparing the state of the quantum computer faces many challenges:

   (a) The ability of controlling some of or all the parts of the system, for example, how to individually manipulate the state of a (target) qubit among many qubits.

   (b) Decoherence: every physical system (except the whole universe) is in a continuous interaction with its environment. This interaction may affect the prepared state of the quantum computer, which in turn leads to unwanted input state, and this will give wrong output from the quantum computer. This unwanted behaviour is called *decoherence* and it is the result of *noise* in the system [44, 50–56].

[6] Bosons used in CV QIP are photons or phonons.

3. **perform a universal set of unitary transformations on the state of the system:** Quantum computation is the time evolution of the state of the quantum computer where the initial state is the input of computation and the final state is the output of computation. Therefore, a quantum algorithm is a unitary evolution governed by an appropriate Hamiltonian. But, there is always decoherence that will affect the dynamics of the system which in turn will result in errors in the output.

4. **measure the system quantities:** To obtain the output information, one have to do an appropriate measurement of the system at the end of computation.

The different stages, mentioned above, which are involved in quantum computation do suffer from the effects of noise. These stages are summarized in figure 1.1. When building a quantum computer, one must take into account the *decoherence*[7] of the system. There are many proposals to overcome or lower the effects of decoherence on the system:

1. **Quantum error correction protocols:** To protect information from the effects of noise, it is encoded in a way that it can be recovered after the action of noise [57–65]. For example, the information can be encoded by repeating it many times then if probably some of the encoded information is lost (as a result of the noise), we can recover the original information by extracting it from the unaffected encoded information.

2. **Time optimal quantum control theory (TO-QCT):** TO-QCT [66–71] is a framework that enables us to find the optimal Hamiltonian implementing a given quantum algorithm in a given time. We can use TO-QCT framework to build a quantum computer that is reliable against the effects of decoherence: Say that we know the decoherence time τ_d of the quantum computer, then we must find a Hamiltonian that implements the quantum algorithm in time τ such that $\tau << \tau_d$.

3. **Dissipation engineering:** As we have previously said, every quantum computer interacts with its environment. This interaction will affect the input, the dynamics, and/or the the output of computation. To overcome this issue, it is proposed to use this interaction[8] as a resource to drive the system to a desired steady state. The obtained steady state must be robust against decoherence, so one can use dissipation engineering to do reliable quantum computation [72–81].

4. **Decoherence free subspaces (DFS):** In DFS scheme, information is encoded in states belonging to sub-spaces of Hilbert space of the system (quantum computer) that are decoupled from the envirenoment, *i.e.,* its dynamics is unitary and conserved from the effects of decoherence processes. [82–87]

[7] I will use the two terms *decoherence* and *noise* interchangeably

[8] We will call it dissipation, because the interaction will cause energy dissipation between the system and its environment.

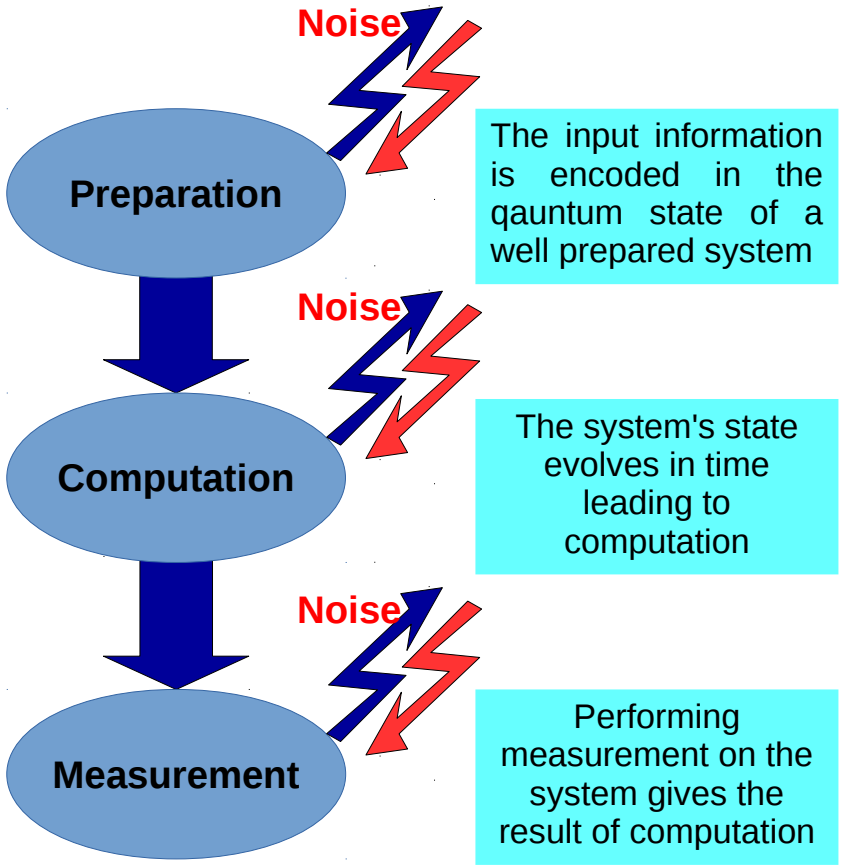

Figure 1.1: Quantum computation steps: each phase of quantum computation is affected by decoherence. First step is the preparation of the input state. Then, this input evolves according to the quantum algorithm. The last step in quantum computation is extracting information from output by measuring the final state of the system.

1.4 Motivation of this work

Many recent experiments have shown that the degrees of freedom of mechanical oscillators can operate in the quantum regime [88–90], which can lead to interesting applications in quantum information technologies. In particular, advances in quantum optomechanical theory and experiments [90] allowed the demonstration and implementations of many quantum processes such as squeezing [91–93] and entanglement [94]. Also, it has been shown that optomechanical systems can be scaled up to build larger systems [95–98]. These achievements can lead to important applications in QIP [99, 100] and quantum many body simulation [101–103].

A promising domain of QIP is the CV one-way model of computation [28, 49, 104–108], where a cluster state is prepared then a sequence of measurements are performed on it. Much research had been devoted towards the study and generation of cluster states of light [108–110]. However, protocols and schemes to generate cluster states of mechanical degrees of freedom are still lacking.

This thesis has the intention of introducing a scheme to generate CV cluster states in mechanical oscillators. The proposed scheme should be robust against the

unavoidable environmental noise, namely the mechanical bath interaction with the oscillators. One way to generate the cluster state is by using dissipation engineering and switching scheme [111–113]. Such a scheme will pave the way towards building scalable and reliable solid-state based QIP devices. We propose to work with optomechanical systems where one cavity mode is coupled to many mechanical oscillators via radiation pressure force [114–118]. The generation of the desired (target) cluster state in the mechanical modes is done with the help of the optomechanical coupling and the cavity dissipation.

1.5 Outline

This thesis introduces a scheme for generating cluster states in the mechanical resonators of an optomechanical system. A suitable choice of the driving lasers with the help of cavity decay will generate the desired cluster state in the mechanical oscillators. In **Chapter 2**, the CV quantum information framework is introduced and some notions of Gaussian states are given. In particular, we talk about cluster states, their definition, canonical preparation and the definition of approximate cluster sates. Also we give the definition of quantum fidelity that will play an important role in quantifying the quality of the generated cluster states by our scheme. **Chapter 3** starts by briefly introducing the theory of quantum optomechanics. Our optomechanical system that will host the cluster state is studied in details, and then we explain a scheme that enables the control of the system via a tunable linearised Hamiltonian. This chapter is concluded by extending our scheme to other configurations of optomechanical systems. **Chapter 4** shows how to generate the cluster state in the mechanical degrees of freedom, where we gave the general protocol and some examples of generic cluster states. We also study the realistic case of generating the cluster state in a finite time. In **Chapter 5**, the analysis of the robustness of the cluster state generation in presence of mechanical noise is presented. Namely, we considered *quantum–optical like noise* for the mechanical oscillators. Finally, **Chapter 6** resumes the obtained results and possible extensions of this work are discussed.

Chapter 2

Gaussian quantum information

Gaussian quantum information is attracting more consideration in theoretical research works as well as in experimental implementations. Because of the simple theoretical study of Gaussian states and the wealthy toolbox and framework developed for quantum optics, Gaussian quantum information theory shows a promising path towards developing reliable and scalable quantum computers.

In this chapter, we give a short introduction to CV systems where we introduce the necessary language and tools that will be exploited in the subsequent chapters. This chapter is organized as follows: after we define the most important concepts of bosonic field quadratures and some quantities and properties related to them such as symplectic transformations and the covariance matrix, we introduce some basic but important examples of Gaussian quantum states. Then, a section is dedicated to cluster states which their generation is the main subject of this thesis. This chapter is concluded by introducing the concept of quantum fidelity which we will extensively be using in the following chapters as a tool to quantify the quality of the generated cluster states by our protocol.

2.1 Quadratures of bosonic fields

A system consisting of N quantized bosonic field modes is called a *continuous variable* (CV) system [49]. A CV system has infinite dimensional Hilbert space with continuous eigen-spectra of its observables.

Associated with the k^{th} mode, is a pair of dimensionless operators a_k and $a_k^\dagger$ that, respectively, lower and raise the number of quanta of that mode:

$$a_k \left|n\right\rangle_k = \sqrt{n}\left|n-1\right\rangle_k \qquad n \geq 1 \ , \tag{2.1}$$

$$a_k \left|0\right\rangle_k = 0 \ , \tag{2.2}$$

$$a_k^\dagger \left|n\right\rangle_k = \sqrt{n+1}\left|n+1\right\rangle_k \qquad n \geq 0 \ , \tag{2.3}$$

where $\left|n\right\rangle_k$ is the state of the k^{th} mode containing n quanta.

The quadratures of the bosonic field are observables of the system and are defined as follows:

$$q_k = \frac{1}{\sqrt{2}}(a_k + a_k^\dagger) \ , \tag{2.4}$$

$$p_k = \frac{1}{i\sqrt{2}}(a_k - a_k^\dagger) \ , \tag{2.5}$$

with the property:

$$[q_k, p_k] = i \ , \tag{2.6}$$

and the Heisenberg uncertainty principle :

$$\Delta q_k \Delta p_k \geq \frac{1}{2} \ . \tag{2.7}$$

The different modes are independent from each other, therefore we can write:

$$[a_k, a_\ell] = 0 \ , \tag{2.8}$$
$$[a_k, a_\ell^\dagger] = \delta_{k\ell} \ , \tag{2.9}$$

and in terms of the quadratures :

$$[q_k, p_\ell] = i\delta_{k\ell} \ . \tag{2.10}$$

We arrange the quadratures in one vector as:

$$x = (q_1, \ldots, q_N; p_1, \ldots, p_N)^T \ , \tag{2.11}$$

where T denotes the transpose operation, then the commutation relations are written in the condensed form:

$$[x_k, x_\ell] = i\Omega_{k\ell} \ , \tag{2.12}$$

where $\Omega_{k\ell}$ are the elements of the $2N \times 2N$ matrix

$$\Omega = \begin{pmatrix} 0_N & \mathbb{1}_N \\ -\mathbb{1}_N & 0_N \end{pmatrix} \ , \tag{2.13}$$

with 0_N and $\mathbb{1}_N$ denoting the zero and identity $N \times N$ matrices, respectively. The Matrix Ω is known as the *symplectic form* [119, 120].

2.2 Wigner function

In quantum mechanics, all the physical information about the system is contained in its state. This state can be represented by a *ket* vector belonging to the Hilbert space associated with the system, or by a trace one positive operator called *density operator*.

It is convenient to use an equivalent representation of the system's state called *Wigner function* [121], defined as

$$W(x) = \int_{\mathbb{R}^{2N}} \frac{\mathrm{d}^{2N}\xi}{(2\pi)^{2N}} \, \mathrm{e}^{-iX^T\Omega\xi} \, \chi(\xi) \ , \tag{2.14}$$

with $\chi(\xi)$ being the Wigner characteristic function given by :

$$\chi(\xi) = \mathrm{Tr}\left[\rho \ D(\xi)\right] \ , \tag{2.15}$$

where $D(\xi)$ is the Weyl operator

$$D(\xi) = \mathrm{e}^{iX^T\Omega\xi} \ . \tag{2.16}$$

The vector $X \in \mathbb{R}^{2N}$ that shows in equations (2.14) and (2.16) consists of the eigenvalues of the quadratures x of the system in the state ρ. The Wigner function is a quasi-probability distribution which normalizes to one and may acquire negative values [122, 123].

2.3 Displacement vector and covariance matrix

The Wigner function W (or equivalently, the corresponding characteristic function χ) is characterized by the statistical moments of the quantum state of the system [124]. In particular, we will be interested in the first and second moments. The first moment is the *displacement vector* given by

$$\overline{x} \equiv \langle x \rangle = \mathrm{Tr}(\rho x) \ , \tag{2.17}$$

and the second moment is called *the covariance matrix* and its elements are given by

$$V_{ij} = \frac{1}{2}\langle \{\Delta x_i, \Delta x_j\} \rangle = \frac{1}{2}\mathrm{Tr}\left(\rho \{\Delta x_i, \Delta x_j\}\right) \ , \tag{2.18}$$

where Δx_i is *variance* of the quadrature x_i :

$$\Delta x_i = x_i - \langle x_i \rangle \ . \tag{2.19}$$

It is clear from Eq. (2.18) that the covariance matrix is symmetric, *i.e.*, $V_{ij} = V_{ji}$, and from the uncertainty principle, see Eq. (2.7), it must satisfy [125]

$$V + \frac{i}{2}\Omega \geq 0 \ , \tag{2.20}$$

which leads to the positive semi-definiteness property

$$V > 0 \ . \tag{2.21}$$

In other words, the following statements are equivalent [125, 126]:

1. V describes a physical state.
2. Eq. (2.20) is true.
3. Eq. (2.21) is true.

2.4 Gaussian states and Gaussian unitaries

2.4.1 Gaussian states

If the Wigner function (and equivalently the characteristic function χ) has a gaussian form, then the corresponding quantum state is called *Gaussian state* [126–128]. The Wigner function W and the characteristic function χ are written as:

$$\chi(\xi) = \exp\{-\frac{1}{2}\xi^T(\Omega V \Omega^T)\xi - i(\Omega\ \overline{x})^T\xi\} \ , \tag{2.22}$$

$$W(x) = \frac{\exp\{-\frac{1}{2}(X-\overline{x})^T V^{-1}(X-\overline{x})\}}{(2\pi)^N\sqrt{\det V}} \ . \tag{2.23}$$

Gaussian states are completely characterized by the displacement vector $\overline{x}$ and the covariance matrix V. We write in this case, $\rho = \rho(\overline{x}, V)$.

2.4.2 Gaussian unitaries - Symplectic transformations

The class of quantum operations that transform a gaussian state into gaussian state is called *gaussian transformation*. A gaussian unitary U is generated by at most a quadratic Hamiltonian H of the field operators a_k and $a_k^\dagger$:

$$U = \mathrm{e}^{-iH} \ . \tag{2.24}$$

In the state space, the quantum state ρ of a system transforms as:

$$\rho \longrightarrow \rho' = U\rho U^\dagger \ . \tag{2.25}$$

Correspondingly, the quadratures x of the field transform, in the phase-space, as follows:

$$x \longrightarrow x' = S \cdot x + d \ , \tag{2.26}$$

with $d \in \mathbb{R}^{2N}$ and $S \in \mathbb{R}^{2N\times 2N}$. The new quadratures must satisfy the commutation relation :

$$\begin{aligned} [x'_k, x'_\ell] &= i\Omega_{k\ell} \ , && (2.27)\\ \Rightarrow \sum_{i,j} S_{ki}S_{\ell j}[x_i, x_j] &= i\Omega_{k\ell} \ , \\ \Rightarrow \sum_{i,j} S_{ki}S_{\ell j} i\Omega_{ij} &= i\Omega_{k\ell} \ , \\ \Rightarrow \sum_{i,j} S_{ki}\Omega_{ij}S_{\ell j} &= \Omega_{k\ell} \ , \\ \Rightarrow S\Omega S^T &= \Omega \ , && (2.28) \end{aligned}$$

where the matrix S satisfying Eq. (2.28) is called *Symplectic matrix*, and the transformation Eq. (2.26) is known as *linear symplectic map*.

Every gaussian unitary U can be decomposed as:

$$U = D(d) \cdot U_S \ . \tag{2.29}$$

The unitary $D(d)$ corresponds to the symplectic map :

$$x \longrightarrow x + d \ , \tag{2.30}$$

therefore, $D(d)$ is nothing then the Weyl displacement operator:

$$D(d) = \mathrm{e}^{ix^T\Omega d} \ . \tag{2.31}$$

The unitary transformation U_S corresponds to the symplectic map :

$$x \longrightarrow S \cdot x \ . \tag{2.32}$$

The displacement vector $\langle x \rangle$ transforms as

$$\overline{x} \longrightarrow \overline{x} + d \ , \tag{2.33}$$

and the covariance matrix V as

$$V \longrightarrow SVS^T \ . \tag{2.34}$$

2.4.3 Vacuum states

The state of a system where there are no quanta in all the bosonic modes of the field is called *vacuum state*, denoted by $|0\rangle$, and defined for an N modes system as :

$$|0\rangle \equiv |0\rangle_1 \otimes \cdots \otimes |0\rangle_N \ . \tag{2.35}$$

The displacement vector and covariance matrix that correspond to the vacuum state are:

$$\overline{x}_0 = (0 \ldots 0)^T \equiv 0 \ , \tag{2.36}$$

$$V_0 = \frac{1}{2}\mathbb{1}_{2N} \ . \tag{2.37}$$

The vacuum state is a state that minimizes the uncertainty principle. The diagonal elements of the covariance matrix are the quadratures' variances, and therefore it is clear from Eq. (2.37) that

$$\Delta x_j \Delta x_{N+j} = \frac{1}{2} \ , \tag{2.38}$$

which minimizes the uncertainty principle as said.

2.4.4 Thermal states

The state of a system in thermal equilibrium with a bath is called *thermal state*. This state has displacement vector $\overline{x}_{th}$ and covariance matrix V_{th} as follows:

$$\overline{x}_{th} = 0 \ , \tag{2.39}$$

$$V_{th} = \frac{1}{2}\,\mathrm{Diag}(2\overline{n}_1 + 1, \ldots, 2\overline{n}_N + 1) \ , \tag{2.40}$$

where Diag is the diagonal matrix with the diagonal elements are given by its argument. $\overline{n}_k$ is the mean number of quanta present in the k^{th} bosonic mode of the field, and it is defined by

$$\overline{n}_k =_k \langle n|a_k^\dagger a_k|n\rangle_k \ , \tag{2.41}$$

and explicitly for the thermal state as :

$$\overline{n}_k = \left(\exp\left(\frac{\hbar\omega_k}{K_B T_k}\right) - 1\right)^{-1} \ , \tag{2.42}$$

where ω_k is the frequency of the k^{th} bosonic mode (modelled as a harmonic oscillator) that is coupled to a bath at temperature T_k. K_B and $\hbar$ are the Boltzmann and reduced Planck constants respectively.

If the bath's temperature is zero, then from Eq. (2.42) we have $\overline{n}_k = 0$ and the system's state is the vacuum.

2.4.5 Coherent states

Consider a bosonic system consisting of N modes. The vacuum state of the system is given by Eq. (2.35). A *coherent state* is defined as the displaced vacuum state.

Let $D(\alpha)$ be the displacement operator acting on the k^{th} mode:

$$|\alpha_k\rangle = D(\alpha_k)\,|0\rangle_k \ . \tag{2.43}$$

$|\alpha_k\rangle$ is the coherent state of the k^{th} mode, and α_k is called *the complex amplitude*.

The displacement operator is generated by the linear Hamiltonian

$$H_k = i(\alpha_k a_k^\dagger - \alpha_k^* a_k) \ . \tag{2.44}$$

The Bogoliubov transformations [129] for the field operators a_k are:

$$a_k \longrightarrow a_k + \alpha_k \ , \tag{2.45}$$

and the quadratures as :

$$x_k \longrightarrow x_k + d_k \ , \tag{2.46}$$

with

$$d_k = \sqrt{2}(\Re\alpha_k, \Im\alpha_k)^T \ . \tag{2.47}$$

Put $\alpha \equiv (\alpha_1, \ldots, \alpha_N)^T$ and $d = \sqrt{(2)}(\Re\alpha_1, \ldots, \Re\alpha_N; \Im\alpha_1, \ldots, \Im\alpha_N)^T$, then the field's quadratures transform as

$$x_0 \longrightarrow x_{\rm c} = x_0 + d \ . \tag{2.48}$$

The displacement vector of the coherent state is $\overline{x}_c = \overline{x}_0 + d$, but the vacuum state has zero displacement, *i.e.,* $\overline{x}_0 = 0$, therefore the displacement of the coherent state is

$$\overline{x}_c = d \ . \tag{2.49}$$

The covariance matrix of a coherent state is calculated from Eq. (2.34), with $S = \mathbb{1}$, as follows:

$$\begin{aligned} V_c &= \mathbb{1}_{2N} \cdot V_0 \cdot (\mathbb{1}_{2N})^T \ , \\ &= \frac{1}{2}\mathbb{1}_{2N} \ . \end{aligned} \tag{2.50}$$

From Eq. (2.50) it is clear that coherent states minimize also the uncertainty principle given in Eq. (2.7).

2.4.6 Squeezed states

Consider one mode vacuum state $|0\rangle$ with annihilation (creation) operator a ($a^\dagger$). Define the operator

$$U_s = \exp\left[\frac{r}{2}(a^2 - a^{\dagger 2})\right] \ , \tag{2.51}$$

generated by the Hamiltonian

$$H_s = \frac{ir}{2}(a^2 - a^{\dagger 2}) \ . \tag{2.52}$$

The state $|0, r\rangle$ defined as

$$|0, r\rangle = U_s\,|0\rangle \ , \tag{2.53}$$

is called *the squeezed vacuum*, where U_s and r are the *squeezing operator* and *squeezing parameter* respectively.

The field operator a transforms by the Bogoliubov transformations as

$$a \longrightarrow \cosh r\ a - \sinh r\ a^\dagger \ , \tag{2.54}$$

which results in the symplectic map

$$x_0 \longrightarrow x_s = S x_0 \ , \tag{2.55}$$

with

$$S = \begin{pmatrix} \mathrm{e}^{-r} & 0 \\ 0 & \mathrm{e}^{r} \end{pmatrix} \ . \tag{2.56}$$

Therefore, the squeezed vacuum has zero displacement vector

$$\overline{x}_s = 0 \ , \tag{2.57}$$

and the covariance matrix V_s, calculated using Eq. (2.34) and Eq. (2.56) :

$$V_s = \frac{1}{2} \begin{pmatrix} \mathrm{e}^{-2r} & 0 \\ 0 & \mathrm{e}^{2r} \end{pmatrix} \ . \tag{2.58}$$

Notice that, from Eq. (2.58), the system has a quadrature with variance smaller than the vacuum noise level[1], while the other (conjugate) quadrature has variance greater than that. The quadrature with variance smaller than the vacuum noise level is called the *squeezed quadrature*.

Although the variances are bellow and above the vacuum noise level, the squeezed vacuum state minimizes the uncertainty principle. From Eq. (2.58), we have $\Delta q \Delta p \equiv \sqrt{V_{11} V_{22}} = 1/2$, which as said, is the minimum of the uncertainty principle given in Eq. (2.7).

The state described by the covariance matrix (2.58) is said to have a level of squeezing [2] equal to [130]

$$10 \log_{10} \mathrm{e}^{2r} \ \mathrm{dB} \ . \tag{2.59}$$

2.4.7 Two–modes squeezed state

Consider two modes defined by the field operators a_1, $a_1^\dagger$, a_2 and $a_2^\dagger$. The two–mode operator U_{S_2} defined by

$$U_{S_2} = \exp \frac{r}{2} \left(a_1 a_2 - a_1^\dagger a_2^\dagger \right) \ , \tag{2.60}$$

and generated by the Hamiltonian

$$H_{S_2} = i \frac{r}{2} \left(a_1 a_2 - a_1^\dagger a_2^\dagger \right) \ , \tag{2.61}$$

is called the *two–modes squeezing operator*, where r is the squeezing parameter. The state obtained when applying this operator on the vacuum state $|0\rangle \otimes |0\rangle$ is known as the *two–modes squeezed state* (TMSS) or Einstein–Podolsky–Rosen (EPR) state [131, 132], denoted by $|r\rangle_{\mathrm{EPR}}$, and it is equal to [127]

$$|r\rangle_{\mathrm{EPR}} = U_{S_2} \ |0\rangle \otimes |0\rangle = \sqrt{1 - \tanh^2 r} \ \sum_{n=0}^{\infty} \left(- \tanh r \right)^n |n\rangle \otimes |n\rangle \ . \tag{2.62}$$

[1] The vacuum noise level is normalized to 1/2.

[2] The squeezing level is usually quantified in units of *deci bell* (dB) .

The two–modes squeezing operator (2.60) induces the symplectic transformation

$$x_0 \to x_{\text{TMSS}} = S_2(r)\ x_0\ , \tag{2.63}$$

where x_0 is the quadratures vector of the two mode vacuum state, and $S_2(r)$ is given by

$$S_2 = \begin{pmatrix} \cosh r & \sinh r & 0 & 0 \\ \sinh r & \cosh r & 0 & 0 \\ 0 & 0 & \cosh r & -\sinh r \\ 0 & 0 & -\sinh r & \cosh r \end{pmatrix} . \tag{2.64}$$

From Eq. (2.63) it is clear that the TMSS has zero displacement

$$\bar{x}_{\text{TMSS}} = 0\ , \tag{2.65}$$

and covariance matrix

$$V_{\text{TMSS}} = \frac{1}{2} S_2 S_2^T = \frac{1}{2} \begin{pmatrix} \cosh 2r & \sinh 2r & 0 & 0 \\ \sinh 2r & \cosh 2r & 0 & 0 \\ 0 & 0 & \cosh 2r & -\sinh 2r \\ 0 & 0 & -\sinh 2r & \cosh 2r \end{pmatrix} . \tag{2.66}$$

2.5 Cluster states

Cluster states are pure, multi–partite, highly entangled quantum states. Briegel and Raussendorf [133] introduced the cluster state in qubit systems. Cluster states over CV were proposed by J. Zhang and S. L. Braustein [134] where they studied *ideal cluster states*. Then, N. M. Menicucci *et al.* [107] developed a graphical approach for studying Gaussian pure states and in particular CV cluster states including the physical case where the cluster contains finite squeezing *i.e., approximate cluster states*. Cluster states are important because they allow universal quantum computation given that *homodyne detection* [135, 136] and a *non-Gaussian measurement* are available [104]. This model of quantum computation that uses CV cluster states is the extension of the one–way model of computation originally developed for qubit systems [137].

Consider N–party system with N modes, and consider that every mode is in an eigenstate of the momentum quadrature of that mode. In particular, we are interested in the state where all the modes are in the zero–momentum eigenstate. If we call this state $|\psi_0\rangle$ then:

$$|\psi_0\rangle = |0\rangle_1 \otimes \cdots \otimes |0\rangle_N\ , \tag{2.67}$$

where $|0\rangle_k$ is the eigenstate of the momentum quadrature of the k^{th} mode ($k = 0, \ldots, N$). Since every mode is in a definite momentum state, then this means that the momentum variance is zero. According to the uncertainty principle, the variance of the position must be infinite. Therefore, every mode is in an infinite momentum–squeezed state. By creating entanglement between the modes, one obtains the so called *ideal cluster states*. The entangling operation between the i^{th} and j^{th} modes is performed via the application of the controlled–Z unitary defined by

$$C_Z^{ij} = \exp\left(i g_{ij}\ q_i \otimes q_j\right)\ , \tag{2.68}$$

which is generated by the Hamiltonian

$$H_{ij} = -\chi_{ij}\ q_i \otimes q_j\ , \tag{2.69}$$

where $g_{ij} = \hbar\chi_{ij}t$ and χ are, respectively, the gain of the interaction and coupling strength between the i^{th} and j^{th} modes, and t denotes the time. The Hamiltonian (2.69) is known as the *quantum non–demolition* (QND) coupling [138–140]. The constants g_{ij}, with $i, j = 1, \ldots, N$, form a real symmetric matrix, denoted by A, and called *the adjacency matrix* :

$$A_{ij} = g_{ij}\ . \tag{2.70}$$

The adjacency matrix has zero elements on the diagonal and this is because the couplings g_{ij} are associated to different modes. The cluster state is therefore written as

$$|\psi_A\rangle = C_Z(A)\ \ |\psi_0\rangle\ \ , \tag{2.71}$$

where $C_Z(A)$ is the resultant of applying all the controlled–Z operations between the modes according to the adjacency matrix A :

$$\begin{aligned} C_Z(A) &= \prod_{i,j=1,\ j>i}^{N} C_Z^{ij}\ , \\ &= \prod_{i,j=1,\ j>i}^{N} \exp\left(iA_{ij}q_iq_j\right) = \exp\left(i\sum_{i,j=1,\ j>i}^{N} A_{ij}q_iq_j\right)\ . \end{aligned} \tag{2.72}$$

We should mention here that since all the position quadratures commute two by two, then the order in which the controlled–Z operations are applied is unimportant. Since A is symmetric and has null diagonal elements, then $C_Z(A)$ can be written as

$$C_Z(A) = \exp\left(\frac{i}{2}q^T A\ q\right)\ , \tag{2.73}$$

where q is the vector of the position quadratures of the N–modes:

$$q = (q_1, \ldots, q_N)^T\ . \tag{2.74}$$

Therefore, the cluster state is given by the equation

$$|\psi_A\rangle = \exp\left(\frac{i}{2}q^T A\ q\right)|\psi_0\rangle\ . \tag{2.75}$$

Cluster states are represented graphically by a set of nodes connected by edges. Every node corresponds to a zero–momentum eigenstate, and edges connecting two nodes represents the coupling between the corresponding modes. The coupling (gain) constants are put as a label for the edges, see Fig. 2.1. Since the couplings g_{ij} depends on the choice of labelling the modes then the same cluster state can be represented by many adjacency matrices. In the special case where all the couplings between modes equal to one (unit), then the labels of the edges can be omitted.

Cluster states described so far are non-physical states, since momentum eigenstates can not be normalized. In real world states, systems can only have finite amount of squeezing (and not infinite squeezing as in the case of the ideal cluster states). This leads to considering *approximate cluster states* instead of their *ideal*

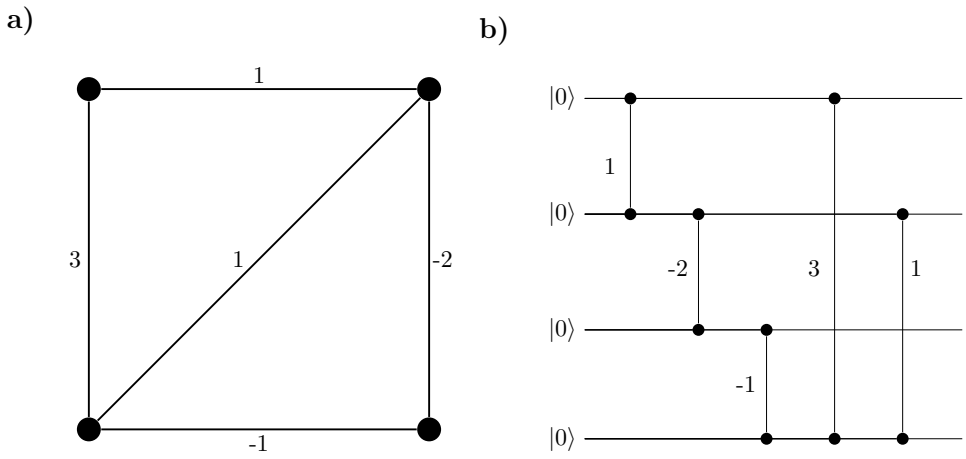

Figure 2.1: Cluster state representation by graph and a circuit. a) Graph representation of 4–modes cluster state. b) Circuit showing how to prepare the cluster state. A vertical line connecting two nodes represents the controlled–Z operation between the modes and the labels of the lines correspond to the coupling strength. The initial states $|0\rangle$'s are the zero–momentum eigenstates.

and non-physical counter part. Approximate cluster states must approach the ideal one when considering big squeezing: If we denote by $|\psi_A\rangle$ the ideal cluster state and by $|\psi_A(r)\rangle$ the approximate cluster state, then the following limit must hold:

$$\lim_{r\to\infty} |\psi_A(r)\rangle = |\psi_A\rangle \ , \tag{2.76}$$

where r is a parameter that quantifies the squeezing present in the state. In terms of the quadratures and the adjacency matrix, approximate cluster states must satisfy

$$\lim_{r\to\infty} \ \mathrm{cov}\,(p - Aq) = 0 \ , \tag{2.77}$$

where q, p and A are the position vector, momentum vector and adjacency matrix respectively, and $\mathrm{cov}\,(\cdot)$ is the covariance matrix defined for a vector x of N quadratures as [107]

$$(\ \mathrm{cov}\,(x))_{ij} = \frac{1}{2}\langle\{x_i, x_j\}\rangle \ , \tag{2.78}$$

with the expectation values are calculated in the state $|\psi_A(r)\rangle$.

In this thesis, when the term *cluster state* is mentioned, it is *approximate cluster state* that is meant unless otherwise is stated.

2.6 Quantum fidelity for Gaussian states

Being able to distinguish two quantum states is a crucial matter in quantum information and computation theory.

The degree of distinguishibility between two states is quantified by a suitable measure. There are many distance measures in use in QIP [141] such as *the fidelity*.

Fidelity in quantum information theory gives a measure of how close two quantum states are. It is defined, for two states ρ_1 and ρ_2 as:

$$F(\rho_1, \rho_2) \equiv \left(\mathrm{Tr}\sqrt{\sqrt{\rho_1}\rho_2\sqrt{\rho_1}}\right)^2 \ . \tag{2.79}$$

The fidelity given in Eq. (2.79) is known as *Uhlmann-Jozsa fidelity* [142, 143], and it satisfies the following properties:
Let ρ_1 and ρ_2 be two quantum states belonging to the state space of a physical system:

1. $0 \leq F(\rho_1, \rho_2) \leq 1$.
2. $F(\rho_1, \rho_2) = 0 \Leftrightarrow \rho_1$ and ρ_2 are orthogonal.
3. $F(\rho_1, \rho_2) = 1 \Leftrightarrow \rho_1$ and ρ_2 are identical.
4. $F(\rho_1, \rho_2)$ is invariant under unitary transformations: Let U be a unitary transformation, then ρ_1 and ρ_2 transforms as

$$\rho_j \longrightarrow U\rho_j U^\dagger \qquad , \qquad j = 1, 2 \ ,$$

and we have $F(U\rho_1 U^\dagger, U\rho_2 U^\dagger) = F(\rho_1, \rho_2)$.

In particular, for two Gaussian states $\rho_1(\overline{x}_1, V_1)$ and $\rho_2(\overline{x}_2, V_2)$, the Uhlman fidelity becomes [144]:

$$F(\rho_1, \rho_2) = \sqrt{\frac{\det \mathcal{O} \det\left(\mathbb{1}_{2N} + \sqrt{\mathbb{1}_{2N} + (\Omega\mathcal{O})^{-2}}\right)}{\det(V_1 + V_2)}} \ , \tag{2.80}$$

where the matrix $\mathcal{O}$ is given by

$$\begin{aligned} \mathcal{O} \ = \ & \Phi(V_1) - [\Phi(V_1) - i\Omega]\Big\{2V_2 + \Phi(V_1) \\ & -(2V_2 - i\Omega)[\Phi(V_1) + 2V_2]^{-1}(2V_2 + i\Omega)\Big\}^{-1}[\Phi(V_1) + i\Omega] \ , \end{aligned} \tag{2.81}$$

with the function Φ is defined as

$$\Phi(V) = 2V\left(\mathbb{1}_{2N} + \sqrt{\mathbb{1}_{2N} + (2\Omega V)^{-2}}\right) \ . \tag{2.82}$$

Furthermore, when at least one of the two states is pure, the fidelity becomes [145]:

$$F(\rho_1, \rho_2) = \frac{2^N}{\sqrt{\det(V_1 + V_2)}} \exp\left[-\frac{1}{2}\delta^T(V_1 + V_2)\delta\right] \ , \tag{2.83}$$

with $\delta = \overline{x}_1 - \overline{x}_2$.

Chapter 3

Optomechanical systems

Cavity optomechanics is a field of quantum physics that studies the interaction between mechanical and optical degrees of freedom in quantum systems. Cavity optomechanics gained much interest both in the theoretical and experimental sides leading to very precise devices with high controllability. These theoretical and technological advances rendered optomechanical systems good candidates for quantum information processing devices.

In this chapter we aim to develop a framework enabling us to control the state of an optomechanical system and driving it to a target quantum state. This chapter is organized as follows: First, we introduce the simplest system that exploits radiation pressure, *Fabry–Pérot cavity* with a movable mirror, where we describe its dynamics in terms of a master equation. In the subsequent section the model optomechanical system is introduced where we extend the simple Fabry–Pérot optomechanical system to the case of many movable membranes inside an optical cavity. In **Section 3.3** we derive the Hamiltonian of the model system in the case of weak optomechanical interactions which will be the basis of the next section to develop a scheme for controlling the quantum state of the model system. Then we conclude this chapter by extending our scheme to other configurations of optomechanical systems to overcome some limitations put by our model system.

3.1 Radiation pressure

The light can show a pressure force, called *radiation pressure*, when it hits an object. This pressure force is explained by the fact that light possesses momentum and when it collides another object its momentum (or part of it) is transferred to that object. Much theoretical and experimental effort was devoted to the study of the radiation pressure [114–118]. After the invention of the laser [146, 147], many other sophisticated experiments were established such as cooling the vibrational motion (of both micro and macro) objects to their ground state [148–152] which opened the door for many other theoretical and experimental advances.

A typical system exploiting radiation pressure is the *cavity optomechanics* [90]. A simple cavity optomechanical system is shown in Fig. 3.1. This system consists of a Fabry–Pérot cavity with a movable end–mirror. The cavity mode has a frequency ω and annihilation operator a, and the movable mirror has frequency Ω and annihilation operator b. The Hamiltonian of this system is

$$H_0 = \omega a^\dagger a + \Omega b^\dagger b \ . \tag{3.1}$$

The photons inside the cavity applies a pressure force on the movable mirror which leads to a small displacement x. This results in a change of the resonance frequency of the cavity and therefore ω is a function of the mirror's displacement x *i.e.,* $\omega = \omega(x)$, and we can write

$$\omega(x) = \omega_c + x\frac{\mathrm{d}\omega}{\mathrm{d}x} + \frac{x^2}{2}\frac{\mathrm{d}\omega}{\mathrm{d}x} + \cdots \ , \tag{3.2}$$

where ω_c is the cavity's frequency for the uncoupled system *i.e.,* the same cavity with fixed end–mirrors. For small displacement x we can stop at the second term in Eq. (3.2) and we write

$$\omega(x) = \omega_c - Gx \ , \tag{3.3}$$

where $G = -\frac{\mathrm{d}\omega}{\mathrm{d}x}$. The Hamiltonian (3.1) becomes

$$H_0 = \omega_c a^\dagger a + \Omega b^\dagger b - G a^\dagger a x \ . \tag{3.4}$$

The first term in Eq. (3.4) is the uncoupled cavity Hamiltonian and the second term is the uncoupled mechanical oscillator (the moving mirror) Hamiltonian. The optomechanical interaction between the optical cavity and the mechanical oscillator is given by the third term.

The mirror's position operator is written in terms of the annihilation and creation operators as

$$x = \sqrt{\frac{\hbar}{2m\Omega}}\ (b + b^\dagger) \ , \tag{3.5}$$

where m is the effective mass of the mirror. We put

$$g = \sqrt{\frac{\hbar}{m\Omega}}\ G \ , \tag{3.6}$$

then the optomechanical interaction Hamiltonian is written as

$$H_{cm} = -g\ a^\dagger a\ \frac{b + b^\dagger}{\sqrt{2}} \ , \tag{3.7}$$

and the Hamiltonian of the system becomes

$$H_0 = \omega_c\ a^\dagger a + \Omega\ b^\dagger b - g\ a^\dagger a\ \frac{b + b^\dagger}{\sqrt{2}} \ . \tag{3.8}$$

The parameter g is called *the vacuum optomechanical strength* [90].

In **Section 3.2**, we consider a system with many mechanical modes where the cavity mode is coupled to many movable mirrors (membranes) inside an optical cavity (with unmovable end–mirrors). Systems similar to this one were studied in the literature and implemented experimentally [100–103].

Up to now we considered a perfectly isolated optomechanical system where the end–mirrors are totally reflective and no photons inside the cavity can leak out, and also the mirrors were considered isolated from their phononic bath. But in real world optomechanical systems, some intra–cavity photons leak out the cavity and the movable mirrors are in a thermal equilibrium with their bath, see Fig. 3.2.

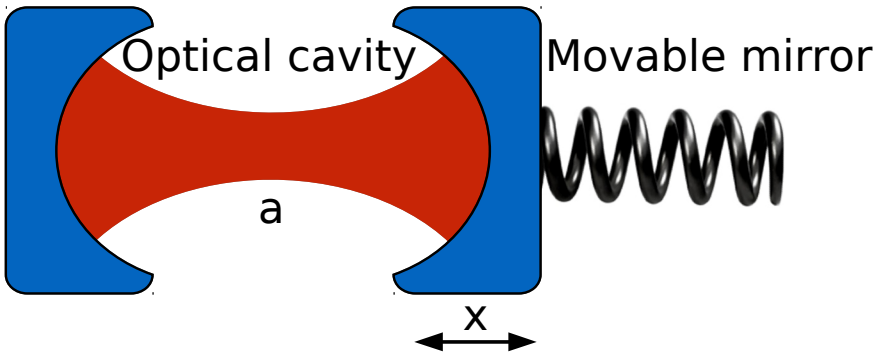

Figure 3.1: An optomechanical setup: This device consists of a fixed mirror and a movable mirror that can be modeled by a harmonic oscillator. There are two bosonic modes, an optical mode $\hat{a}$ (intra-cavity photon) and a mechanical mode $\hat{b}$ (phonon).

Therefore the Hamiltonian of the system will contain other terms that characterize these dissipation processes. The Hamiltonian becomes

$$H = H_0 + H_d + H_\gamma + H_\kappa \ , \tag{3.9}$$

where H_0 is the Hamiltonian given in Eq. (3.8), H_d is the Hamiltonian that describes driving the cavity with external laser fields, and H_γ and H_κ are the Hamiltonians that take into account the dissipation of the mirror and the cavity respectively.

The dynamics of the system shown in Fig. 3.2 is usually described by a master equation of the form

$$\dot{\rho}(t) = -i[H_0 + H_d, \rho(t)] + \mathcal{L}_c(t)[\rho] + \mathcal{L}_m(t)[\rho] \ , \tag{3.10}$$

where $\rho(t)$ is the density operator for the system, and $\mathcal{L}_c$ and $\mathcal{L}_m$ characterize the dissipation processes for the cavity and the mirror respectively.

3.2 The model

We consider an optomechanical system consisting of one cavity mode coupled to N non interacting mechanical oscillators. The cavity is driven by M classical laser fields. The cavity decays with the rate κ. This configuration is sketched in Fig. 3.3. Systems similar to this were suggested and realized in several experiments (see **Chapter 6** for references).

Since the optomechanical system shown in Fig. 3.3 interacts with the reservoirs of both the cavity field and the mechanical oscillators, then the dynamics is described by a unitary part and dissipative terms [52]. The unitary evolution of the system is generated by the Hamiltonian

$$\mathcal{H} = \mathcal{H}_c + \mathcal{H}_m + \mathcal{H}_{cm} + \mathcal{H}_D \ , \tag{3.11}$$

where $\mathcal{H}_c$ is the cavity's free Hamiltonian and it is given by

$$\mathcal{H}_c = \omega_c(c^\dagger c + \frac{1}{2}) \ , \tag{3.12}$$

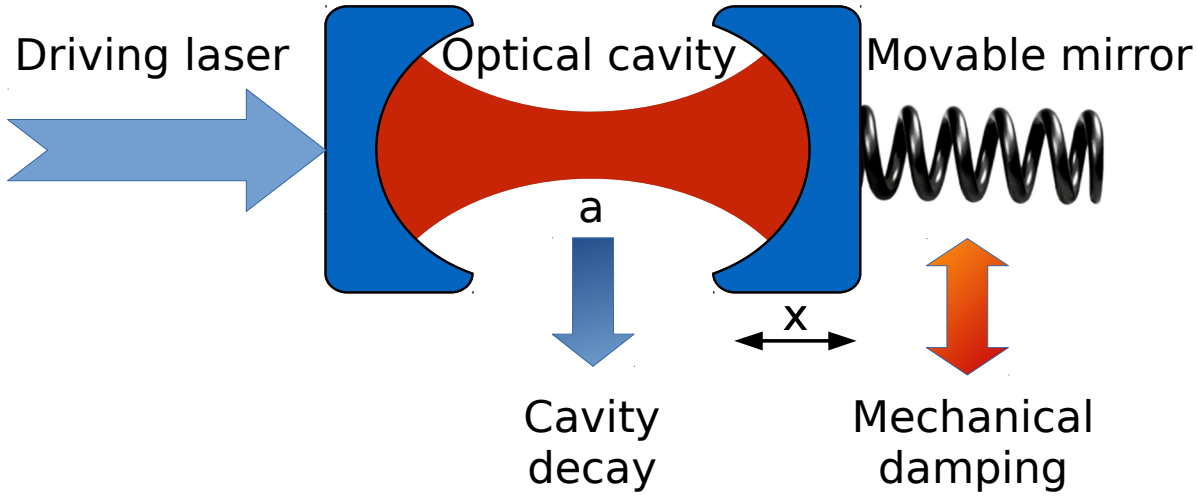

Figure 3.2: An optomechanical system where the mirror is in thermal equilibrium with its bath (damping rate Γ) and the cavity photons decay with a rate κ.

with ω_c and c ($c^\dagger$) are the frequency and annihilation (creation) operator respectively. $\mathcal{H}_m$ is the Hamiltonian of the mechanical oscillators given by

$$\mathcal{H}_m = \sum_{j=1}^{N} \Omega_j (d_j^\dagger d_j + \frac{1}{2}) \ , \tag{3.13}$$

with Ω_j and d_j ($d_j^\dagger$) are the frequency and the annihilation (creation) operator of the j^{th} mechanical oscillator. $\mathcal{H}_{cm}$ is the Hamiltonian describing the interaction between the cavity mode and the mechanical modes, and it is given by [90]

$$\mathcal{H}_{cm} = -\sum_{j=1}^{N} g_j \ c^\dagger c \ q_j \ , \tag{3.14}$$

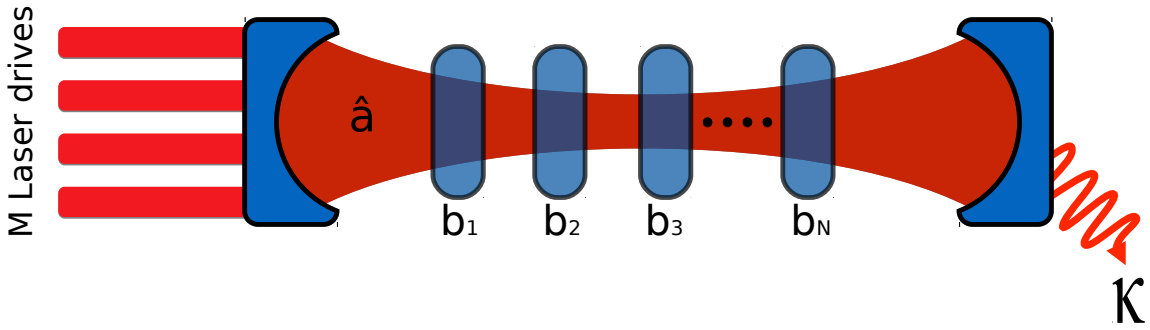

Figure 3.3: An optomechanical system consisting of one cavity mode and N mechanical oscillators. The cavity losses are characterised by the decay rate κ.

where g_j is the coupling rate between the cavity mode and the j^{th} mechanical oscillator and it is called *the optomechanical coupling constant* where it quantifies the strength of the interaction between one photon and one phonon [90]. The operator $q_j = 1/\sqrt{2}\ (d_j + d_j^\dagger)$ is the *position quadrature* of the j^{th} mechanical oscillator. $\mathcal{H}_D$ is the Hamiltonian describing the coupling of the cavity mode with the pump laser fields. We consider here that the pump consists of M lasers that are regarded as classical fields. $\mathcal{H}_D$ is given by

$$\mathcal{H}_D = \epsilon(t)\ c^\dagger + \epsilon^*(t)\ c\ , \tag{3.15}$$

with $\epsilon(t)$ is the laser pump and it is given by

$$\epsilon(t) = \sum_{k=1}^{M} \epsilon_k \mathrm{e}^{-i(\omega_k t + \Phi_k)}\ , \tag{3.16}$$

where ϵ_k, ω_k and Φ_k are, respectively, the intensity, frequency and the phase of the k^{th} laser field.

We should mention here that the Hamiltonians in equations (3.12) and (3.13) contain constant terms ($1/2\ \omega_c$ and $1/2\ \Omega_j$). It is more convenient to drop writing them in the subsequent equations by implementing a suitable shift of the energy reference as follows:

$$\mathcal{H}_c \longrightarrow \mathcal{H}_c - \frac{\omega_c}{2} = \omega_c c^\dagger c\ , \tag{3.17}$$

$$\mathcal{H}_m \longrightarrow \mathcal{H}_m - \sum_{j=1}^{N} \frac{\Omega_j}{2} = \sum_{j=1}^{N} \Omega_j d_j^\dagger d_j\ . \tag{3.18}$$

The Hamiltonian of the system, therefore, is written as:

$$\begin{aligned} \mathcal{H} \ &= \ \omega_c\ c^\dagger c + \sum_{j=1}^{N} \left\{ \Omega_j\ d_j^\dagger d_j - g_j\ c^\dagger c\ q_j \right\} \\ &\quad + \sum_{k=1}^{M} \left\{ \epsilon_k \mathrm{e}^{-i(\omega_k t + \Phi_k)} c^\dagger + \epsilon_k^* \mathrm{e}^{i(\omega_k t + \Phi_k)} c \right\}\ . \end{aligned} \tag{3.19}$$

3.3 Linearised Hamiltonian

The Hamiltonian given in Eq. (3.19) contains cubic terms of the field operators. We are interested in the weak coupling regime where the optomechanical coupling constants are negligible compared to the other frequencies present in the system ,*i.e.*,

$$g_j \ \ll \ \Omega_j\ , \tag{3.20}$$

$$g_j \ \ll \ \omega_c\ . \tag{3.21}$$

In this regime, the Hamiltonian given in Eq. (3.19) can be approximated to an expression that contains, at most, quadratic terms of the field operators[1]. This approximate Hamiltonian contains an interaction term that is *bilinear* in the cavity and mechanical field operators, and it is called *linear Hamiltonian*.

[1] Gaussian states are generated by quadratic Hamiltonians

The first step to linearise the Hamiltonian given in Eq. (3.19) is to consider that the cavity field consists of a coherent part with complex amplitude α and a fluctuating part that we denote a, and we write

$$c = a + \alpha \ , \tag{3.22}$$

where $\langle c \rangle = \alpha$.

Also we split the the mechanical motion as follows:

$$d_j = b_j + \beta_j \quad , \quad j = 1, \cdots, N \ , \tag{3.23}$$

where $\langle d_j \rangle = \beta_j$ and b_j is the operator that describes the fluctuations in the j^{th} mechanical oscillator.

Equations of motion of the cavity field and the mechanical one are:

$$\begin{aligned} \frac{\mathrm{d}c(t)}{\mathrm{d}t} &= -i\omega_c \, c(t) + \frac{i}{\sqrt{2}} \, c(t) \sum_{j=1}^{N} g_j \left(d_j(t) + d_j^\dagger(t) \right) \\ &\quad -i\epsilon(t) - \frac{\kappa}{2} c(t) - \sqrt{\kappa} a_{\text{in}} \ , \end{aligned} \tag{3.24}$$

$$\frac{\mathrm{d}d_j(t)}{\mathrm{d}t} = -i\Omega_j \, d_j(t) + \frac{i}{\sqrt{2}} \, g_j \, c(t)^\dagger c(t) \ , \tag{3.25}$$

where $c(t)$ and $d(t)$ are the Heisenberg picture field operators, and κ is the decay rate of the cavity field, and a_{in} is the input noise operator of the cavity mode [51]. We should mention here that the mechanical noise was neglected, but it will be considered in **Chapter 5** where we study the robustness of the generation of cluster states in the mechanical degrees of freedom.

Substituting Eq. (3.22) and Eq. (3.23) in Eq. (3.24) and Eq. (3.25), one obtains

$$\begin{aligned} \frac{\mathrm{d}a(t)}{\mathrm{d}t} &= -\left[\frac{\kappa}{2} + i \left(\omega_c - \sqrt{2} \sum_{j=1}^{N} g_j \Re\beta_j \right) \right] a(t) \\ &\quad -\frac{i}{\sqrt{2}} \sum_{j=1}^{N} g_j \, a(t) \left(b_j(t) + b_j^\dagger(t) \right) - \sqrt{\kappa} \, a_{\text{in}} \ , \end{aligned} \tag{3.26}$$

$$\frac{\mathrm{d}b_j(t)}{\mathrm{d}t} = -i\Omega_j b_j(t) + \frac{i}{\sqrt{2}} \, g_j \left(a^\dagger(t) a(t) + \alpha a^\dagger(t) + \alpha^* a(t) \right) \ , \tag{3.27}$$

$$\dot{\alpha} = -\left[\frac{\kappa}{2} + i \left(\omega_c - \sqrt{2} \sum_{j=1}^{N} g_j \Re\beta_j \right) \right] \alpha - i\epsilon(t) \ , \tag{3.28}$$

$$\dot{\beta}_j = -i\Omega_j \beta_j + \frac{i}{\sqrt{2}} g_j |\alpha|^2 \ . \tag{3.29}$$

Since a and b_j are the fluctuations in the cavity and mechanical movement fields respectively, then one can neglect second order terms of a and b_j in Eq. (3.26) and 3.27 and obtain

$$\dot{a} \approx -\left[\frac{\kappa}{2} + i \left(\omega_c - \sqrt{2} \sum_{j=1}^{N} g_j \, \Re\beta_j \right) \right] a - \sqrt{\kappa} \, a_{\text{in}} \ , \tag{3.30}$$

$$\dot{b}_j \approx -i\Omega_j b_j + \frac{i}{\sqrt{2}} g_j \, (\alpha a^\dagger + \alpha^* a) \ . \tag{3.31}$$

From equations (3.30) and (3.31) one obtains the Hamiltonian

$$\mathcal{H} = \omega_c' a^\dagger a + \sum_{j=1}^{N} \left[\Omega_j b_j^\dagger b_j - \frac{g_j}{\sqrt{2}} (\alpha a^\dagger + \alpha^* a)(b_j + b_j^\dagger) \right] , \tag{3.32}$$

with ω_c' is given by

$$\omega_c' = \omega_c - \sqrt{2} \sum_{j=1}^{N} g_j \ \Re\beta_j \ . \tag{3.33}$$

3.4 Controlling the optomechanical system by external lasers

The state of the system shown if Fig. 3.3 can be controlled by tuning the frequency, phase and intensity of the lasers pumping the cavity. The driving lasers parameters enter in the system's Hamiltonian through the cavity's complex amplitude α. To simplify the calculations and obtain analytical expressions for α,we assume that

$$g_j \Re\beta_j \ll \omega_c \ . \tag{3.34}$$

Relation (3.34) is valid in the weak coupling regime (see Eq. (3.21)) for small mechanical vibration amplitude β_j. In this case we have $\omega_c' \approx \omega_c$ and

$$\dot{\alpha} \approx -(\frac{\kappa}{2} + i\omega_c)\alpha - i\epsilon(t) \ , \tag{3.35}$$

which has the solution

$$\alpha(t) = \alpha_0 \mathrm{e}^{-(\frac{\kappa}{2} + i\omega_c)t} + \sum_{k=1}^{M} \frac{\epsilon_k}{(\omega_k - \omega_c) + i \ \frac{\kappa}{2}} \mathrm{e}^{-i(\omega_k t + \Phi_k)} \ , \tag{3.36}$$

where α_0 is a constant. We are interested in the stationary regime of the cavity, *i.e.,* when $t \to +\infty$, then $\alpha(t)$ becomes

$$\alpha(t) = \sum_{k=1}^{M} \frac{\epsilon_k \mathrm{e}^{-i(\omega_k t + \Phi_k)}}{\Delta_k + i \ \frac{\kappa}{2}} \ , \tag{3.37}$$

where Δ_k is the detuning of the k^{th} laser with the cavity, and it is given by

$$\Delta_k = \omega_k - \omega_c \ . \tag{3.38}$$

We write $\alpha(t)$ as

$$\alpha(t) = \sum_{k=1}^{M} \alpha_k \ \mathrm{e}^{-i(\omega_k \ t + \phi_k)} \ , \tag{3.39}$$

with α_k and ϕ_k are given by

$$\alpha_k = \frac{\epsilon_k}{\sqrt{\Delta_k^2 + (\frac{\kappa}{2})^2}} \ , \tag{3.40}$$

$$\phi_k = \Phi_k + \arctan \frac{\kappa}{2\Delta_k} \ . \tag{3.41}$$

The Hamiltonian in Eq. (3.32) becomes

$$\mathcal{H} = \omega_c\ a^\dagger a + \sum_{j=1}^{N}\left\{\Omega_j\ b_j^\dagger b_j - \frac{1}{\sqrt{2}}\sum_{k=1}^{M}\alpha_k\ g_j\left(\mathrm{e}^{-i(\omega_k t+\phi_k)}\ a^\dagger + \mathrm{e}^{i(\omega_k t+\phi_k)}\ a\right)(b_j + b_j^\dagger)\right\}\ . \tag{3.42}$$

Now we want to eliminate the time dependence in this Hamiltonian. To do that, we first transform into the interaction picture with respect to the free Hamiltonian of the optomechanical system, and therefore we are considering the following transformation operator:

$$\mathcal{U} = \exp\left\{it\left(\omega_c\ a^\dagger a + \sum_{j=1}^{N}\Omega_j\ b_l^\dagger b_j\right)\right\}\ , \tag{3.43}$$

and we obtain the following Hamiltonian

$$\begin{aligned} H &= \mathcal{U}\mathcal{H}\mathcal{U}^\dagger - i\mathcal{U}\frac{\partial\mathcal{U}^\dagger}{\partial t} \\ &= -\frac{1}{\sqrt{2}}\sum_{k=1}^{M}\sum_{j=1}^{N}\alpha_k g_k\left(\mathrm{e}^{-i(\Delta_k t+\phi_k)}\ a^\dagger + \mathrm{e}^{i(\Delta_k t+\phi_k)}\ a\right)\left(\mathrm{e}^{-i\Omega_j}\ b_j + \mathrm{e}^{i\Omega_j}\ b_j^\dagger\right) \end{aligned} \tag{3.44}$$

We then associate for the j^{th} mechanical oscillator, two laser drives with the frequencies ω_j^+ and ω_j^-, amplitudes α_j^+ and α_j^-, and phases ϕ_j^+ and ϕ_j^- with the following convention

$$\omega_j^- \equiv \omega_j \quad , \quad \omega_j^+ \equiv \omega_{N+j}\ , \tag{3.45}$$
$$\alpha_j^- \equiv \alpha_j \quad , \quad \alpha_j^+ \equiv \alpha_{N+j}\ , \tag{3.46}$$
$$\phi_j^- \equiv \phi_j \quad , \quad \phi_j^+ \equiv \phi_{N+j}\ . \tag{3.47}$$

The detunings of these two lasers are

$$\Delta_j^- \equiv \Delta_j \quad , \quad \Delta_j^+ \equiv \Delta_{N+j}\ . \tag{3.48}$$

The Hamiltonian (3.44) is written

$$\begin{aligned} H &= -\sum_{j,\ell=1}^{N}\frac{g_j}{\sqrt{2}}\ a^\dagger\left\{\left(\alpha_\ell^-\mathrm{e}^{-i[(\Delta_\ell^-+\Omega_j)t+\phi_\ell^-]} + \alpha_\ell^+\mathrm{e}^{-i[(\Delta_\ell^++\Omega_j)t+\phi_\ell^+]}\right)\ b_j\right. \\ &\quad \left. + \left(\alpha_\ell^-\mathrm{e}^{-i[(\Delta_\ell^--\Omega_j)t+\phi_\ell^-]} + \alpha_\ell^+\mathrm{e}^{-i[(\Delta_\ell^+-\Omega_j)t+\phi_\ell^+]}\right)\ b_j^\dagger\right\} + \text{H.C.}\ , \end{aligned} \tag{3.49}$$

where H.C. denotes the hermitian conjugate.

In order to control the dynamics of the optomechanical system shown in Fig. 3.3, one should be able to tune independently the coefficients of $a^\dagger b_j$ and $a^\dagger b_j^\dagger$ in Eq. (3.49). To achieve this, we assume that the following conditions are satisfied:

- The mechanical oscillators have non overlapping frequencies.
- In addition to the weak coupling condition (3.20), we should have

$$\alpha_j^\pm g_j \ll \Omega_j\ . \tag{3.50}$$

We put

$$\omega_j^{\pm} = \omega_c \pm \Omega_j \ , \tag{3.51}$$

then, the detunings of the driving lasers become

$$\Delta_j^{\pm} = \pm\Omega_j \ , \tag{3.52}$$

and the Hamiltonian (3.49) writes

$$\begin{aligned} H \ = \ & -\sum_{j,\ell=1}^{N} \frac{g_j}{\sqrt{2}}\, a^\dagger \Big\{ \Big(\alpha_\ell^- \mathrm{e}^{-i[(-\Omega_\ell+\Omega_j)t+\phi_\ell^-]} + \alpha_\ell^+ \mathrm{e}^{-i[(\Omega_\ell+\Omega_j)t+\phi_\ell^+]} \Big)\ b_j \\ & + \Big(\alpha_\ell^- \mathrm{e}^{-i[-(\Omega_\ell+\Omega_j)t+\phi_\ell^-]} + \alpha_\ell^+ \mathrm{e}^{-i[(\Omega_\ell-\Omega_j)t+\phi_\ell^+]} \Big)\ b_j^\dagger \Big\} + \mathrm{H.C.} \end{aligned} \tag{3.53}$$

Applying the rotating wave approximation (RWA) to the Hamiltonian (3.53) one obtains

$$H = -\sum_{j=1}^{N} \frac{g_j}{\sqrt{2}}\, a^\dagger \left(\alpha_j^- \mathrm{e}^{-i\phi_j^-}\ b_j + \alpha_j^+ \mathrm{e}^{-i\phi_j^+}\ b_j^\dagger \right) + \mathrm{H.C.} \tag{3.54}$$

The Hamiltonian (3.54) generates controlled dynamics by tuning the intensities and phases of the driving lasers. These later enter in (3.54) through the parameters $\alpha_j^{\pm}$ and $\phi_j^{\pm}$ that are now written as

$$\alpha_j^{\pm} \ = \ \frac{\epsilon_j^{\pm}}{\sqrt{\Omega_j^2 + (\frac{\kappa}{2})^2}} \ , \tag{3.55}$$

$$\phi_j^{\pm} \ = \ \Phi_j^{\pm} \pm \arctan \frac{\kappa}{2\Omega_j} \ , \tag{3.56}$$

where equations (3.40), (3.41) and (3.52) are used to obtain equations (3.55) and (3.56). $\epsilon_j^{\pm}$ and $\Phi_j^{\pm}$ are defined as

$$\epsilon_j^- \equiv \epsilon_j \qquad , \qquad \epsilon_j^+ \equiv \epsilon_{N+j} \ , \tag{3.57}$$

$$\Phi_j^- \equiv \Phi_j \qquad , \qquad \Phi_j^+ \equiv \Phi_{N+j} \ . \tag{3.58}$$

In this work we are interested in driving the system's steady state to a desired quantum state. This is done with the help of the cavity losses. The open system dynamics of the system shown in Fig. 3.3 is governed by the following master equation [50–55]

$$\dot{\rho}(t) = -i[H, \rho(t)] + \mathcal{L}_c[\rho(t)] \ , \tag{3.59}$$

where $\rho(t)$ is the system's density operator ,*i.e.,* the system's quantum state, and $\dot{\rho}(t)$ is its time derivative, H is the Hamiltonian given in Eq. (3.54), and $\mathcal{L}_c[\rho(t)]$ describing the cavity's losses is given by [153]

$$\mathcal{L}_c[\rho(t)] = \kappa\ D[a]\rho(t) \ , \tag{3.60}$$

with κ is the decay rate of the cavity mode, and $D[a]\rho(t)$ is the super operator defined as

$$D[a]\rho(t) = a\rho(t)a^\dagger - \frac{1}{2}\{a^\dagger a, \rho(t)\} \ , \tag{3.61}$$

where the symbol $\{\cdot,\cdot\}$ denotes the anti-commutator.

The asymptotic solution of Eq. (3.59), if it exists, is called *steady state*:

$$\rho_{\text{steady}} = \lim_{t\to\infty} \rho(t) \ . \tag{3.62}$$

The existence and uniqueness of a steady state solution of the master equation (3.59) is studied in **Section 4.1**. It is shown there that the master equation (3.59) have a unique steady state if and only if the cavity mode is coupled to only one mechanical mode. A scheme to overcome this issue, *i.e.,* when considering more than one mechanical mode, is given in **Section 4.3**, and an example of generating two modes squeezed state is demonstrated in **Appendix A**.

3.5 Interacting mechanical modes

When we studied the quantum state of the system shown in figure Fig. 3.3, we required that the frequencies of the mechanical modes do not overlap (see **Section 3.4**). One can overcome this limitation and consider mechanical modes frequencies that overlap with each other. But this comes with the price of requiring the existence of couplings between the mechanical modes. Figure 3.4 shows a schematic representation of the couplings between different modes of the optomechanical system.

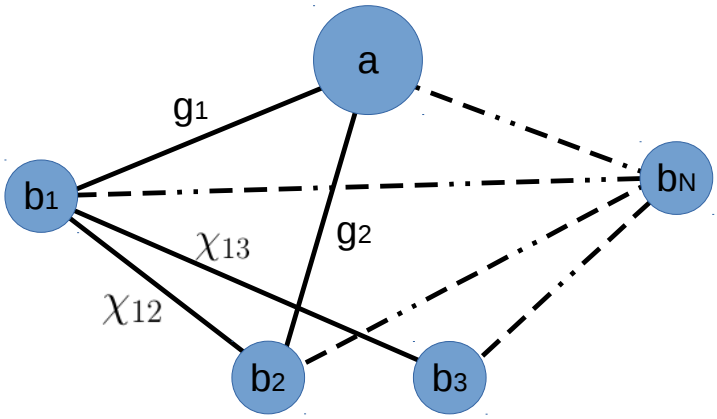

Figure 3.4: Graphical representation of the couplings between different parts of the optomechanical system. Every circle denotes a bosonic mode, and each line connecting two circles represents interaction between the two corresponding modes. The g's are the optomechanical coupling constants while the χ's are the mechanical couplings.

The Hamiltonian of such a system writes

$$H = H_c + H_m + H_{cm} \ , \tag{3.63}$$

with H_c is the cavity Hamiltonian and it is given by

$$H_c = \omega_c a^\dagger a \ , \tag{3.64}$$

and H_m is the Hamiltonian of the mechanical modes in the absence of the optomechanical interaction and it is given by:

$$H_m = \sum_{j=1}^{N} \Omega_j b_j^\dagger b_j + \sum_{\ell,\ s>\ell}^{N} \chi_{\ell s}^{qq} q_\ell q_s + \sum_{\ell,s}^{N} \chi_{\ell s}^{qp} q_\ell p_s + \sum_{\ell,\ s>\ell}^{N} \chi_{\ell s}^{pp} p_\ell p_s \ , \tag{3.65}$$

where the first summation is the free Hamiltonian of the mechanical oscillators, while the second, third and fourth summations are respectively the position–position, position–momentum and momentum–momentum interactions between different mechanical modes with coupling constants $\chi_{\ell s}^{qq}$, $\chi_{\ell s}^{qp}$ and $\chi_{\ell s}^{pp}$ respectively. H_{cm} is the optomechanical Hamiltonian that describes the coupling of the cavity mode with the mechanical ones and it equals

$$H_{cm} = \frac{-1}{\sqrt{2}} \left(\alpha a^\dagger + \alpha^* a\right) \sum_{j=1}^{N} g_j \left(b_j + b_j^\dagger\right) \ . \tag{3.66}$$

We can arrive at the form of the Hamiltonian (3.54) even if some or all the mechanical modes frequencies overlap. The idea is to consider the normal modes of the mechanical oscillators and obtain a controllable configuration in this new space of modes. By applying an appropriate transformation, the Hamiltonian (3.63) becomes

$$\tilde{H} = \omega_c a^\dagger a + \sum_{j=1}^{N} \tilde{\Omega}_j \tilde{b}_j^\dagger \tilde{b}_j - \frac{1}{\sqrt{2}} \left(\alpha a^\dagger + \alpha^* a\right) \sum_{j=1}^{N} \tilde{g}_j \left(\tilde{b}_j^\dagger + \tilde{b}_j\right) \ , \tag{3.67}$$

where $\tilde{\Omega}_j = \tilde{\Omega}_j(\Omega_1, \ldots, \Omega_N, \chi_1^{qq}, \ldots, \chi_N^{qq}, \chi_1^{qp}, \ldots, \chi_N^{qp}, \chi_1^{pp}, \ldots, \chi_N^{pp})$ are the frequencies of the normal modes of the mechanical oscillators. Also, the new optomechanical coupling constants $\tilde{g}_j$ are functions of the g's, Ω's and χ's as a result of the considered transformation.

We should mention here that only some systems with carefully chosen frequencies (Ω's) and couplings (g's and χ's) will give non overlapping normal frequencies $\tilde{\Omega}$'s with optomechanical couplings that satisfy the following conditions:

$$\alpha_j^{\pm} \tilde{g}_j \ \ll \ \tilde{\Omega}_j \ , \tag{3.68}$$

$$\tilde{g}_j \ \ll \ \omega_c \ . \tag{3.69}$$

Indeed, if one can find the normal modes, then the non overlappness of the frequencies $\tilde{\Omega}$'s and the conditions (3.68) and (3.69) can be controlled by tuning the coupling between the mechanical modes (χ^{qq}'s, χ^{qp}'s and χ^{pp}'s). As an example, we consider an optomechanical system consisting of one cavity mode coupled to one mechanical mode, and the later is coupled to a chain of mechanical oscillators as shown in Fig. 3.5. Let the frequencies of the mechanical oscillators be all equal[2] and assuming that only position–position interactions are present between the modes, then the Hamiltonian (3.63) becomes

$$H = \omega_c a^\dagger a + \Omega \sum_{j=1}^{N} b_j^\dagger b_j + \sum_{j=1}^{N-1} \frac{\chi_j}{2} \left(b_j + b_j^\dagger\right) \left(b_{j+1} + b_{j+1}^\dagger\right) - \frac{g}{\sqrt{2}} \left(\alpha a^\dagger + \alpha^* a\right) \left(b_1 + b_1^\dagger\right) \ , \tag{3.70}$$

[2]This is not mandatory, one can have a situation where only a subset of the mechanical frequencies do overlap, and this study will remain valid.

where χ_j is the position–position coupling between the j^{th} and the $(j+1)^{\text{th}}$ mechanical oscillators. This Hamiltonian can be put in normal modes form as

$$\tilde{H} = \omega_c a^\dagger a + \sum_{j=1}^{N} \Omega_j \tilde{b}_j^\dagger \tilde{b}_j - \frac{1}{\sqrt{2}} \left(\alpha a^\dagger + \alpha^* a\right) \sum_{j=1}^{N} g_j \left(\tilde{b}_1 + \tilde{b}_1^\dagger\right) \ , \tag{3.71}$$

with $\Omega_j = \Omega_j(\Omega, \chi_1, \ldots, \chi_N)$ and $g_j = g_j(\Omega, \chi_1, \ldots, \chi_N)$. These two later quantities should be controllable via changing the couplings χ's and one will obtain non overlapping frequencies as required by our scheme described in **Section 3.4**.

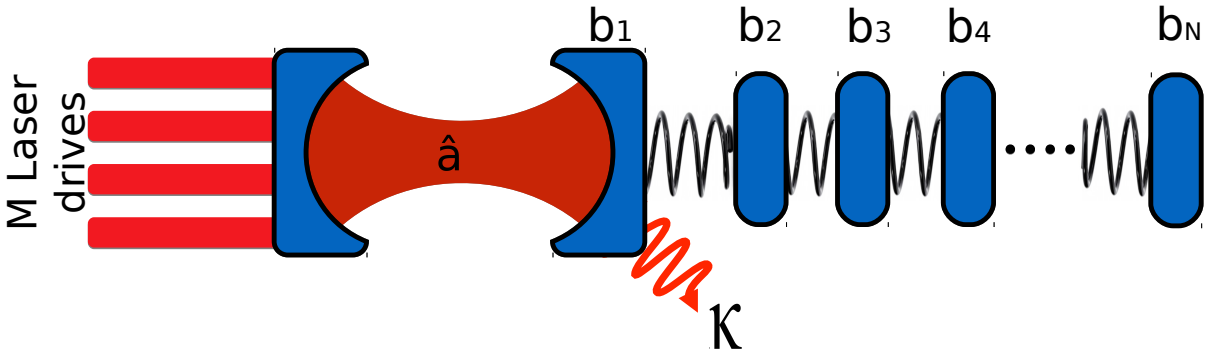

Figure 3.5: An optomechanical system consisting of one cavity mode and N mechanical oscillators. The mechanical modes have equal frequencies and are coupled with chain interaction. Only the first mechanical oscillator interacts with the cavity mode while the other modes do not.

Chapter 4

Cluster states generation by dissipation in optomechanical systems

Cluster states are the key resource in the measurement based model of quantum computation, being able to generate them will allow the building of quantum computers. In this chapter we aim to generate the cluster state in optomechanical system and namely in the mechanical degrees of freedom of the model system studied in **Chapter 3**.

This chapter introduces a scheme for generating cluster states in mechanical oscillators with the help of the optomechanical coupling and the cavity dissipation. This chapter considers the case of noiseless mechanical oscillators *i.e.,* mechanical modes that do not couple to a bath, but this later will be considered in **Chapter 5**. This chapter is organized as follows: in **Section 4.1** we study the existence of a steady state of the model system described in **Chapter 3**, and in **Section 4.2** we show how to obtain the one mode squeezed state which will be the basis for **Section 4.3** where we introduce the switching scheme that allows us to generate a given target quantum state. **Section 4.4** uses the results of preceding section and introduces the protocol for generating cluster states in the mechanical modes of the considered model optomechanical system. Then we conclude this chapter in **Section 4.5** with studying the impact of finite time dynamics on the quality of the generated cluster state.

4.1 Existence and uniqueness of Gaussian steady state

We write the master equation (3.59) for the Hamiltonian (3.54) and cavity losses (3.60) in terms of the covariance matrix[1] instead of the density matrix $\rho(t)$.

First, we write the master equation (3.59) as

$$\dot{\rho}(t) = -i[H, \rho(t)] + \left(L_c \rho(t) L_c^\dagger - \frac{1}{2}\{L_c^\dagger L_c, \rho(t)\} \right) , \tag{4.1}$$

[1]Read **Chapter 2** for definitions, notations and details regarding quadratures and covariance matrices.

with the operator L_c is defined by

$$L_c = \sqrt{\kappa}\, a \ , \tag{4.2}$$

and we write the Hamiltonian (3.54) in the form

$$H = \frac{1}{2} x^T G x \ , \tag{4.3}$$

with x is the vector of quadratures defined as

$$x = (q_1, \ldots, q_N, q_c; p_1, \ldots, p_N, p_c)^T \ , \tag{4.4}$$

and G is $2(N+1) \times 2(N+1)$ real matrix. Since H is hermitian, then G must be symmetric. In Eq. (4.4) the quadratures q_j, p_j, q_c and p_c are given by

$$q_j = \frac{1}{\sqrt{2}} \left(b_j + b_j^\dagger\right) , \tag{4.5}$$

$$p_j = \frac{1}{i\sqrt{2}} \left(b_j - b_j^\dagger\right) , \tag{4.6}$$

$$q_c = \frac{1}{\sqrt{2}} \left(a + a^\dagger\right) , \tag{4.7}$$

$$p_c = \frac{1}{i\sqrt{2}} \left(a - a^\dagger\right) . \tag{4.8}$$

From Eq. (3.54), one can show that the matrix G is equal to

$$G = \begin{pmatrix} 0_N & \mathcal{A} & 0_N & \mathcal{B} \\ \mathcal{A}^T & 0 & \mathcal{C}^T & 0 \\ 0_N & \mathcal{C} & 0_N & \mathcal{D} \\ \mathcal{B}^T & 0 & \mathcal{D}^T & 0 \end{pmatrix} , \tag{4.9}$$

where $\mathcal{A}$, $\mathcal{B}$, $\mathcal{C}$ and $\mathcal{D}$ are $N \times 1$ vectors whose elements are given by

$$\mathcal{A}_j = \frac{-g_j}{\sqrt{2}} \left(\alpha_j^+ \cos\phi_j^+ + \alpha_j^- \cos\phi_j^-\right) , \tag{4.10}$$

$$\mathcal{B}_j = \frac{g_j}{\sqrt{2}} \left(\alpha_j^+ \sin\phi_j^+ + \alpha_j^- \sin\phi_j^-\right) , \tag{4.11}$$

$$\mathcal{C}_j = \frac{-g_j}{\sqrt{2}} \left(-\alpha_j^+ \sin\phi_j^+ + \alpha_j^- \sin\phi_j^-\right) , \tag{4.12}$$

$$\mathcal{D}_j = \frac{-g_j}{\sqrt{2}} \left(-\alpha_j^+ \cos\phi_j^+ + \alpha_j^- \cos\phi_j^-\right) . \tag{4.13}$$

Writing L_c in Eq. (4.2) as

$$L_c = Cx \ , \tag{4.14}$$

it is easy to show that the $1 \times (2N+1)$ complex matrix C is equal to

$$C = \sqrt{\frac{\kappa}{2}} \left(\ 0_{1\times N} \ , \ 1 \ , \ 0_{1\times N} \ , \ i \ \right) . \tag{4.15}$$

One can show that the master equation (4.1) is equivalent to [112]

$$\frac{\mathrm{d}\langle x\rangle}{\mathrm{d}t} = A\langle x\rangle \ , \tag{4.16}$$

$$\frac{\mathrm{d}V}{\mathrm{d}t} = AV + VA^T + B \ , \tag{4.17}$$

where the matrices A and B are given by

$$A = \Omega \left[G + \Im\left(C^\dagger C\right) \right] , \tag{4.18}$$

$$B = -\Omega \, \Re\left(C^\dagger C\right) \, \Omega , \tag{4.19}$$

with the symplectic form Ω [119, 120] is equal to[2]

$$\Omega = \begin{pmatrix} O_{N+1} & \mathbb{1}_{N+1} \\ -\mathbb{1}_{N+1} & 0_{N+1} \end{pmatrix} . \tag{4.20}$$

Substituting equations (4.9) and (4.15) in equations (4.18) and (4.19), one finds matrices A and B as follows:

$$A = \begin{pmatrix} 0_N & \mathcal{C} & 0_N & \mathcal{D} \\ \mathcal{B}^T & -\frac{\kappa}{2} & \mathcal{D}^T & 0 \\ 0_N & -\mathcal{A} & 0_N & -\mathcal{B} \\ -\mathcal{A}^T & 0 & -\mathcal{C}^T & -\frac{\kappa}{2} \end{pmatrix} , \tag{4.21}$$

$$B = \frac{\kappa}{2} \, \mathrm{Diag}\left(\underbrace{0, \ldots, 0}_{N}, \; 1 \, , \underbrace{0, \ldots, 0}_{N}, \; 1 \right) . \tag{4.22}$$

The existence and uniqueness of a steady state for the system shown in Fig. 3.3 with the master equation (4.1) depends on whether the matrix A given in Eq. (4.21) is *Hirwitz* or not. There exists a unique steady state if and only if A is Hirwitz, *i.e.,* all its eigenvalues have negative real part [154]. One can show that the eigenvalues of the matrix A are

$$\underbrace{\frac{-\kappa}{4} \pm \sqrt{\left(\frac{\kappa}{4}\right)^2 - \mathcal{A}^T \cdot \mathcal{D} + \mathcal{C}^T \cdot \mathcal{B}}}_{\text{2–degenerate}} \quad , \quad \underbrace{0, \ldots, 0}_{2(N-1)} . \tag{4.23}$$

It is clear from Eq. (4.23) that the matrix A is Hirwitz if and only if:

$$N = 1 , \tag{4.24}$$

$$\Re\sqrt{\left(\frac{\kappa}{4}\right)^2 - \mathcal{A}^T \cdot \mathcal{D} + \mathcal{C}^T \cdot \mathcal{B}} < \frac{\kappa}{4} . \tag{4.25}$$

Therefore, condition (4.24) says that if the system of Fig. 3.3 contains more than one mechanical mode then it will not have a unique steady state. Condition (4.25) when $N = 1$ translates to

$$\alpha^+ < \alpha^- , \tag{4.26}$$

$$g \neq 0 . \tag{4.27}$$

While condition (4.27) is always satisfied because the optomechanical coupling is different from zero, one must satisfy condition (4.26) .

[2] See **Section 2.1** for more details about the symplectic form Ω.

4.2 One–mode squeezed state

We have proved in **Section 4.1** that the system shown in Fig. 3.3 obeying the master equation (4.1) has a unique steady state while condition (4.27) is satisfied. In this section we investigate further on the reachable steady states that can be obtained by tuning the system parameters $\alpha^{\pm}$ and $\phi^{\pm}$. In particular, we are interested in finding the conditions to obtain the one–mode squeezed state.

The covariance matrix $V(t)$ of the considered system obeys the differential equation (4.17). We put $V(t)$ in the following form:

$$V(t) = \mathrm{e}^{At} M(t) \mathrm{e}^{A^T t} \ , \tag{4.28}$$

and substituting in Eq. (4.17), we obtain:

$$\frac{\mathrm{d}M(t)}{\mathrm{d}t} = \mathrm{e}^{-At} B \mathrm{e}^{-A^T t} \Rightarrow M(t) = M(t_0) + \int_{t_0}^{t} \mathrm{e}^{-As} B \mathrm{e}^{-A^T s} \, \mathrm{d}s \ , \tag{4.29}$$

and $V(t)$ becomes:

$$V(t) = \mathrm{e}^{At} M(t_0) \mathrm{e}^{A^T t} + \int_{t_0}^{t} \mathrm{e}^{A(t-s)} B \mathrm{e}^{A^T (t-s)} \, \mathrm{d}s \ . \tag{4.30}$$

But we have the following:

$$V(t_0) = \mathrm{e}^{At_0} M(t_0) \mathrm{e}^{A^T t_0} \Rightarrow M(t_0) = \mathrm{e}^{-At_0} V(t_0) \mathrm{e}^{-A^T t_0} \ , \tag{4.31}$$

where $V(t_0)$ is the initial state of the system, then we obtain the formal solution of Eq. (4.17):

$$V(t) = \mathrm{e}^{A(t-t_0)} V(t_0) \mathrm{e}^{A^T (t-t_0)} + \int_{t_0}^{t} \mathrm{e}^{A(t-s)} B \mathrm{e}^{A^T (t-s)} \, \mathrm{d}s \ , \tag{4.32}$$

with the matrices A and B are calculated from equations (4.21) and (4.22) and are given by

$$A = \begin{pmatrix} 0 & \mathcal{C}_1 & 0 & \mathcal{D}_1 \\ \mathcal{B}_1 & -\frac{\kappa}{2} & \mathcal{D}_1 & 0 \\ 0 & -\mathcal{A}_1 & 0 & -\mathcal{B}_1 \\ -\mathcal{A}_1 & 0 & -\mathcal{C}_1 & -\frac{\kappa}{2} \end{pmatrix} \ , \tag{4.33}$$

$$B = \frac{\kappa}{2} \, \mathrm{Diag}\left(0 \ , \ 1 \ , \ 0 \ , \ 1\right) \ , \tag{4.34}$$

where $\mathcal{A}_1$, $\mathcal{B}_1$, $\mathcal{C}_1$ and $\mathcal{D}_1$ are given by

$$\mathcal{A}_1 = \frac{-g}{\sqrt{2}} \left(\alpha^+ \cos\phi^+ + \alpha^- \cos\phi^- \right) \ , \tag{4.35}$$

$$\mathcal{B}_1 = \frac{g}{\sqrt{2}} \left(\alpha^+ \sin\phi^+ + \alpha^- \sin\phi^- \right) \ , \tag{4.36}$$

$$\mathcal{C}_1 = \frac{-g}{\sqrt{2}} \left(-\alpha^+ \sin\phi^+ + \alpha^- \sin\phi^- \right) \ , \tag{4.37}$$

$$\mathcal{D}_1 = \frac{-g}{\sqrt{2}} \left(-\alpha^+ \cos\phi^+ + \alpha^- \cos\phi^- \right) \ . \tag{4.38}$$

We diagonalize the matrix A as

$$A = PDP^{-1} \ , \tag{4.39}$$

where the columns of the matrix P are the eigenvectors of A and D is the diagonal matrix containing the eigenvalues of A. The covariance matrix (4.32) becomes:

$$V(t) = P\mathrm{e}^{D(t-t_0)}P^{-1}V(t_0){P^{-1}}^T\mathrm{e}^{D(t-t_0)}P^T + \int_{t_0}^{t} P\mathrm{e}^{D(t-s)}P^{-1}B{P^{-1}}^T\mathrm{e}^{D(t-s)}P^T \ \mathrm{d}s \ . \tag{4.40}$$

The steady state (V_s) is given by the limit

$$V_s = \lim_{t\to\infty} \ V(t) \ , \tag{4.41}$$

and since the real part of the eigenvalues of the matrix A (and hence the elements of the matrix D) are strictly negative (because A is Hirwitz, see **Section 4.1**), then the steady state V_s becomes

$$V_s = \int_0^{\infty} P\mathrm{e}^{Dt}P^{-1}B{P^{-1}}^T\mathrm{e}^{Dt}P^T \ \mathrm{d}t \ . \tag{4.42}$$

Remark that Eq. (4.42) can also be put in terms of the matrix A in the following form

$$V_s = \int_0^{\infty} \mathrm{e}^{At}B\mathrm{e}^{A^Tt} \ \mathrm{d}t \ . \tag{4.43}$$

After lengthy but simple algebra, one finds the steady state to be equal to

$$V_s = \frac{1}{2}\begin{pmatrix} \frac{{\alpha^-}^2+{\alpha^+}^2-2\alpha^-\alpha^+\cos(\phi^- -\phi^+)}{{\alpha^-}^2-{\alpha^+}^2} & 0 & \frac{-2\alpha^-\alpha^+\sin(\phi^- -\phi^+)}{{\alpha^-}^2-{\alpha^+}^2} & 0 \\ 0 & 1 & 0 & 0 \\ \frac{-2\alpha^-\alpha^+\sin(\phi^- -\phi^+)}{{\alpha^-}^2-{\alpha^+}^2} & 0 & \frac{{\alpha^-}^2+{\alpha^+}^2+2\alpha^-\alpha^+\cos(\phi^- -\phi^+)}{{\alpha^-}^2-{\alpha^+}^2} & 0 \\ 0 & 0 & 0 & 1 \end{pmatrix} \ . \tag{4.44}$$

The covariance matrix (4.44) represents the steady state of the system of one cavity mode coupled to one mechanical mode. One can extract from it the following informations:

1. The cavity and the mechanical modes are uncorrelated,

2. the cavity mode is in the vacuum state:

$$V_s^{\text{cavity}} = \frac{1}{2}\ \mathbb{1}_2 \ , \tag{4.45}$$

3. and the mechanical mode is in a state given by the covariance matrix

$$V_s^{\text{mech}} = \frac{1}{2}\begin{pmatrix} \frac{{\alpha^-}^2+{\alpha^+}^2-2\alpha^-\alpha^+\cos(\phi^- -\phi^+)}{{\alpha^-}^2-{\alpha^+}^2} & \frac{-2\alpha^-\alpha^+\sin(\phi^- -\phi^+)}{{\alpha^-}^2-{\alpha^+}^2} \\ \frac{-2\alpha^-\alpha^+\sin(\phi^- -\phi^+)}{{\alpha^-}^2-{\alpha^+}^2} & \frac{{\alpha^-}^2+{\alpha^+}^2+2\alpha^-\alpha^+\cos(\phi^- -\phi^+)}{{\alpha^-}^2-{\alpha^+}^2} \end{pmatrix} \ . \tag{4.46}$$

In particular, the one–mode squeezed state of the mechanical mode can be obtained (as the steady state) if we put:

$$\alpha^+ = r\alpha^- , \tag{4.47}$$
$$\phi^+ = \phi^- = 0 . \tag{4.48}$$

Since condition (4.26) must be satisfied, and because $\alpha^\pm \geq 0$, then we have

$$0 \leq r < 1 , \tag{4.49}$$

and the covariance matrix becomes:

$$V_s^{\text{mech}} = \frac{1}{2} \begin{pmatrix} \frac{1-r}{1+r} & 0 \\ 0 & \frac{1+r}{1-r} \end{pmatrix} , \tag{4.50}$$

which can be put into the form

$$V_s^{\text{mech}} = \frac{1}{2} \begin{pmatrix} \mathrm{e}^{-2\xi} & 0 \\ 0 & \mathrm{e}^{2\xi} \end{pmatrix} , \tag{4.51}$$

with the parameter ξ is given by

$$\xi = \frac{1}{2} \log \frac{1+r}{1-r} = \tanh^{-1} r . \tag{4.52}$$

The mechanical mode state has squeezing equal to (see **Section 2.4.6**)

$$10 \log_{10} \frac{1+r}{1-r} \text{ dB} . \tag{4.53}$$

4.3 Switching protocol to generate steady states

We consider the optomechanical system shown in Fig. 3.3. The dynamics of this system is governed by the master equation (3.59) with the effective Hamiltonian (3.54) and cavity dissipation (3.60). We have shown in **Section 4.1** that the master equation (3.59) has a unique steady state if and only if the cavity mode is coupled to one mechanical mode. Therefore, the system of Fig. 3.3 with $N > 1$ has no unique steady state. To overcome this issue, one should couple the cavity mode to one effective mechanical mode at any instant of time. In particular, one can reach the target steady state in N steps where in each step the cavity mode is coupled to one collective mechanical mode, then the system is let to reach an intermediate steady state, and the target steady state is obtained as the steady state of the system at the N^{th} step. This scheme was first proposed by Li *et al.* [111] and was generalized by Y. Ikeda and N Yamamoto [113]. Although they studied the generation of cluster states in atomic ensembles, this scheme can be easily applied to the optomechanical system shown in Fig. 3.3 with the effective Hamiltonian (3.54).

Consider the transformation U defined by

$$e = Ub , \tag{4.54}$$

where b and e are vectors of operators defined as

$$b = (b_1, \ldots, , b_N)^T \quad , \quad e = (e_1, \ldots, e_N)^T , \tag{4.55}$$

and U is $N \times N$ complex matrix.

Equation (4.54) can be written as

$$e_\ell = \sum_{j=1}^{N} U_{\ell j} b_j \ . \tag{4.56}$$

We impose the following commutation relation on the operators e's

$$[e_i^\dagger, e_j] = \delta_{ij} \ , \tag{4.57}$$

and since $[b_i^\dagger, b_j] = \delta_{ij}$, therefore the matrix U must be unitary, *i.e.*, $UU^\dagger = \mathbb{1}_N$.

Let x and x' be quadrature vectors defined by $x = (q_1, \ldots, q_N;\ p_1, \ldots, p_N)^T$ and $x' = (q'_1, \ldots, q'_N;\ p'_1, \ldots, p'_N)^T$ with

$$q_j = \frac{1}{\sqrt{2}}(b_j + b_j^\dagger) \quad , \quad p_j = \frac{1}{i\sqrt{2}}(b_j - b_j^\dagger) \ , \tag{4.58}$$

$$q'_j = \frac{1}{\sqrt{2}}(b'_j + b'^\dagger_j) \quad , \quad p'_j = \frac{1}{i\sqrt{2}}(b'_j - b'^\dagger_j) \ , \tag{4.59}$$

then, using Eq. (4.56), one can arrive to

$$x' = Sx \ , \tag{4.60}$$

with the matrix S is given as the following bloc matrix

$$S = \begin{pmatrix} \Re U & -\Im U \\ \Im U & \Re U \end{pmatrix} \ . \tag{4.61}$$

Equation (4.60) is a symplectic transformation of the system's mechanical modes quadratures, and the covariance matrix transforms as (see **Chapter 2**)

$$V' = SVS^T \ , \tag{4.62}$$

where V and V' are respectively the covariance matrix of the mechanical modes subsystem in the space of the b's and e's operators.

Since U is unitary and using Eq. (4.61) one can show that

$$S^T S = SS^T = \mathbb{1}_N \ , \tag{4.63}$$

then, from Eq. (4.62), one arrives to

$$V = S^T V' S \ . \tag{4.64}$$

Now, we return to the Hamiltonian (3.54), and we impose

$$\phi_j^+ = -\phi_j^- \ , \tag{4.65}$$

$$\alpha_j^+ = r\alpha_j^- \ , \tag{4.66}$$

with r being a real parameter satisfying

$$0 \leq r < 1 \ . \tag{4.67}$$

Condition (4.67) ensures the existence and uniqueness of a steady state solution of the master equation (3.59) (see **Section 4.2** for the proof).

By substituting Eq. (4.65) and Eq. (4.66) in Eq. (3.54), one finds

$$H = -\sum_{j=1}^{N} \frac{g_j}{\sqrt{2}}\alpha_j^- \; a^\dagger \left\{ \mathrm{e}^{-i\phi_j^-} \; b_j + r \left(\mathrm{e}^{-i\phi_j^-} \; b_j \right)^\dagger \right\} + \; H.C. \tag{4.68}$$

We put:

$$\frac{1}{\sqrt{2}} \, g_j \alpha_j^- \mathrm{e}^{-i\phi_j^-} = \beta_\ell U_{\ell j} \; , \tag{4.69}$$

where β_ℓ is a positive real parameter. By using Eq. (4.56), one arrives to the Hamiltonian

$$H_\ell = -\beta_\ell a^\dagger (e_\ell + r e_\ell^\dagger) + \; H.C. \tag{4.70}$$

The dynamics of the system in terms of the collective modes $\{e_\ell\}_{\ell=1}^N$ obeys the following master equation:

$$\dot{\rho}_\ell(t) = -i[H_\ell, \rho_\ell(t)] + \mathcal{L}_c[a]\rho_\ell(t) \; , \tag{4.71}$$

where $\rho_\ell(t)$ is the state of the subsystem (cavity–ℓ^{th} mechanical collective mode), and the term $\mathcal{L}_c[a]\rho_\ell(t)$ describes the cavity losses and it is given by [155]:

$$\mathcal{L}_c[a]\rho_\ell(t) = \sqrt{\kappa} \; D[a]\rho_\ell(t) \; , \tag{4.72}$$

with the super operator $D[a]$ is defined in Eq. (3.61).

The master equation (4.71) has the unique steady state denoted by $|0, r\rangle$, where the cavity (mechanical) mode is in the vacuum (squeezed) state. The corresponding covariance matrix is (see **Section 4.2** for detailed derivation)

$$V_\ell = \frac{1}{2} \begin{pmatrix} 1 & 0 & 0 & 0 \\ 0 & \mathrm{e}^{-2\xi} & 0 & 0 \\ 0 & 0 & 1 & 0 \\ 0 & 0 & 0 & \mathrm{e}^{2\xi} \end{pmatrix} \; , \tag{4.73}$$

where ξ, the squeezing parameter, is given by the formula

$$\xi = \tanh^{-1} r \; . \tag{4.74}$$

Since the collective mechanical modes e's are independent (see Eq. (4.57)), one can squeeze each collective mode e_ℓ independently by setting the Hamiltonian to H_ℓ and wait sufficient time to reach the steady state. By repeating this procedure for all the collective mechannical modes, they become all squeezed. The covarinace matrix of the optomechanical system is then written as

$$V' = \frac{1}{2} \begin{pmatrix} \mathrm{e}^{-2\xi} \mathbb{1}_N & 0_N \\ 0_N & \mathrm{e}^{2\xi} \mathbb{1}_N \end{pmatrix} \; . \tag{4.75}$$

In the space of modes $\{b_j\}_{j=1}^N$ the covariance matrix is given by Eq. (4.64), which is written explicitly as

$$V = \begin{pmatrix} -\sinh(2\xi) \; (\Re U)^T \Re U + \frac{1}{2}\mathrm{e}^{2\xi} & \sinh(2\xi) \; (\Re U)^T \Im U \\ \\ \sinh(2\xi) \; (\Re U)^T \Im U & \sinh(2\xi) \; (\Re U)^T \Re U + \frac{1}{2}\mathrm{e}^{-2\xi} \end{pmatrix} \; . \tag{4.76}$$

It is clear that the system's steady state depends on the choice of the unitary matrix U. One can find system parameters, namely driving lasers phases and amplitudes that drives the system to a target steady state. An example demonstrating the generation of the two modes squeezed state in the mechanical modes of the optomechanical system is given in **Appendix A**, and a protocol to generate the approximate cluster state is given in **Section 4.4**.

4.4 Cluster states in the mechanical modes

In this section, we give the scheme to generate cluster states in the mechanical modes of the optomechanical system shown in Fig. 3.3 where its dynamics is described by the Hamiltonian (4.68) and obeys the master equation (3.59). As said in **Section 4.3**, we will use Hamiltonian switching scheme where the switching program is given by the unitary transformation U (see Eq. (4.54)). For the generation of cluster states, the switching program U can be determined in a systematic way using the method developped by Ikeda and Yamamoto[3] [113] and will be presented in **Section 4.4.1**.

4.4.1 Switching program

Canonical cluster states (see **Section 2.5**) satisfy the condition

$$\lim_{\xi\to\infty} \operatorname{cov}(p - Aq) = 0 \ , \tag{4.77}$$

where ξ is the squeezing parameter, q and p are the quadratures, A is the adjacency matrix [134, 158] of the cluster state, and $\operatorname{cov}(x)$ denotes the covariance matrix and it is defined as

$$\operatorname{cov}(x) = \frac{1}{2}\langle\left\{\Delta x, (\Delta x)^T\right\}\rangle \ . \tag{4.78}$$

In practice, we can not have quantum states with infinite squeezing, and in this case we talk about *approximate cluster state*: for big enough squeezing, approximate cluster states can be regarded as (ideal or canonical) cluster states. In the following, when we mention *cluster state* we mean *approximate cluster state* (**Section 2.5**).

Let A be the adjacency matrix of the graph of the cluster state that one wants to generate, and consider a system in the state described by the covariance matrix (4.76), then $\operatorname{cov}(p - Aq)$ is written as [113]

$$\begin{aligned}
\operatorname{cov}(p - Aq) &= (-A, \mathbb{1}_N)\ V \begin{pmatrix} -A \\ \mathbb{1}_N \end{pmatrix} \\
&= \frac{1}{2}\,\mathrm{e}^{2\xi}\left(-A(\Re U)^T\Re U A - (\Re U)^T\Im U A - A(\Re U)^T\Im U + (\Re U)^T\Re U + A^2\right) \\
&\quad + \frac{1}{2}\,\mathrm{e}^{-2\xi}\left(A(\Re U)^T\Re U A + (\Re U)^T\Im U A + A(\Re U)^T\Im U - (\Re U)^T\Re U + \mathbb{1}_N\right) \ .
\end{aligned}$$

We define the matrices F_1 and F_2 as the following:

$$F_1 = \Re U A + \Im U \qquad , \qquad F_2 = \Im U A - \Re U \ , \tag{4.79}$$

[3] Ikeda and Yamamoto generalized previous works of P. Loock *et al.* [156], X. Li *et al.* [111] and A. Furusawa *et al.* [157]

then, $\mathrm{cov}\,(p - Aq)$ becomes:

$$\mathrm{cov}\,(p - Aq) = \frac{1}{2}\,\mathrm{e}^{-2\xi}\,F_1^T F_1 + \frac{1}{2}\,\mathrm{e}^{2\xi}\,F_2^T F_2\ . \tag{4.80}$$

In order Eq. (4.80) to be consistent with Eq. (4.77), we must have

$$F_2^T F_2 = 0 \Rightarrow \Re U = \Im U A\ , \tag{4.81}$$

and therefore, the unitary transformation U becomes

$$U = \Im U(A + i\mathbb{1}_N)\ , \tag{4.82}$$

or equivalently

$$A + i\mathbb{1}_N = (\Im U)^{-1}\ U\ . \tag{4.83}$$

Now, we want to find $(\Im U)^{-1}$ in terms of the adjacency matrix A. We calculate $(A + i\mathbb{1}_N)\,(A + i\mathbb{1}_N)^\dagger$

$$(A + i\mathbb{1}_N)\,(A + i\mathbb{1}_N)^\dagger = A^2 + \mathbb{1}_N = (\Im U)^{-1}\,(\Im U)^{-1^T}\ . \tag{4.84}$$

If we assume that $\Im U$ is symmetric, then we obtain

$$(\Im U)^{-1} = \sqrt{A^2 + \mathbb{1}_N}\ , \tag{4.85}$$

and the unitary matrix U is written

$$U = (A^2 + \mathbb{1}_N)^{-1/2}(A + i\mathbb{1}_N)\ . \tag{4.86}$$

Therefore, one can find the switching program (unitary U) for a given cluster state described by its adjacency matrix A by using Eq. (4.86) .

Before concluding this section, we should mention that if we relabel the modes of the cluster state while keeping the same geometry of the graph, this will change the adjacency matrix A of the corresponding graph which also change the switching program U given by Eq. (4.86). In **Appendix B** we give explicit formula for expression of the matrix U when relabelling the modes. We show in **Appendix B** that the switching programs for different relabelling of the modes of the target cluster state are equivalent (they are related by a transformation that corresponds to modes permutations).

In the following, we give explicit examples of generating different cluster states in optomechanical systems using the switching scheme presented so far.

4.4.2 Linear cluster states

A linear cluster state consisting of N modes is represented in Fig. 4.1. Its adjacency matrix A is given by

$$A = \begin{pmatrix} 0 & 1 & 0 & \cdots & 0 \\ 1 & \ddots & \ddots & \ddots & \vdots \\ 0 & \ddots & \ddots & \ddots & 0 \\ \vdots & \ddots & \ddots & \ddots & 1 \\ 0 & \cdots & 0 & 1 & 0 \end{pmatrix}\ . \tag{4.87}$$

Figure 4.1: A graph representation of N modes linear cluster state.

In particular, we consider two modes and four modes linear cluster states: The adjacency matrix of the two modes cluster state is

$$A_2 = \begin{pmatrix} 0 & 1 \\ 1 & 0 \end{pmatrix} , \tag{4.88}$$

and from Eq. (4.86) one obtains

$$U = \frac{1}{\sqrt{2}} \begin{pmatrix} i & 1 \\ 1 & i \end{pmatrix} . \tag{4.89}$$

Without loss of generality, we assume that, for $j = 1, \ldots, N$, we have :

$$\beta_j = \beta , \tag{4.90}$$

$$g_j = g , \tag{4.91}$$

then the system parameters that generate the two modes cluster state are obtained using Eq. (4.69) with U being replaced by Eq. (4.89) and they are given in Table. 4.1.

Step	α_1^-	α_2^-	ϕ_1^-	ϕ_2^-
1	$1/\sqrt{2}$	$1/\sqrt{2}$	$-\pi/2$	0
2	$1/\sqrt{2}$	$1/\sqrt{2}$	0	$-\pi/2$

Table 4.1: System parameters for generating the two modes cluster state. The α^-'s are given in units of $\sqrt{2}\beta/g$. The ϕ^+'s and α^+'s parameters are obtained from Eq. (4.65) and Eq. (4.66) respectively.

The adjacency matrix of the four modes linear cluster state (Fig. 4.2-a) is

$$A_4^{\text{linear}} = \begin{pmatrix} 0 & 1 & 0 & 0 \\ 1 & 0 & 1 & 0 \\ 0 & 1 & 0 & 1 \\ 0 & 0 & 1 & 0 \end{pmatrix} , \tag{4.92}$$

the switching program is

$$U = \frac{1}{5} \begin{pmatrix} i\sqrt{2(5+\sqrt{5})} & \sqrt{5+2\sqrt{5}} & -i\sqrt{5-2\sqrt{5}} & -\sqrt{5-2\sqrt{5}} \\ \sqrt{5+2\sqrt{5}} & i\sqrt{5+2\sqrt{5}} & \sqrt{10-2\sqrt{5}} & -i\sqrt{5-2\sqrt{5}} \\ -i\sqrt{5-2\sqrt{5}} & \sqrt{10-2\sqrt{5}} & i\sqrt{5+2\sqrt{5}} & \sqrt{5+2\sqrt{5}} \\ -\sqrt{5-2\sqrt{5}} & -i\sqrt{5-2\sqrt{5}} & \sqrt{5+2\sqrt{5}} & i\sqrt{2(5+\sqrt{5})} \end{pmatrix} , \tag{4.93}$$

and the system parameters that generate the four modes linear cluster state are given in Table. 4.2.

Step	α_1^-	α_2^-	α_3^-	α_4^-	ϕ_1^-	ϕ_2^-	ϕ_3^-	ϕ_4^-
1	$\frac{\sqrt{2(5+\sqrt{5})}}{5}$	$\frac{\sqrt{5+2\sqrt{5}}}{5}$	$\frac{\sqrt{5-2\sqrt{5}}}{5}$	$\frac{\sqrt{5-2\sqrt{5}}}{5}$	$-\pi/2$	0	$\pi/2$	π
2	$\frac{\sqrt{5+2\sqrt{5}}}{5}$	$\frac{\sqrt{5+2\sqrt{5}}}{5}$	$\frac{\sqrt{2(5-\sqrt{5})}}{5}$	$\frac{\sqrt{5-2\sqrt{5}}}{5}$	0	$-\pi/2$	0	$\pi/2$
3	$\frac{\sqrt{5-2\sqrt{5}}}{5}$	$\frac{\sqrt{2(5-\sqrt{5})}}{5}$	$\frac{\sqrt{5+2\sqrt{5}}}{5}$	$\frac{\sqrt{5+2\sqrt{5}}}{5}$	$\pi/2$	0	$-\pi/2$	0
4	$\frac{\sqrt{5-2\sqrt{5}}}{5}$	$\frac{\sqrt{5-2\sqrt{5}}}{5}$	$\frac{\sqrt{5+2\sqrt{5}}}{5}$	$\frac{\sqrt{2(5+\sqrt{5})}}{5}$	π	$\pi/2$	0	$-\pi/2$

Table 4.2: System parameters for generating the four modes linear cluster state. The α^-'s are given in units of $\sqrt{2}\beta/g$. The ϕ^+'s and α^+'s parameters are obtained from Eq. (4.65) and Eq. (4.66) respectively.

4.4.3 Four modes square cluster state

The graph representation of the four modes square cluster state is given in Fig. 4.2-b. Its adjacency matrix is

$$A_4^{\text{square}} = \begin{pmatrix} 0 & 1 & 0 & 1 \\ 1 & 0 & 1 & 0 \\ 0 & 1 & 0 & 1 \\ 1 & 0 & 1 & 0 \end{pmatrix}, \tag{4.94}$$

the switching program is

$$U = \frac{1}{10}\begin{pmatrix} i(5+\sqrt{5}) & 2\sqrt{5} & i(-5+\sqrt{5}) & 2\sqrt{5} \\ 2\sqrt{5} & i(5+\sqrt{5}) & 2\sqrt{5} & i(-5+\sqrt{5}) \\ i(-5+\sqrt{5}) & 2\sqrt{5} & i(5+\sqrt{5}) & 2\sqrt{5} \\ 2\sqrt{5} & i(-5+\sqrt{5}) & 2\sqrt{5} & i(5+\sqrt{5}) \end{pmatrix}, \tag{4.95}$$

and the system parameters that generate the four modes square cluster state are given in Table. 4.3.

Step	α_1^-	α_2^-	α_3^-	α_4^-	ϕ_1^-	ϕ_2^-	ϕ_3^-	ϕ_4^-
1	$(5+\sqrt{5})/10$	$1/\sqrt{5}$	$(5-\sqrt{5})/10$	$1/\sqrt{5}$	$-\pi/2$	0	$\pi/2$	0
2	$1/\sqrt{5}$	$(5+\sqrt{5})/10$	$1/\sqrt{5}$	$(5-\sqrt{5})/10$	0	$-\pi/2$	0	$\pi/2$
3	$(5-\sqrt{5})/10$	$1/\sqrt{5}$	$(5+\sqrt{5})/10$	$1/\sqrt{5}$	$\pi/2$	0	$-\pi/2$	0
4	$1/\sqrt{5}$	$(5-\sqrt{5})/10$	$1/\sqrt{5}$	$(5+\sqrt{5})/10$	0	$\pi/2$	0	$-\pi/2$

Table 4.3: System parameters for generating the four modes square cluster state. The α^-'s are given in units of $\sqrt{2}\beta/g$. The ϕ^+'s and α^+'s parameters are obtained from Eq. (4.65) and Eq. (4.66) respectively.

4.5 Finite time dynamics

The described protocol for generating the cluster state given in **Section 4.3** and **Section 4.4** requires one to wait infinite time to reach the steady state. But in practice we spend finite time in each step of the switching scheme. This results in deviations of the system's steady state from the (ideal) target state. We quantify this deviation by the fidelity, namely the Uhlmann fidelity [142, 143] introduced in **Section 2.6**.

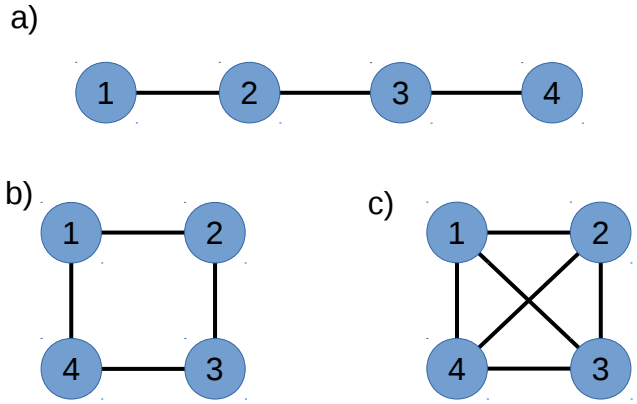

Figure 4.2: A graph representation of 4 modes cluster states of different geometries. a) Linear cluster state. b) Square cluster state. c) Full–interaction cluster state.

4.5.1 Speed of approaching the steady state

At the ℓ^{th} step of the switching scheme described in **Section 4.3**, the system's dynamics is described by the master equation (4.71) with Hamiltonian (4.70) and dissipator (4.72). The covariance matrix $V_\ell(t)$ of this system at the ℓ^{th} step is given by

$$V_\ell(t) = \mathrm{e}^{A^{(\ell)}t} V_\ell(0) \mathrm{e}^{A^{(\ell)^T}t} + \int_0^t \mathrm{e}^{A^{(\ell)}s} B \mathrm{e}^{A^{(\ell)^T}s}\, \mathrm{d}s \ , \tag{4.96}$$

with $t \geq 0$, B is given by Eq. (4.34) and $A^{(\ell)}$ is given by:

$$A^{(\ell)} = \begin{pmatrix} 0 & 0 & 0 & -\beta_\ell(1-r) \\ 0 & -\frac{\kappa}{2} & -\beta_\ell(1-r) & 0 \\ 0 & \beta_\ell(1+r) & 0 & 0 \\ \beta_\ell(1+r) & 0 & 0 & -\frac{\kappa}{2} \end{pmatrix} . \tag{4.97}$$

Equation (4.96) was obtained by following the same steps to arrive to Eq. (4.32) then we made appropriate time transformations so that time t starts from zero at the beginning of each switching step. We should mention that $V_\ell(0)$ is the initial state of the system at the ℓ^{th} step and it equals the final state of the system in the preceding switching step, except for the first switching step where it is the system's state before starting the switching protocol.

Hence the matrix $A^{(\ell)}$ has eigenvalues:

$$\lambda_\ell^{\pm} = -\frac{\kappa}{4} \pm \sqrt{\left(\frac{\kappa}{4}\right)^2 - \beta_\ell^2(1-r^2)} \ , \tag{4.98}$$

and since $0 \leq r < 1$ (Eq. (4.67)) then it is always true that

$$\left(\frac{\kappa}{4}\right)^2 > \left(\frac{\kappa}{4}\right)^2 - \beta_\ell^2(1-r^2) \ , \tag{4.99}$$

which leads to

$$\frac{\kappa}{4} > \Re\sqrt{\left(\frac{\kappa}{4}\right)^2 - \beta_\ell^2(1-r^2)} \ , \tag{4.100}$$

and hence the eigenvalues $\lambda_\ell^\pm$ satisfy

$$\Re\lambda_\ell^\pm < 0 \ . \tag{4.101}$$

Eq. (4.101) tells us that the matrix $A^{(\ell)}$ (Eq. (4.97)) is Hirwitz *i.e.,* the system's dynamics has always a unique steady state. The system approaches its steady state with speed that depends only on the negativity of the the real part of the eigenvalues (4.98): The more negative $\Re\lambda_\ell^\pm$, the faster to reach the steady state. This later statement is clear from Eq. (4.96) because the matrices $A^{(\ell)}$ and $A^{(\ell)^T}$ appear in exponentials and since the eigenvalues of $A^{(\ell)}$ have negative real part then the exponentials will decay when the time increases.

Since we always have

$$|\Re\lambda_\ell^-| \geq |\Re\lambda_\ell^+| \ , \tag{4.102}$$

then the system reaches its steady state in time of the order of few multiples of $\tau^{(\ell)}$:

$$\tau^{(\ell)} = \frac{1}{|\Re\lambda_\ell^+|} \ . \tag{4.103}$$

From Eq. (4.98) we also have

$$|\Re\lambda_\ell^+| \leq \frac{\kappa}{4} \Rightarrow |\Re\lambda_\ell^+|_{\max} = \frac{\kappa}{4} \ , \tag{4.104}$$

therefore the minimum value for $\tau^{(\ell)}$ is

$$\tau_{\min} = \frac{4}{\kappa} \ , \tag{4.105}$$

which represents the limit of speed one can reach in order to approach the steady state of the system. Using Eq. (4.98) once more this limit translates to

$$\left(\frac{\kappa}{4}\right)^2 - \beta_\ell^2(1-r^2) \leq 0 \Rightarrow \beta_\ell \geq \frac{\kappa}{4\sqrt{1-r^2}} \ . \tag{4.106}$$

As said in **Section 2.5**, our cluster state approaches the ideal (canonical) one for large squeezing strength *i.e.,* when $\xi \to \infty$ or equivalently when $r \to 1$ (we used Eq. (4.74)), but in this situation Eq. (4.106) tells us that κ must be very small *i.e.,*

$$\kappa \to \ 0 \ , \tag{4.107}$$

in order to render β_ℓ a finite quantity satisfying condition

$$\beta_\ell \ll \Omega_\ell \tag{4.108}$$

obtained from Eq. (3.50) and Eq. (4.69).
But when $\kappa \to 0$ the time to reach the steady state given in Eq. (4.105) will be infinite, therefore if we want to prepare a cluster state that has large squeezing we have to consider very good cavity ($\kappa \to 0$) and we must wait a very long time to generate it.

4.5.2 Four–modes linear cluster state

Without loss of generality, we study the case of four modes cluster states with the mechanical oscillators having the frequencies

$$\Omega_j = 2\pi j \text{ MHz} . \tag{4.109}$$

The choice of the frequencies in Eq. (4.109) is for demonstration only. In fact, one can choose any other values as long as the RWA used in the derivation of the Hamiltonian (3.54) must be valid. Indeed, choosing non-overlapping mechanical frequencies (as in Eq. (4.109)) and the weak coupling assumptions (Eq. (3.20) and Eq. (3.50)) should be enough for the RWA to be valid, *i.e.,* Hamiltonian (3.54) is a good approximation of the dynamics of the optomechanical system shown in Fig. 3.3.

First, we study the evolution of the fidelity[4]. In Fig. 4.3 we plot the fidelity versus time for the four-modes linear cluster state for different squeezing strengths: 5 dB, 12.7 dB[5] and 20.5 dB[6]. We see that the fidelity increases monotonically in each step, and step by step, up to the value of 1 where the target cluster state is reached. Also notice that regardless of the squeezing strength, the target cluster state is obtained after the same time (around 80 κ^{-1} when we spend time equal to 20 κ^{-1} in each step).

In the numerical simulations (see **Appendix C** for a brief outline of the codes used to simulate the dynamics of the system) shown in Fig. 4.3, the parameter β was set to

$$\beta = \frac{\kappa}{4\sqrt{1-r^2}} . \tag{4.110}$$

This choice is to guarantee reaching the steady state in minimal time while keeping the driving laser power at its minimum (See **Section 4.5.1**). Taking into account Eq. (3.50) one arrives to

$$\kappa \ll 4\sqrt{1-r^2} \min_{k,j=1,\ldots,N} \frac{\Omega_j}{|U_{kj}|} . \tag{4.111}$$

This means that the cavity must operate in the resolved-sideband regime [149, 150, 160–165]. Also, from Eq. (4.111) it is clear that the higher the squeezing strength the deeper the cavity should operate in the resolved-sideband regime. On the other hand, Eq. (4.111) puts an upper bound limit on how fast one can reach the target cluster steady state: In order to obtain the cluster state quickly, the cavity decay rate should be as big as possible as long as condition (4.111) is satisfied (resolved sideband regime).

We now study the fidelity of the generated state and the target cluster state when we change the duration of each step of the switching scheme. For this, we consider again the target cluster state to be the four modes linear cluster state (Fig. 4.2-a) with mechanical oscillators frequencies (4.109). We calculate the fidelity of the system's state at the end of the last switching step and that of the target cluster

[4] what we mean by the word *fidelity* here and in the subsequent sections is the Uhlmann fidelity of the system's state at time t (with $t \in [0, \infty[$) and the target (approximate) cluster state.

[5] 12.7 dB is the highest achieved squeezing of one optical mode in experiment [159].

[6] It is shown in [108] that squeezing of 20.7 dB is the threshold to perform universal fault–tolerant quantum computation in CV.

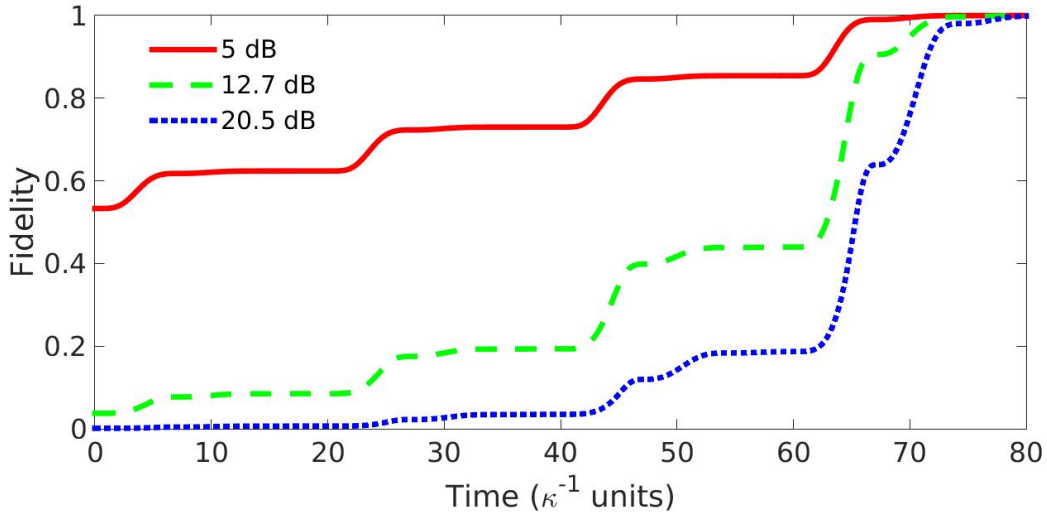

Figure 4.3: Fidelity evolution in time for the four-modes linear cluster state. Squeezing strengths of 5 dB, 12.7 dB and 20.5 dB are considered. The frequency of the j^{th} mechanical oscillator is chosen to be equal to $2\pi j$ MHz (see text). The duration of each step is $t_s = 20\ \kappa^{-1}$ where κ is the cavity's decay rate.

state. We call this fidelity *the final fidelity*. In Fig. 4.4 we plot the final fidelity as function of the total evolution time per switching step for the same squeezing strengths used in Fig. 4.3. Also we have set the total evolution time in each step to be equal in all steps. This choice should not lead to any prime difference in the results and conclusions of this analysis.

We notice that the final fidelity reaches one when enough time is allowed in each switching step. Also we see that the more the squeezing strength the longer time one has to spend in each step. In other words, when the squeezing strength of the target cluster state is big[7], then the system needs more time to reach the steady state at each step.

One would ask the question whether the geometry of the target cluster state affects the evolution of the fidelity in time. To answer this question we consider the four-modes and eight-modes cluster states represented in Fig. 4.2 and Fig. 4.5 respectively, then we plot the fidelity versus time for a squeezing strength 12.7 dB with β set to the value as in (4.110). The results of the simulations are shown in Fig. 4.6 and Fig. 4.7. We see that the geometry of the target cluster state does not affect the fidelity in time of the state of the system during the generation of that target cluster state. This observation should be the subject of further study where

[7]Remember that cluster states generated by the switching scheme approach the canonical cluster states when considering infinite squeezing (read **Section 2.5**)

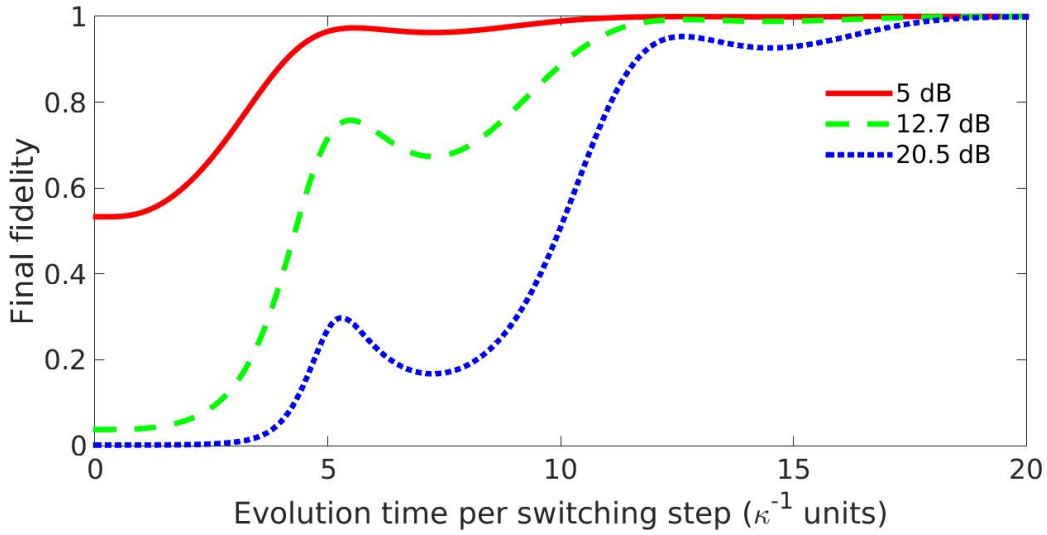

Figure 4.4: Final fidelity function of total evolution time per switching step for the four-modes linear cluster state. Squeezing strengths of 5 dB, 12.7 dB and 20.5 dB are considered. The frequency of the j^{th} mechanical oscillator is chosen to be equal to $2\pi j$ MHz (see text).

one should show analytically that the fidelity in time is independent of the geometry of the target cluster state for fixed number of modes.

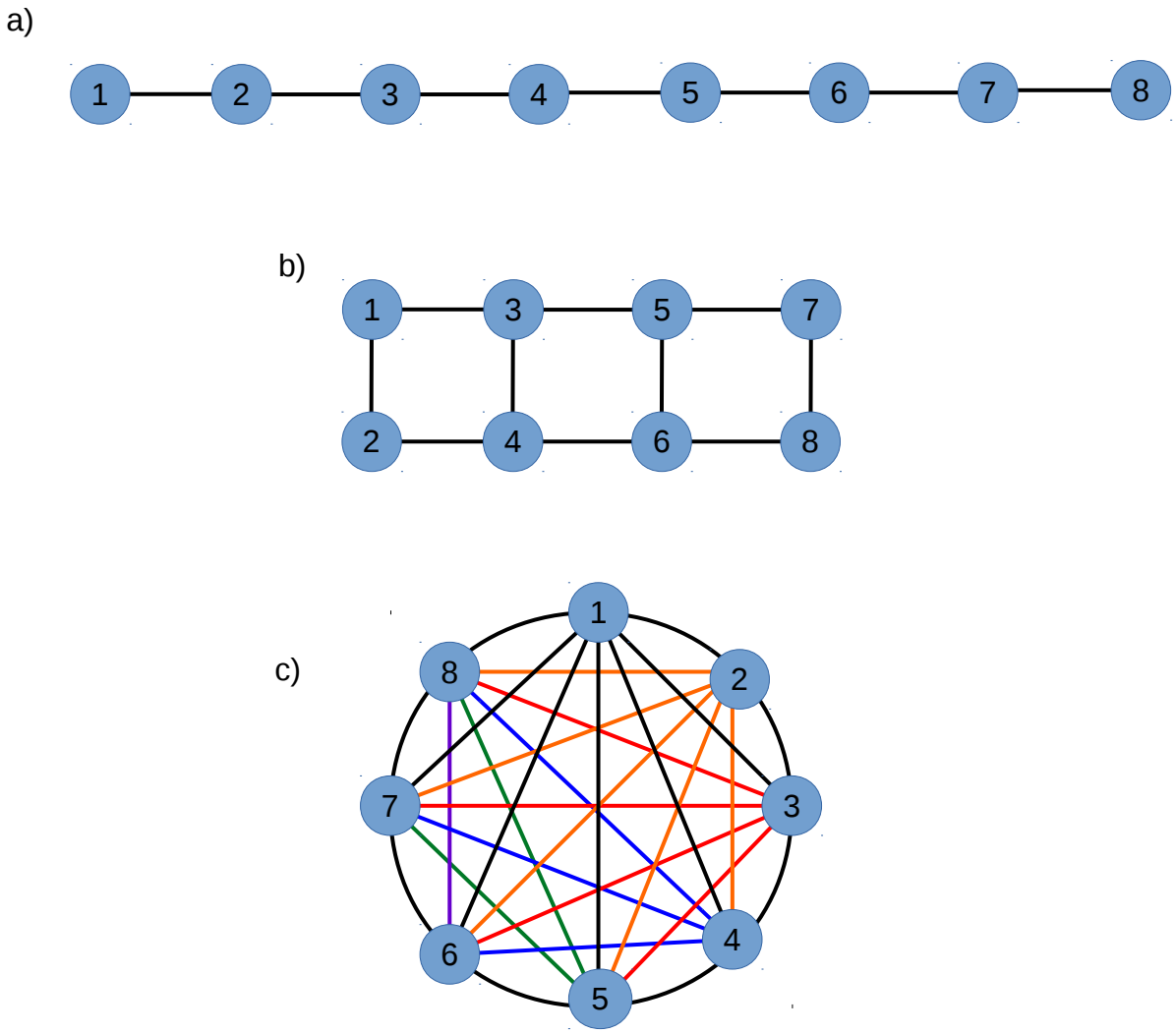

Figure 4.5: A graph representation of 8 modes cluster states of different geometries. a) Linear cluster state. b) Dual-rail cluster state. c) Full–interaction cluster state.

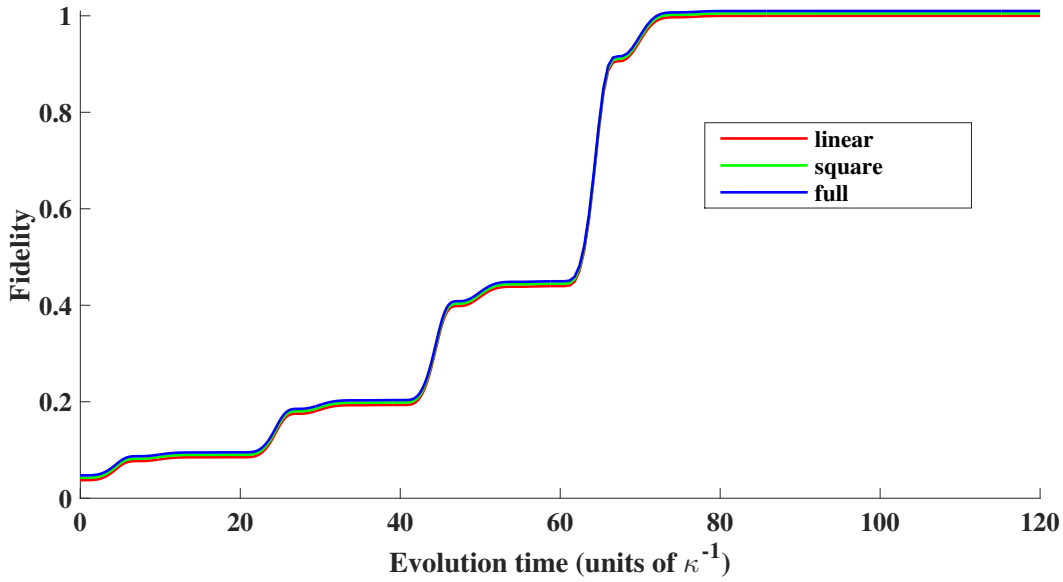

Figure 4.6: Fidelity evolution in time for different four-modes cluster state geometries. The squeezing strengths was chosen to be equal to 12.7 dB. The frequency of the j^{th} mechanical oscillator is chosen, as before, to be equal to $2\pi j$ MHz with $j = 1, \ldots, 4$ (see text). The duration of each step is $t_s = 20\ \kappa^{-1}$ where κ is the cavity's decay rate.

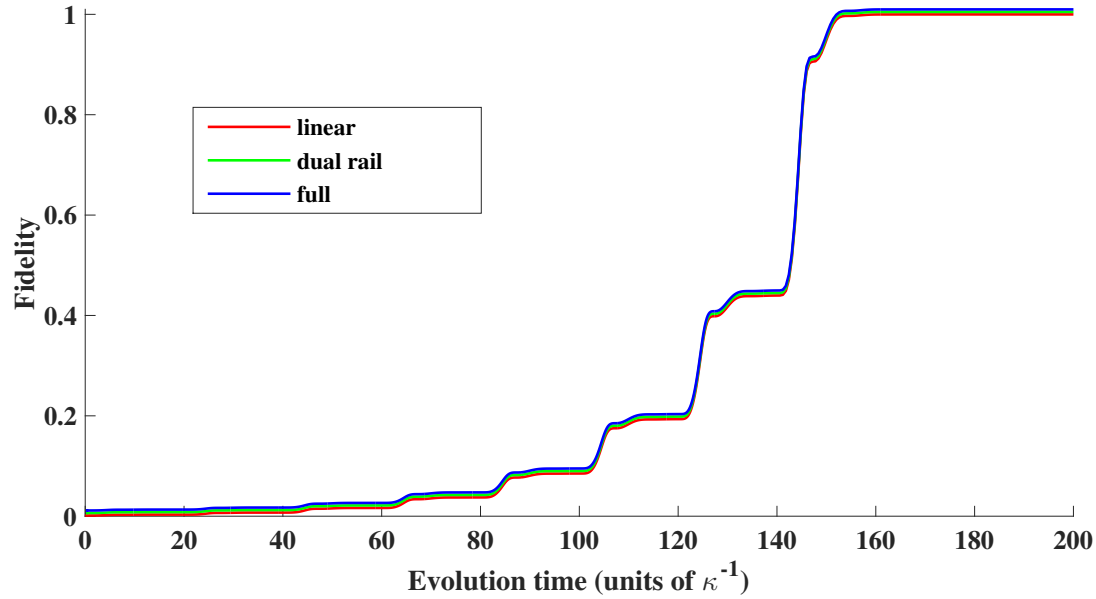

Figure 4.7: Fidelity evolution in time for different eight-modes cluster state geometries. The system parameters are as follow: squeezing strengths 12.7 dB, frequency of the j^{th} mechanical oscillator $2\pi j$ MHz with $j = 1, \ldots, 4$, and the duration of each step $t_s = 20\ \kappa^{-1}$

Chapter 5

Cluster state generation in the presence of mechanical noise

We showed in **Chapter 4** how to generate cluster states in the mechanical modes of the optomechanical system shown in Fig. 3.3. The scheme developed there to obtain the cluster state assumes the ideal situation where the mechanical modes are decoupled from their bath[1]. In this chapter we study the effects of the (unwanted) mechanical noise[2] on the generation of cluster states using the switching protocol presented in **Chapter 4**. This will be quantified in terms of the quantum fidelity between the system's state and the target cluster state.

This chapter is organized as follows: in **Section 5.1** we introduce the *quantum optical* noise and in **Section 5.2** we persue the same steps as in **Section 4.1** to prove that the optomechanical system model considered here has always a unique steady state. Then, in **Section 5.3**, we show how the quality of the generated cluster state is affected by the mechanical noise, namely the bath's temperature and the damping of mechanical oscillators.

5.1 *Quantum optical* like noise : The model

Consider an optomechanical system consisting of one (optical) cavity mode coupled to N non interacting mechanical oscillators. The coupling of the cavity mode to its reservoir is characterized by a decay rate κ, and the mechanical modes are also coupled to their (independent) baths with damping rates γ_j $(j = 1, \ldots, N)$. Fig. 5.1 shows a sketch of the considered system.

The dynamics of the system is governed by the master equation

$$\dot{\rho}(t) = -i[H, \rho(t)] + \mathcal{L}_c[\rho(t)] + \mathcal{L}_m[\rho(t)] \ , \tag{5.1}$$

where H is the system's Hamiltonian given by Eq. (4.68) and $\mathcal{L}_c[\rho(t)]$ is the Lindblad term that describes the cavity losses and it is given by Eq. (3.60) rewritten here for convenience as

$$\mathcal{L}_c[\rho(t)] = \kappa \ D[a]\rho(t) \ , \tag{5.2}$$

[1]The bath is a physical system containing infinite number of modes (called *reservoir*) and is in thermal equilibrium state [52].

[2]Mechanical noise results from the coupling of the mechanical system with its bath. For further reading about this topic, one can consult references [50–55].

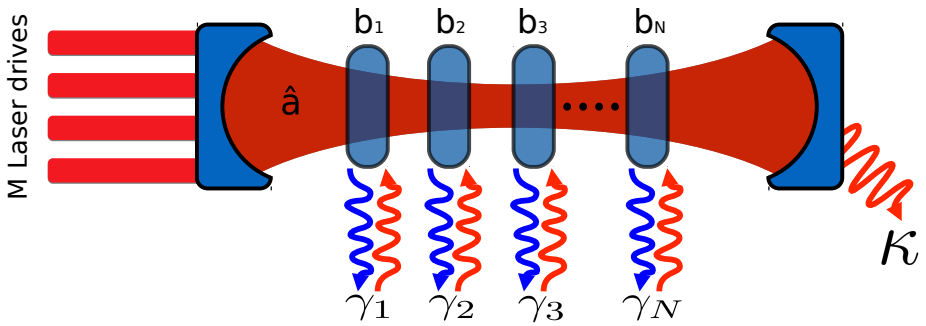

Figure 5.1: An optomechanical system of one cavity mode and N mechanical oscillators. The cavity losses are characterised by the decay rate κ, and the mechanical noise is modelled by damping rates $\gamma_1, \ldots, \gamma_N$, where each mechanical oscillator exchanges quanta (phonons) with its bath. The cavity is pumped by M laser fields.

with a is the annihilation operator for the cavity, and $D[\cdot]\rho(t)$ is the super operator defined as

$$D[v]\rho(t) = v\rho(t)v^\dagger - \frac{1}{2}\{v^\dagger, v\} \ . \tag{5.3}$$

The Lindblad terms for the mechanical oscillators are given by

$$\mathcal{L}_m[\rho(t)] = \sum_{j=0}^{N} \mathcal{L}_j^{(-)}[\rho(t)] + \mathcal{L}_j^{(+)}[\rho(t)] \ , \tag{5.4}$$

where $\mathcal{L}_j^{(-)}[\rho(t)]$ and $\mathcal{L}_j^{(+)}[\rho(t)]$ are given by

$$\mathcal{L}_j^{(-)}[\rho(t)] = \gamma_j(n_j + 1)D[b_j]\rho(t) \ , \tag{5.5}$$
$$\mathcal{L}_j^{(+)}[\rho(t)] = \gamma_j n_j D[b_j^\dagger]\rho(t) \ , \tag{5.6}$$

with γ_j and n_j are, respectively, the damping rate and mean-phonon number of the j^{th} mechanical mode.

The term $\mathcal{L}_j^{(-)}[\rho(t)]$ describes the process of quanta (phonon) leaking from the j^{th} mode into its bath (cooling), while the term $\mathcal{L}_j^{(+)}[\rho(t)]$ describes the opposite process, *i.e.,* phonons entering from the bath to the mechanical mode (heating) [52]. Notice that Lindblad operators (5.5) and (5.6) for the mechanical modes are similar in their form to that for the (optical) cavity mode. For this reason we call the mechanical noise *quantum optical* like noise. The master equation (5.1) is valid if the followings are satisfied:

$$\kappa \ll \omega_c \ , \tag{5.7}$$
$$\gamma_j \ll \Omega_j \ . \tag{5.8}$$

Condition (5.7) is always satisfied for the optical setting[3] [153]. It remains that we assume that condition (5.8) is true for the mechanical modes to ensure that the analysis that will be given in this section is valid.

[3]Typical values of κ are in the range Hz–GHz, while ω_c is of the order of THz.

5.2 Existence and uniqueness of the steady state

In this section, we aim to answer the question whether the system's dynamics governed by the master equation (5.1) has unique steady state. In **Section 4.1** we have proved that the considered system has a unique steady state if and only if one mechanical mode is considered (see conditions (4.24) and (4.26)). In this section we consider the mechanical noise and check if the system still has a steady state.

We will be following the same steps as in **Section 4.1**:
We rewrite the master equation (5.1) as follows:

$$\dot{\rho}(t) = -i[H, \rho(t)] + \sum_{k=1}^{2N+1} \left(L_k \rho(t) L_k^\dagger - \frac{1}{2}\{L_k^\dagger L_k, \rho(t)\} \right) , \tag{5.9}$$

with the operators L_k are defined by

$$\begin{aligned} L_j &= \sqrt{\gamma_j (n_j + 1)}\; b_j , && (5.10)\\ L_{N+j} &= \sqrt{\gamma_j n_j}\; b_j^\dagger , && (5.11)\\ & \quad j = 1, \ldots, N \\ L_{2N+1} &= \sqrt{\kappa}\; a . && (5.12) \end{aligned}$$

Writing the Hamiltonian H in the form $H = \frac{1}{2} x^T G x$, and from Eq. (4.68), one can show that the matrix G is equal to

$$G = \begin{pmatrix} 0_N & \mathcal{A}' & 0_N & \mathcal{B}' \\ \mathcal{A}'^T & 0 & \mathcal{C}'^T & 0 \\ 0_N & \mathcal{C}' & 0_N & \mathcal{D}' \\ \mathcal{B}'^T & 0 & \mathcal{D}'^T & 0 \end{pmatrix} , \tag{5.13}$$

where $\mathcal{A}'$, $\mathcal{B}'$, $\mathcal{C}'$ and $\mathcal{D}'$ are $N \times 1$ vectors whose elements are given by

$$\begin{aligned} \mathcal{A}'_j &= \frac{-1}{\sqrt{2}}\, \alpha_j^- g_j (1 + r) \cos\phi_j^- , && (5.14)\\ \mathcal{B}'_j &= \frac{1}{\sqrt{2}}\, \alpha_j^- g_j (1 - r) \sin\phi_j^- , && (5.15)\\ \mathcal{C}'_j &= \frac{-1}{\sqrt{2}}\, \alpha_j^- g_j (1 + r) \sin\phi_j^- , && (5.16)\\ \mathcal{D}'_j &= \frac{-1}{\sqrt{2}}\, \alpha_j^- g_j (1 - r) \cos\phi_j^- . && (5.17) \end{aligned}$$

Considering the switching scheme, and using Eq. (4.69), then equations (5.14)–(5.17) become

$$\begin{aligned} \mathcal{A}'^{(\ell)}_j &= -\beta_\ell (1 + r) \Re U_{\ell j} , && (5.18)\\ \mathcal{B}'^{(\ell)}_j &= -\beta_\ell (1 - r) \Im U_{\ell j} , && (5.19)\\ \mathcal{C}'^{(\ell)}_j &= \beta_\ell (1 + r) \Im U_{\ell j} , && (5.20)\\ \mathcal{D}'^{(\ell)}_j &= -\beta_\ell (1 - r) \Re U_{\ell j} , && (5.21) \end{aligned}$$

where we put the super script ℓ to indicate the parameters at the ℓ^{th} switching step.

By defining the vector $\mathcal{L}$ as

$$\mathcal{L} = (L_1, \ldots, L_{2N}, L_{2N+1})^T \ , \tag{5.22}$$

and writing

$$\mathcal{L} = C' x \ , \tag{5.23}$$

one can show that the $(2N+1) \times (2N+1)$ complex matrix C' is equal to

$$C' = \begin{pmatrix} C_1 & 0_{N\times 1} & iC_1 & 0_{N\times 1} \\ C_2 & 0_{N\times 1} & -iC_2 & 0_{N\times 1} \\ 0_{1\times N} & \sqrt{\frac{\kappa}{2}} & 0_{1\times N} & i\sqrt{\frac{\kappa}{2}} \end{pmatrix} \ , \tag{5.24}$$

where the matrices C_1 and C_2 are given by their elements as follows:

$$(C_1)_{ij} = \sqrt{\frac{\gamma_j(n_j+1)}{2}}\, \delta_{ij} \ , \tag{5.25}$$

$$(C_2)_{ij} = \sqrt{\frac{\gamma_j n_j}{2}}\, \delta_{ij} \ . \tag{5.26}$$

The master equation (5.9) is equivalent to

$$\frac{\mathrm{d}\langle x\rangle}{\mathrm{d}t} = A\langle x\rangle \ , \tag{5.27}$$

$$\frac{\mathrm{d}V}{\mathrm{d}t} = AV + VA^T + B \ , \tag{5.28}$$

where the matrices A and B are defined in equations (4.18) and (4.19). Using equations (5.13) and (5.24), one finds matrices A and B at the ℓ^{th} switching step as follows:

$$A^{(\ell)} = \begin{pmatrix} \mathcal{E} & \mathcal{C}'^{(\ell)} & 0_N & \mathcal{D}'^{(\ell)} \\ \mathcal{B}'^{(\ell)T} & -\frac{\kappa}{2} & \mathcal{D}'^{(\ell)T} & 0 \\ 0_N & -\mathcal{A}'^{(\ell)} & \mathcal{E} & -\mathcal{B}'^{(\ell)} \\ -\mathcal{A}'^{(\ell)T} & 0 & -\mathcal{C}'^{(\ell)T} & -\frac{\kappa}{2} \end{pmatrix} \ , \tag{5.29}$$

$$B = \left(\begin{array}{cc|cc} \mathcal{F} & 0_{N\times 1} & \multicolumn{2}{c}{\multirow{2}{*}{0_{N+1}}} \\ 0_{1\times N} & \frac{\kappa}{2} & & \\ \hline \multicolumn{2}{c|}{\multirow{2}{*}{0_{N+1}}} & \mathcal{F} & 0_{N\times 1} \\ & & 0_{1\times N} & \frac{\kappa}{2} \end{array}\right) \ , \tag{5.30}$$

where $\mathcal{A}'^{(\ell)}$, $\mathcal{B}'^{(\ell)}$, $\mathcal{C}'^{(\ell)}$ and $\mathcal{D}'^{(\ell)}$ are given by equations (5.18)– (5.21), and the matrices $\mathcal{E}$ and $\mathcal{F}$ are equal to

$$\mathcal{E} = \frac{-1}{2}\ \mathrm{Diag}\left(\gamma_1, \ldots, \gamma_N\right) \ . \tag{5.31}$$

$$\mathcal{F} = \mathrm{Diag}\left(\gamma_1(n_1+\frac{1}{2}), \ldots, \gamma_N(n_N+\frac{1}{2})\right) \ , \tag{5.32}$$

As before, we put the super script ℓ on the matrix A in Eq. (5.29) to indicate that the parameters are given for the ℓ^{th} switching step.

The existence and uniqueness of a steady state at each step of the switching scheme for the system shown in Fig. 5.1 with the master equation (5.1) depends on whether the matrix $A^{(\ell)}$ given in Eq. (5.29) is *Hirwitz* or not. Indeed, one can show that the matrix $A^{(\ell)}$ is Hirwitz by applying the *Routh–Hirwitz stability criterion* [154, 166]. Hence, the system sketched in Fig. 5.1 has always a unique steady state for all (allowed) system parameters at every switching step.

5.3 Robustness of the generation of the cluster state in the presence of mechanical noise

In **Section 5.2**, we proved that the system shown in Fig. 5.1 has a unique steady state in every step of the switching scheme. In this section, we study the impact of the presence of the mechanical noise on the generation of the cluster state. Since the mechanical oscillators interact with their thermal baths, then the system's steady state will deviate from the target cluster state. We quantify this deviation by the Uhlmann-Josza fidelity [142, 143] given in **Section 2.6**.

We start by considering the two modes cluster state. Without loss of generality, we choose mechanical oscillators frequencies as[4] $\Omega_1 = 1$ MHz and $\Omega_2 = 10$ MHz. We choose the duration of the first switching step to be equal to $t_s = 20\kappa^{-1}$ while we give the second step sufficient time so the system can reach its steady state. We calculate the fidelity between the system's state at time t and the target cluster state, the result of the simulation is shown in Fig. 5.2, where we have considered the following cases:

- ideal system where the mechanical modes are not coupled to any other system except the cavity mode.
- the mechanical modes are coupled to their (independent) baths at zero temperature). The damping rates γ_j were chosen to be equal to $\gamma = 10^{-4}\kappa$.
- the mechanical modes are coupled to their baths (with equal damping rates $\gamma = 10^{-4}\kappa$) at temperature $T = 10^{-4}$ kelvin.

Figure 5.2 (main) shows, as expected, that the mechanical noise affects the generation of the cluster state where the fidelity is degraded. Also we see from Fig. 5.2 that in the presence of mechanical damping and/or bath's temperature, the fidelity reaches a maximum value before it starts to decrease. Hence, the (approximate) cluster state is no longer the system's steady state (as in the ideal case), but instead one obtains it as an intermediate state of the system during the application of the switching scheme. Therefore, one must use the cluster state[5] before the decoherence dominates the dynamics, *i.e.,* use the cluster state just after reaching the maximum fidelity.

Since the mechanical noise degrades the quality (in terms of quantum fidelity) of the generated cluster state, one expects that long switching steps implying more decoherence of the system which results in low fidelities. To observe this behaviour, we consider again the two–modes cluster state with the same parameters as before ($\Omega_1 = 1$ MHz, $\Omega_2 = 10$ MHz, $\gamma = 10^{-4}\kappa$ and $T = 10^{-4}$ kelvin) and plot the final fidelity as function of the evolution time per switching step. The results are shown in Fig. 5.3. Indeed, if the switching time is too long then there will be a considerable deviation of the system's state from the target cluster state. On the other hand, too short switching times are not sufficient to let the system evolve to the target cluster state. Therefore, one should consider the *optimal switching time* that yields the

[4]Read **Section 4.5** for more details about the choice of the frequencies of the mechanical oscillators.

[5]for example, one uses the cluster state in one way quantum computation where it is the main resource for computation.

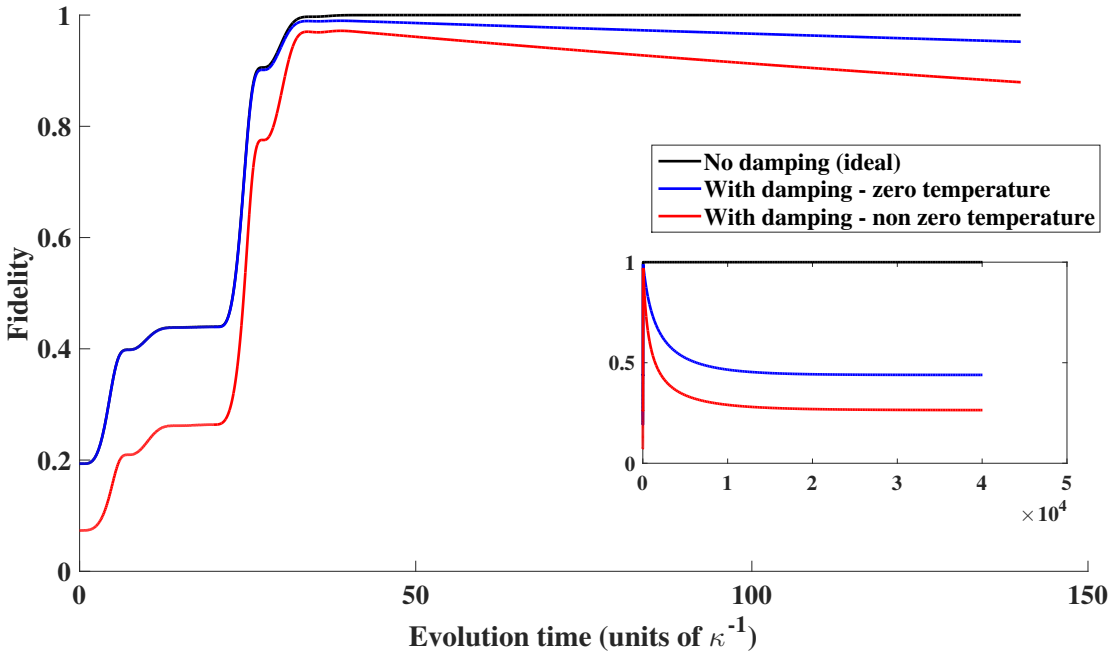

Figure 5.2: Fidelity in time of the two modes cluster state. For the numerical values of the system's parameters, see text.

maximum final fidelity[6] for given mechanical damping and bath's temperature (in the example shown in Fig. 5.3 the optimal switching time is approximately 20 κ^{-1}).

Now, we study the effects of varying the bath's temperature and the couplings of mechanical modes to their baths on the final fidelity of the system's state with the target cluster state. In Fig. 5.4, we show contour plots of the final fidelity as function of both bath's temperature and mechanical couplings to the bath in the case of three different cluster state geometries: two–modes, linear four–modes and eight–modes dual rail cluster states[7]. The simulation data were obtained by assuming the following:

- mechanical modes frequencies: $\Omega_j = 2\pi j$ MHz where j varies from 1 up to the number of mechanical modes (see comments about Eq. (4.109) in **Section 4.5**).
- equal mechanical damping rates: $\gamma_j = \gamma$, and all the mechanical modes baths have the same equilibrium temperature T.
- equal evolution time per switching step.

As we said, there is an optimal evolution time per switching step that yields maximum final fidelity. Every data point in the plots of Fig. 5.4 was calculated by finding

[6] check section **Section 4.5.2** on page 45 for the meaning of the final fidelity

[7] We have chosen these particular cluster states because of their theoretical and practical uses. The two–modes cluster state, up to local symplectic transformations, is equivalent to the two–modes squeezed state. Whereas the linear four–modes and eight–modes dual rail cluster states allow the implementation of one and two modes symplectic operations respectively which are essential in measurement based quantum computation.

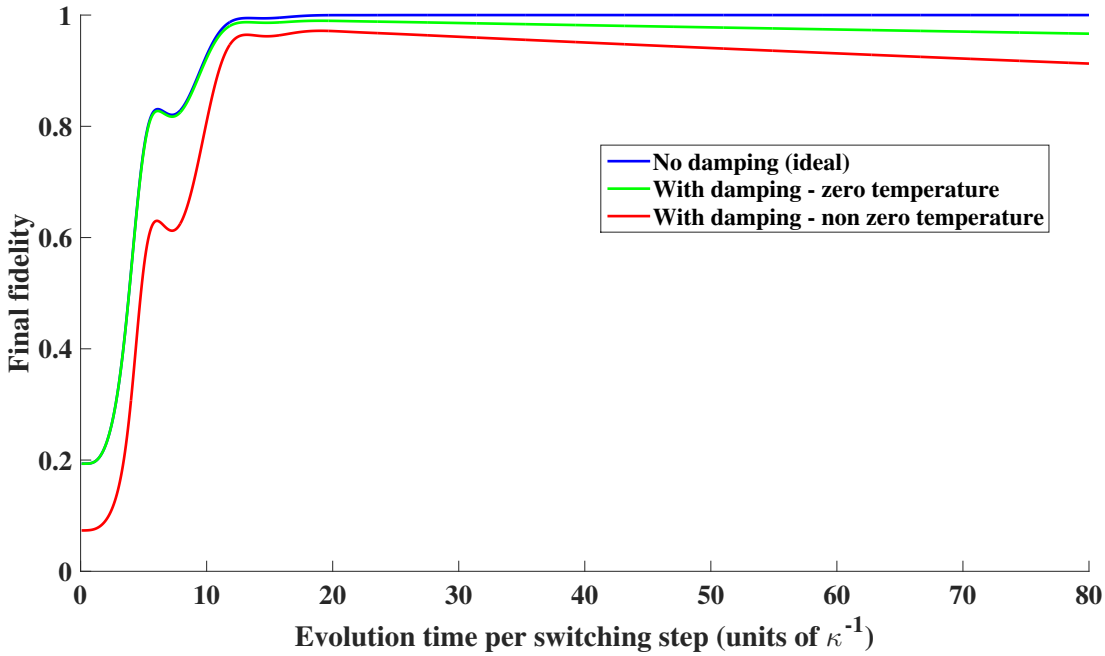

Figure 5.3: Final fidelity function of evolution time per switching step of the two modes cluster state. For the numerical values of the system's parameters, see text.

this optimal evolution time (see **Appendix C** for details about the computer code used for this purpose). Also, we have set the parameter β as in Eq. (4.110) (see comments on Eq. (4.110) on page 44). If we relate mechanical noise to bath's temperature and mechanical damping, then, from Fig. 5.4, one can say that the higher the squeezing or the larger the graph state[8] the less the mechanical noise tolerated.

[8] We quantify the size of the cluster state by the number of modes contained in it

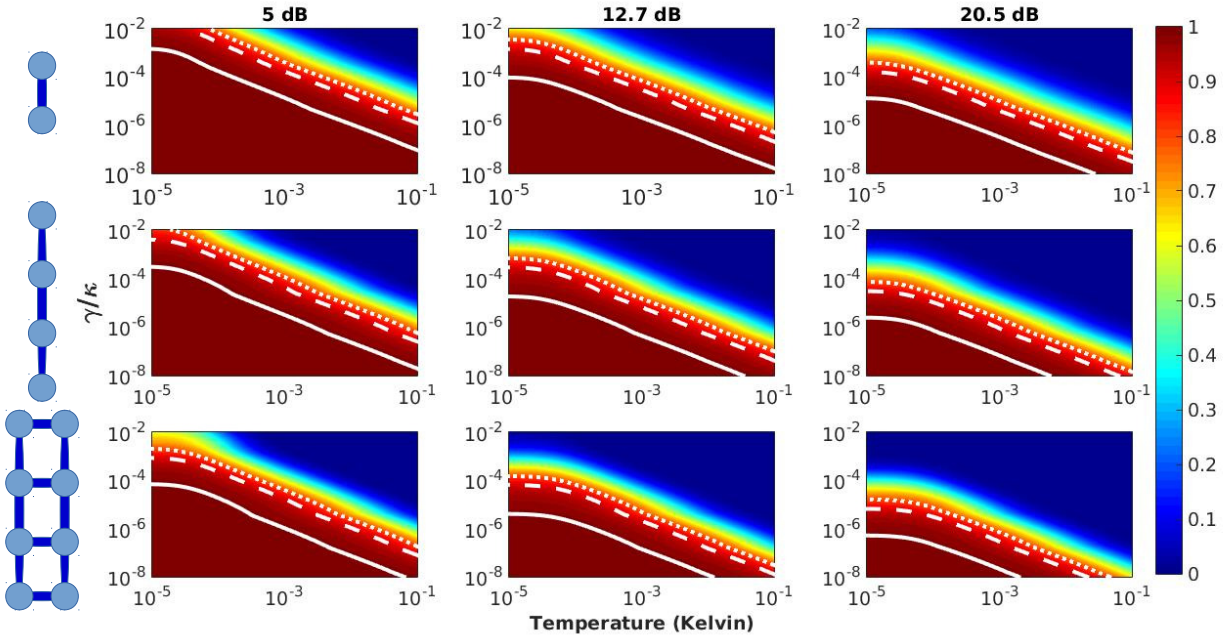

Figure 5.4: Fidelity as function of the mechanical bath's temperature and the mechanical damping rate. The contour plots give the fidelity of the generated state and the target cluster states: two modes, linear four modes, and eight modes dual rail cluster states, with squeezings 5 dB, 12.7 dB and 20.5 dB. The solid, dashed and dotted contour lines correspond respectively to final fidelities 0.99, 0.90 and 0.80. See text for details about the chosen system's parameters.

Chapter 6

Conclusion and suggestions for further works

We introduced a scheme to generate an approximate cluster state encoded in the vibrational modes of a set of mechanical oscillators. The generated cluster state was obtained as the steady state of the oscillators with the help of the optomechanical coupling and cavity dissipation. We used a cavity optomechanical system where the optical cavity mode is coupled to independent mechanical oscillators via radiation pressure.

We were able to control the quantum state of the mechanical oscillators and drive it to the target cluster state via applying multi–tone laser pump on the cavity where each mechanical mode is manipulated by a pair of laser drives operating in the side–band regime. This required us to consider that all mechanical frequencies do not overlap, otherwise it is impossible to address each mechanical oscillator individually. But this later limitation was relaxed by considering an optomechanical system where the cavity mode is coupled to all or a subset of interacting mechanical oscillators and we work in the space of the normal modes of the mechanical modes. We showed that it is possible to tune the normal modes such that they do not overlap, where tuning the normal modes is done via controlling the interactions between the mechanical oscillators.

The quality of the generated cluster state was assessed for finite preparation time and in the presence of mechanical noise. By using quantum fidelity tools, we found that when the target cluster state contains high squeezing level and/or many modes, then the quality is heavily affected. One has to eliminate the mechanical noise as much as possible by cooling down the vibrational modes. A possible solution for this later issue is to extend our scheme to use the mechanical dissipation as a resource in order to obtain cluster states that are also robust against mechanical noise. Another path for extending this study, is to consider non–Markovian mechanical noise instead of the (Markovian) *quantum–optical–like* noise considered in this work.

Since the cluster state generated by our scheme is intended to be used in one–way quantum computation, one would ask how to realize the optomechanical system studied here, and how to perform measurements on the system. To answer the first question we discuss the experimental feasibility of our scheme in the light of previously realized experiments in optomechanics and electromechanics. The second question is reduced to how to devise a strategy to read information out from our generated cluster state.

Our scheme uses an optomechanical system with the following characteristics:

- Many mechanical oscillators with non overlapping frequencies[1], and
- one optical cavity mode that is coupled (via optomechanical interaction) to the mechanical modes.
- The optomechanical interaction is considered weak, and
- the optical cavity is operated in the resolved–sideband regime.

Various experiments have been realized that exploit the weak optomechanical coupling regime [88–90], while optomechanical networks *i.e.,* systems with many mechanical modes, were reported in recent experiments [167–169]. Also, mechanical oscillators with frequencies with values of the order of those used in our simulations are within reach by experiments *e.g.* [170–173].

Returning to the measurement question raised before, we mention here a possible read–out strategy. Using quantum state tomography tools and techniques [174] and the ideas introduced in [175], one can obtain information from the motion of the mechanical oscillators by using a suitable probe that is coupled to the target mechanical mode that we want to measure. Indeed, this later is under study in [176] where they consider optomechanical systems and in particular our cluster state.

Concluding, being able to realize and implement our scheme for generating the cluster states in the vibrational modes of mechanical oscillators, and success in devising a read–out protocol to extract information from our generated cluster state will pave the path towards scalable and integrated solid–state technology for building quantum computers.

[1] But as we said, this condition can be relaxed, see **Section 3.5** for details and requirements.

Appendix A

Generating the two modes squeezed state of optomechanical systems by Hamiltonian switching and cavity dissipation

We will show in this appendix how to dissipatively generate the two modes squeezed state (TMSS) in the mechanical modes of the optomechanical system shown in Fig. A.1. We will use the switching scheme introduced in **Section 4.3**.

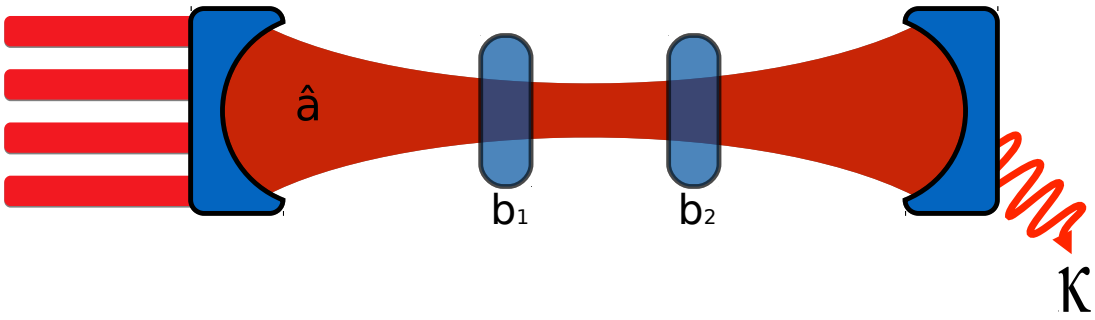

Figure A.1: An optomechanical system consisting of one cavity mode and two mechanical oscillators inside the optical cavity.

The TMSS is characterized with the covariance matrix (see **Section 2.4.7**)

$$V_{\text{TMSS}} = \frac{1}{2}\begin{pmatrix} \cosh 2\xi & \sinh 2\xi & 0 & 0 \\ \sinh 2\xi & \cosh 2\xi & 0 & 0 \\ 0 & 0 & \cosh 2\xi & -\sinh 2\xi \\ 0 & 0 & -\sinh 2\xi & \cosh 2\xi \end{pmatrix}, \tag{A.1}$$

where ξ is the squeezing parameter.

In the other hand, the covariance matrix of the steady state of the system of Fig. A.1 was found to be equal to (see how did we arrive at Eq. (4.76))

$$V = \begin{pmatrix} -\sinh(2\xi)\ (\Re U)^T \Re U + \frac{1}{2}\mathrm{e}^{2\xi} & \sinh(2\xi)\ (\Re U)^T \Im U \\ \sinh(2\xi)\ (\Re U)^T \Im U & \sinh(2\xi)\ (\Re U)^T \Re U + \frac{1}{2}\mathrm{e}^{-2\xi} \end{pmatrix}, \tag{A.2}$$

where U is 2×2 unitary matrix that gives the switching program and $\xi = \arctan^{-1} r$ with r is defined in Eq. (4.66) (see **Section 4.3**).

To simplify the calculations, we put

$$U = X + iY \ , \tag{A.3}$$

where X and Y are 2×2 real symmetric matrices. Comparing Eq. (A.1) and Eq. (A.2) and using Eq. (A.3), one can easily arrive at

$$-2\sinh 2\xi X^2 + \frac{1}{2}\,\mathrm{e}^{2\xi} = \frac{1}{2}\begin{pmatrix} \cosh 2\xi & \sin 2\xi \\ \sinh 2\xi & \cosh 2\xi \end{pmatrix} , \tag{A.4}$$

$$XY = 0 \ , \tag{A.5}$$

which leads to the following expressions for X and Y:

$$X = \frac{1}{2}\begin{pmatrix} 1 & -1 \\ -1 & 1 \end{pmatrix} , \tag{A.6}$$

$$Y = \mu\begin{pmatrix} 1 & 1 \\ 1 & 1 \end{pmatrix} , \tag{A.7}$$

where μ is a real constant that we fix from the unitarity condition for U:

$$U^\dagger U = \mathbb{1}_2 \Rightarrow X^2 + Y^2 = \mathbb{1}_2 \Rightarrow \mu = \pm\frac{1}{2} \ . \tag{A.8}$$

The switching program U is therefore equal to:

$$U = \frac{\pm\mathrm{e}^{i\pi/4}}{\sqrt{2}}\begin{pmatrix} 1 & \mathrm{e}^{-i\pi/2} \\ \mathrm{e}^{-i\pi/2} & 1 \end{pmatrix} . \tag{A.9}$$

Now we have the switching program, we can calculate the intensities and phases of the driving lasers that give the TMSS: using Eq. (4.69) and assuming, for simplicity, that $g_1 = g_2 \equiv g$ and $\beta_1 = \beta_2 \equiv \beta$ we find the following parameters for the four driving lasers , see Table. A.1.

Step	α_1^-	α_2^-	ϕ_1^-	ϕ_2^-
1	1	1	0	$\pi/2$
2	1	1	$\pi/2$	0

Table A.1: System parameters for generating the two modes squeezed state. The α^-'s are given in units of β/g. The ϕ^+'s and α^+'s parameters are obtained from Eq. (4.65) and Eq. (4.66) respectively.

Appendix B

Relabelling modes in the cluster state

In this appendix we aim to find how does relabelling modes in a cluster state change the switching program found in **Section 4.4.1**.

Let A and A' be the adjacency matrices of the same N–modes cluster state geometry but with different mode labels. We will call this *mode relabelling*. A demonstration example is shown in Fig. B.1

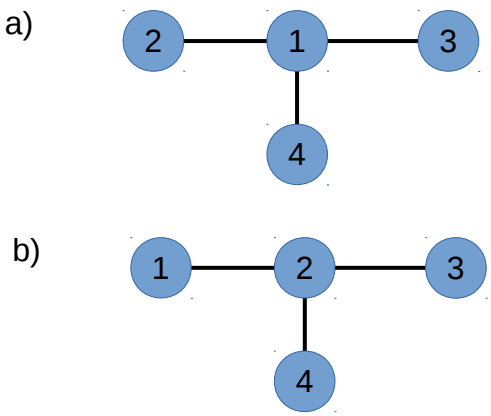

Figure B.1: Two cluster states with the same geometry (T-cluster) and with different mode labels.

The adjacency matrices of the cluster states shown in Fig. B.1–a and Fig. B.1–b are respectively:

$$A = \begin{pmatrix} 0 & 1 & 1 & 1 \\ 1 & 0 & 0 & 0 \\ 1 & 0 & 0 & 0 \\ 1 & 0 & 0 & 0 \end{pmatrix} \quad , \quad A' = \begin{pmatrix} 0 & 1 & 1 & 1 \\ 1 & 0 & 0 & 0 \\ 1 & 0 & 0 & 0 \\ 1 & 0 & 0 & 0 \end{pmatrix} . \tag{B.1}$$

Notice that A and A' are equivalent up to row and column swaps: it is easy to see that when interchanging the first and second rows and then interchanging first and second column of matrix A', then one will obtain the matrix A.

In general, for any relabelling of modes while keeping the same graph geometry, A and A' are related by:

$$A' = TAT \ , \tag{B.2}$$

where T is the row swap matrix and it is the resultant of possibly more than one row swap:

$$T = \prod_{s=1}^{\mathcal{N}} T_{i_s j_s} \ , \tag{B.3}$$

where the $N \times N$ symmetric matrix $T_{i_s j_s}$ is the operation of interchanging between the i_s^{th} and j_s^{th} rows, and it is equal to the identity matrix with rows i_s^{th} and j_s^{th} are swapped. $\mathcal{N}$ is the number of row swaps required to transform A into A'.

Now, we want to see how does the switching program transform as a result of relabelling modes in a given cluster state geometry. We found in **Section 4.4.1** that the switching program for a cluster state with adjacency matrix A is equal to

$$U = -(A^2 + \mathbb{1}_N)^{-1/2}(A + i\mathbb{1}_N) \ , \tag{B.4}$$

and hence for cluster state with adjacency matrix A' we have

$$U' = -(A'^2 + \mathbb{1}_N)^{-1/2}(A' + i\mathbb{1}_N) \ . \tag{B.5}$$

If we replace A' in Eq. (B.5) with its expression (B.2), we obtain:

$$U' = -(TAT^2AT + \mathbb{1}_N)^{-1/2}(TAT + i\mathbb{1}_N) \ , \tag{B.6}$$

and since the matrix T is the product of involutionary matrices [177] then T is also involutionary ,*i.e.,*

$$T^2 = \mathbb{1}_N \ , \tag{B.7}$$

then, Eq. (B.6) simplifies to

$$\begin{aligned} U' &= -(TA^2T + \mathbb{1}_N)^{-1/2}(TAT + i\mathbb{1}_N) \ , \\ &= -T(A^2 + \mathbb{1}_N)^{-1/2}(A + i\mathbb{1}_N)T \ , \\ &= TUT \ . \end{aligned} \tag{B.8}$$

Therefore, relabelling the modes of the cluster state is equivalent to interchanging rows and columns in the corresponding switching program.

Appendix C

Computer codes used to produce the simulations

Numerical simulations given in this thesis were produced by a set of *FORTRAN* programs and *MATLAB* scripts. *FORTRAN* was used to calculate covraiance matrices and quantum fidelities and generate data files, while *MATLAB* was used to produce the plots. In what follows we give flow charts of the most important sections of the *FORTRAN* programs that generated the different types of simulations. Also, an explicit *FORTRAN* code regarding the covariance matrix calculations is given.

C.1 Calculate the covariance matrix of a state prepared by the switchig scheme

The following subroutine will be denoted *cluster–covariance–matrix* in **Section C.3** and **Section C.4**.

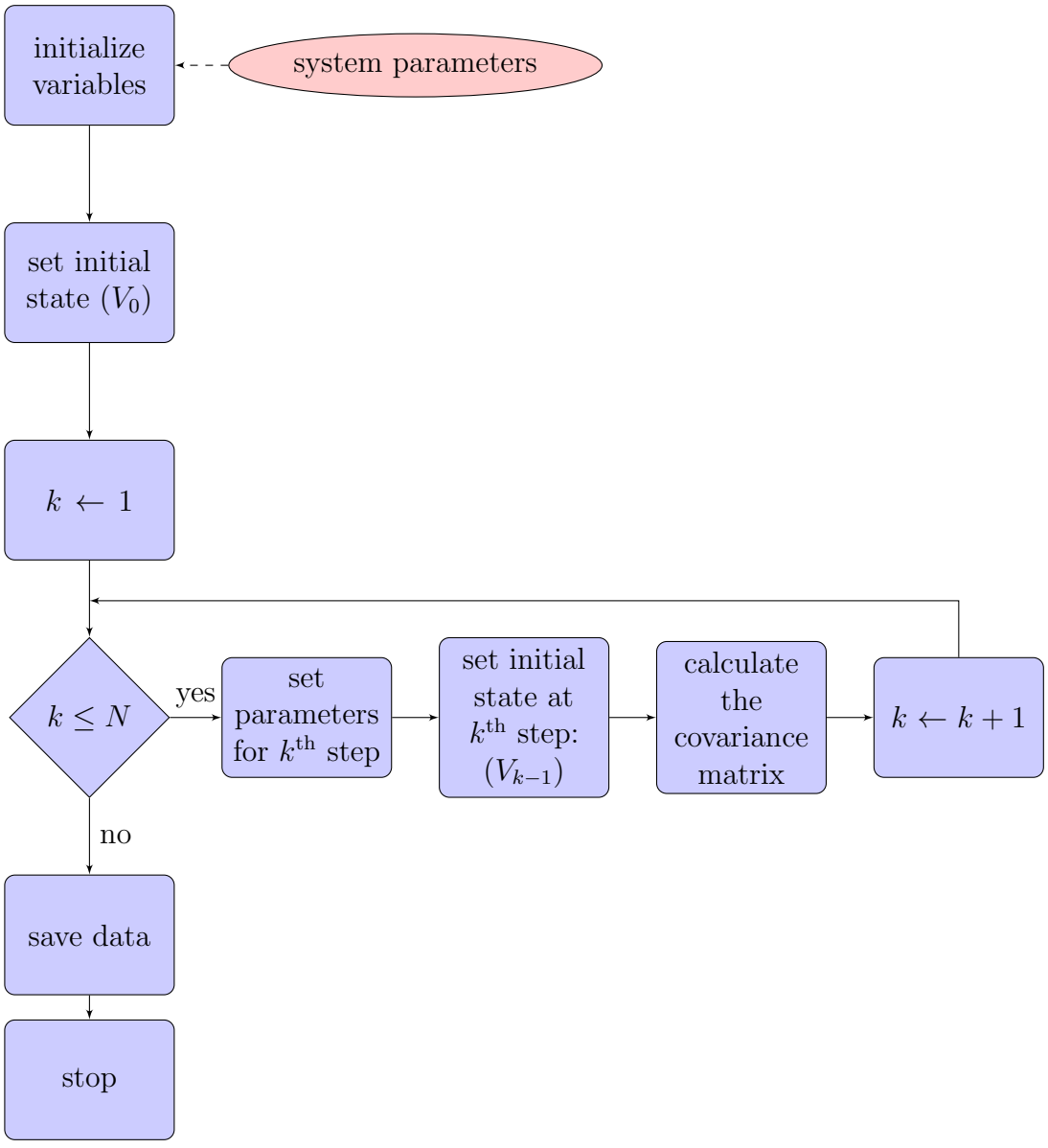

C.2 Fidelity as function of evolution time

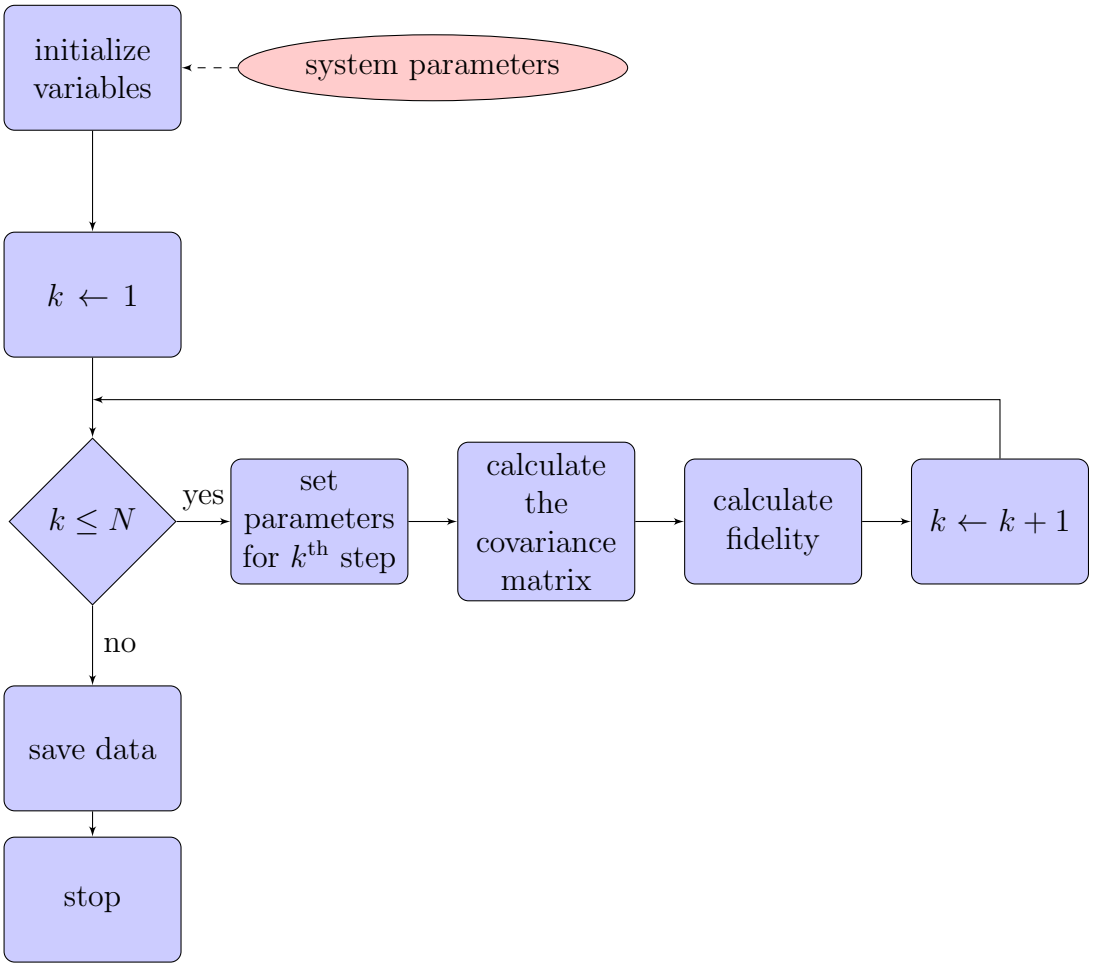

C.3 Final fidelity as function of switching time

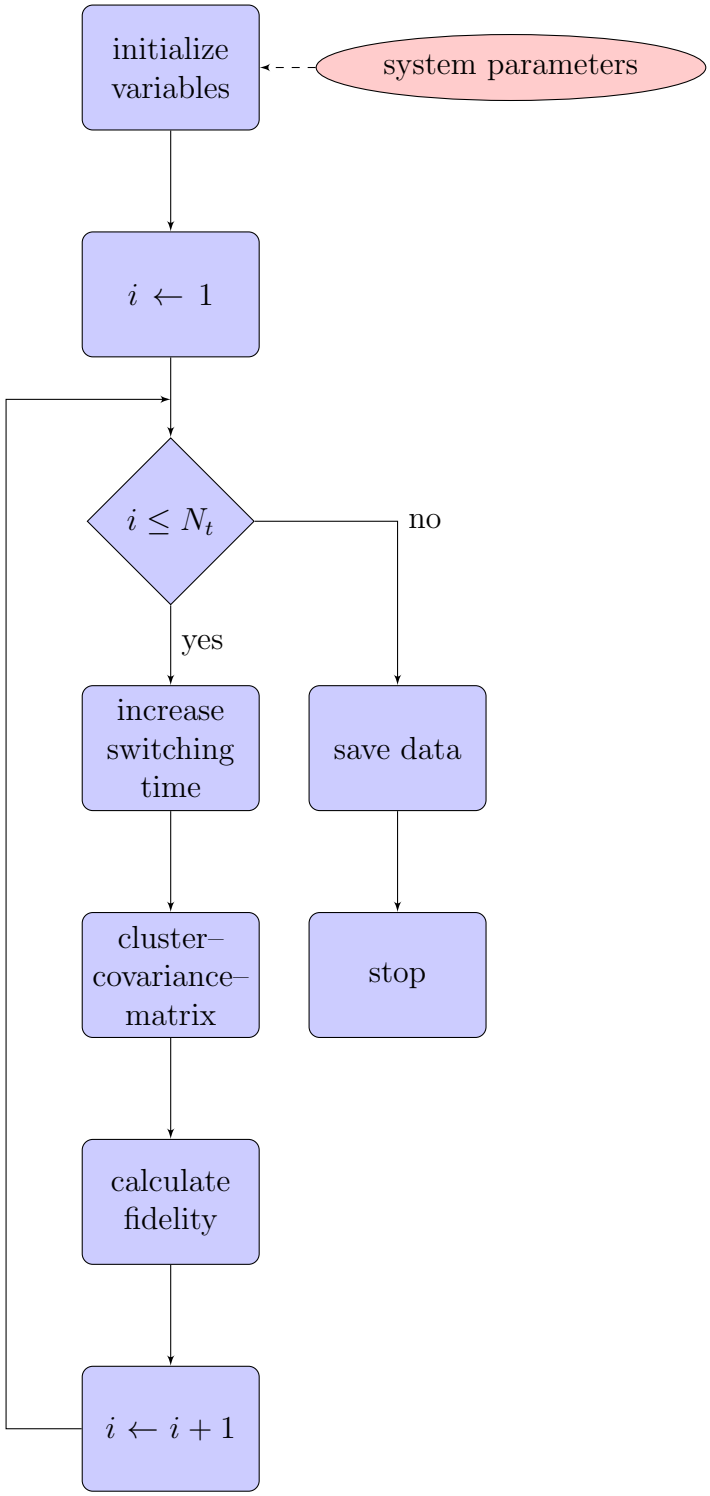

C.4 Maximum fidelity as function of bath's temperature and mechanical damping rate

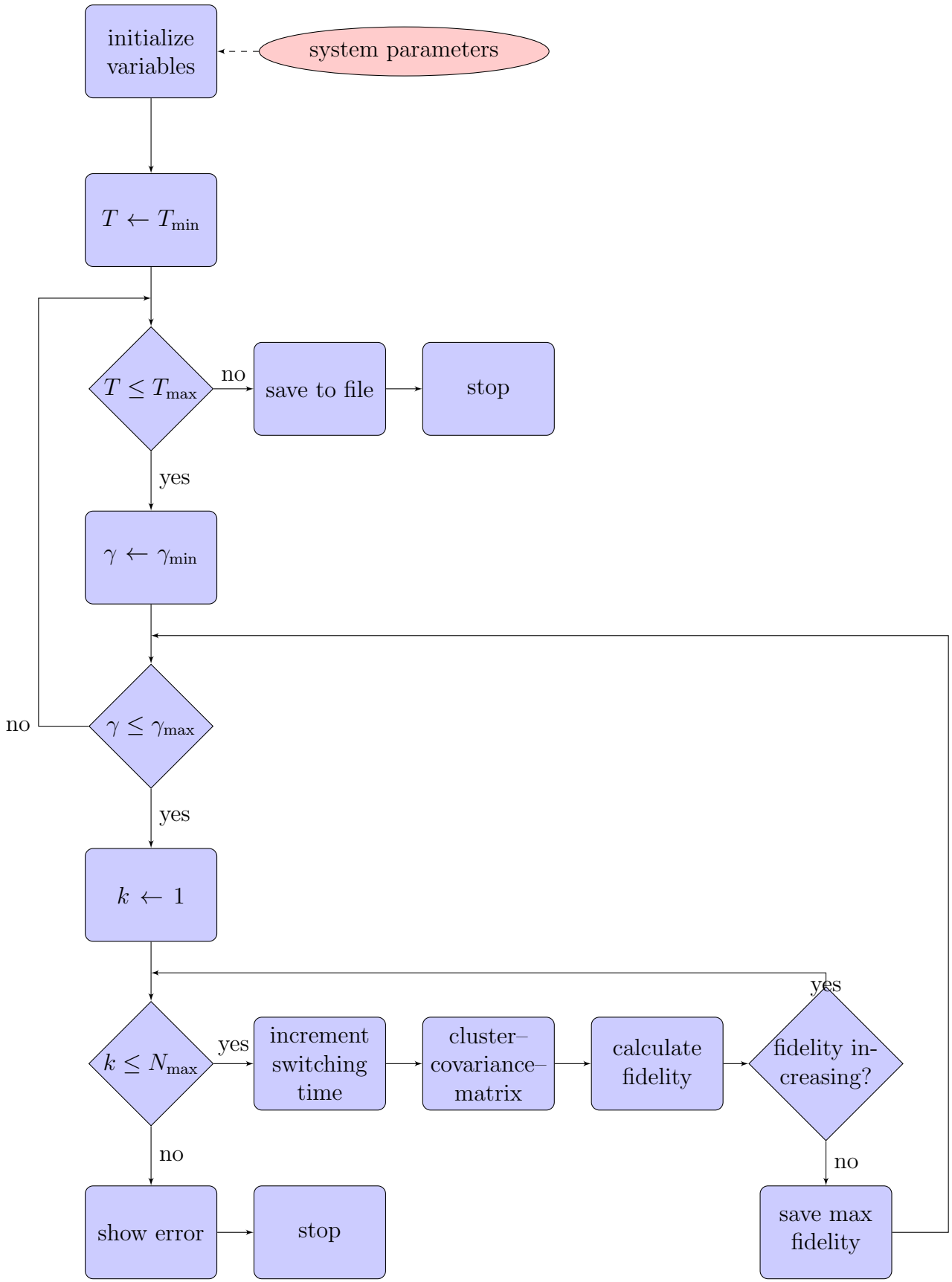

C.5 covmat.f90 subroutines

```
module covmat_module
 use defs_module
 use helper_module

 !standard covariance matrix IDs
 Integer,Parameter   ::  COVMAT_SQUEEZED     =1,  &
          COVMAT_SQUEEZED_VACUUMCAVITY =2
 !Butcher tableau
 real(Kind=Long),parameter:: butcher_a11=0.25_Long,     &
        butcher_a12=0.25_Long-sqrt(3.0_Long)/6, &
        butcher_a21=0.25_Long+sqrt(3.0_Long)/6, &
        butcher_a22=0.25_Long,     &
        butcher_b1=0.5_Long,     &
        butcher_b2=0.5_Long,     &
        butcher_c1=0.5_Long-sqrt(3.0_Long)/6, &
        butcher_c2=0.5_Long+sqrt(3.0_Long)/6
 !COVMAT method IDs
 Integer,Parameter   ::  COVMAT_SOLVER_EULER     =1,  &
          COVMAT_SOLVER_RK4     =2,  &
          COVMAT_SOLVER_RK4_IMPLICIT   =3,  &
          COVMAT_VACUUM_THERMAL    =4,  &
          COVMAT_THERMAL      =5
 !covmat solving method
 integer,parameter::nCovmatMethod=COVMAT_SOLVER_RK4

 contains

!=============================================
 function covmat(A,B,t_f,V_0,Nt,Vfull,t_0)
 !
 !   calculates the covariance matrix
 ! this subroutine uses different methods: explicit/
   implicit Runge-Kutta methods,
 !
 ! PARAMETERS:
 !  input, A,B are the system matrices (may be Time
   dependent: must contain 2*(Nt-1) elements)
 !  input, t_f is the total evolution time
 !  input, V_0 is the initial state
 !  input, Nt, the number of data points used to solve
   the diff equation
 !  output, (optional), Vfull to save the full dynamics
   of the covariance matrix (from time t=0, to time t_f)
 !  input, optional, t_0, initial time
 !
```

```
 implicit none

 !declaration of input/output variables
 real(kind=long),dimension(:,:),intent(in)::V_0
 real(kind=long),intent(in)::t_f
 integer,intent(in)::Nt
 real(kind=long),dimension(:,:,:),intent(in)::A,B
 real(kind=long),dimension(:,:,:),intent(out),optional::
    Vfull
 real(kind=long),intent(in),optional::t_0
 real(kind=long),dimension(1:size(V_0,dim=1),1:size(V_0,
    dim=1))::covmat
 real(kind=Long)::t0

 if(PRESENT(t_0))then
  t0=t_0
 else
  t0=0.0_Long
 end if

 if(PRESENT(Vfull))then
  if(nCovmatMethod==COVMAT_SOLVER_EULER)then
   covmat=covmat_euler(A,B,t0,t_f,V_0,Nt,Vfull)
  elseif(nCovmatMethod==COVMAT_SOLVER_RK4)then
   covmat=covmat_RK4(A,B,t0,t_f,V_0,Nt,Vfull)
  elseif(nCovmatMethod==COVMAT_SOLVER_RK4_IMPLICIT)then
   covmat=covmat_RK4_implicit(A,B,t0,t_f,V_0,Nt,Vfull)
  end if
 else
  if(nCovmatMethod==COVMAT_SOLVER_EULER)then
   covmat=covmat_euler(A,B,t0,t_f,V_0,Nt)
  elseif(nCovmatMethod==COVMAT_SOLVER_RK4)then
   covmat=covmat_RK4(A,B,t0,t_f,V_0,Nt)
  elseif(nCovmatMethod==COVMAT_SOLVER_RK4_IMPLICIT)then
   covmat=covmat_RK4_implicit(A,B,t0,t_f,V_0,Nt)
  end if
 end if

 return
 end function covmat

!=============================================
 function covmat_RK4(A,B,t_0,t_f,V_0,Nt,Vfull)
 !
 !   calculates the covariance matrix using RK4 method
 !
 ! PARAMETERS:
```

```
!  input, A,B are the system matrices (may be Time
   dependent)
!  input, t_0 is the initial time
!  input, t_f is the final time
!  input, V_0 is the initial state
!  input, Nt, the number of data points used to solve
   the diff equation
!  output, (optional), Vfull to save the full dynamics
   of the covariance matrix (from time t=0, to time t_f)
!

 implicit none

 !declaration of input/output variables
       real(kind=long),dimension(:,:),intent(in)::V_0
 real(kind=long),intent(in)::t_0,t_f
 integer,intent(in)::Nt
 real(kind=long),dimension(:,:,:),intent(in)::A,B
 real(kind=long),dimension(:,:,:),intent(out),optional::
    Vfull
 real(kind=long),dimension(1:size(V_0,dim=1),1:size(V_0,
    dim=1))::covmat_RK4

       !local variables
       integer     ::n,i,bTimeDependent=0
       real(kind=Long)  ::h
       real(kind=long),dimension(1:size(V_0,dim=1),1:
          size(V_0,dim=1))::k1,k2,k3,k4,M
       real(kind=long),dimension(:,:,:),allocatable::V

    !cov mat size
    n=size(V_0,dim=1)

    !allocate memory
    allocate(V(1:Nt,1:n,1:n))

 !check if A and B are time dependent
 if(size(A,dim=1)>1)then
  bTimeDependent=1
 end if

 !time step
 h=(t_f-t_0)/(Nt-1)

   !---------------------------------------
   !---------------------------------------
! calculating the covariance matrix
   !---------------------------------------
```

```
    !-------------------------------------
  V(1,:,:)=V_0 !initial state <==> t=0
     do i=2,Nt
   M=MATMUL(A(bTimeDependent*2*(i-2)+1,:,:),V(i-1,:,:))
   K1=M+TRANSPOSE(M)+B(bTimeDependent*2*(i-2)+1,:,:)

   M=MATMUL(A(bTimeDependent*(2*i-3)+1,:,:),V(i-1,:,:)+h*
      k1/2)
   K2=M+TRANSPOSE(M)+B(bTimeDependent*(2*i-3)+1,:,:)

   M=MATMUL(A(bTimeDependent*(2*i-3)+1,:,:),V(i-1,:,:)+h*
      k2/2)
   K3=M+TRANSPOSE(M)+B(bTimeDependent*(2*i-3)+1,:,:)

   M=MATMUL(A(bTimeDependent*2*(i-1)+1,:,:),V(i-1,:,:)+h*
      K3)
   K4=M+TRANSPOSE(M)+B(bTimeDependent*2*(i-1)+1,:,:)

   V(i,:,:)=V(i-1,:,:)+h*(k1+2*k2+2*k3+k4)/6.0_Long
  end do
  covmat_RK4=V(Nt,:,:)

  if(present(Vfull))then
   Vfull=V
  end if

  !free memory
  deallocate(V)

  return
 end function covmat_RK4

!=============================================
 function covmat_RK4_implicit(A,B,t_0,t_f,V_0,Nt,Vfull)
 !
 !   calculates the covariance matrix
 ! this subroutine uses implicit RK4 method
 !
 ! PARAMETERS:
 !  input, A,B are the system matrices (may be Time
    dependent: must contain 2*(Nt-1) elements)
 !  input, t_0 is the initial time
 !  input, t_f is the final time
 !  input, V_0 is the initial state
 !  input, Nt, the number of data points used to solve
    the diff equation
 !  output, (optional), Vfull to save the full dynamics
    of the covariance matrix (from time t=0, to time t_f)
```

```
!

implicit none

!declaration of input/output variables
   real(kind=long),dimension(:,:),intent(in)::V_0
real(kind=long),intent(in)::t_0,t_f
integer,intent(in)::Nt
real(kind=long),dimension(:,:,:),intent(in)::A,B
real(kind=long),dimension(:,:,:),intent(out),optional::
   Vfull
real(kind=long),dimension(1:size(V_0,dim=1),1:size(V_0,
   dim=1))::covmat_RK4_implicit

!local variables
integer     ::n,i,bTD=0
real(kind=Long)  ::h
real(kind=long),dimension(1:size(V_0,dim=1),1:size(V_0,
   dim=1))::K1,K2,Id
real(kind=long),dimension(1:2*size(V_0,dim=1)**2)::KK,FF
real(kind=long),dimension(1:2*size(V_0,dim=1)**2,1:2*
   size(V_0,dim=1)**2)::M
real(kind=long),dimension(:,:,:),allocatable::V

!cov mat size
n=size(V_0,dim=1)

   !allocate memory
   allocate(V(1:Nt,1:n,1:n))

!check if A and B are time dependent
if(size(A,dim=1)>1)then
 bTD=1
end if

!time step
h=(t_f-t_0)/(Nt-1)

!identity matrix
Id=IdentityMatrix(n)

!initial state <==> t=0
V(1,:,:)=V_0

!V(t)=???
do i=1,Nt-1
 FF(1:n**2)=reshape( &
  MATMUL(A(bTD*2*(i-1)+1,:,:),V(i,:,:))     &
```

```
   +MATMUL(V(i,:,:),TRANSPOSE(A(bTD*2*(i-1)+1,:,:))) &
   +B(bTD*2*(i-1)+1,:,:)          &
   ,(/n**2/))
  FF(n**2+1:2*n**2)=reshape( &
   MATMUL(A(bTD*(2*i-1)+1,:,:),V(i,:,:))     &
   +MATMUL(V(i,:,:),TRANSPOSE(A(bTD*(2*i-1)+1,:,:))) &
   +B(bTD*(2*i-1)+1,:,:)          &
   ,(/n**2/))

  M(1:n**2,1:n**2)=KRON(Id,h*butcher_a11*A(bTD*2*(i-1)
     +1,:,:)-Id/2)+KRON(h*butcher_a11*A(bTD*2*(i-1)
     +1,:,:)-Id/2,Id)
  M(1:n**2,n**2+1:2*n**2)=KRON(Id,h*butcher_a12*A(bTD*2*(
     i-1)+1,:,:))+KRON(h*butcher_a12*A(bTD*2*(i-1)+1,:,:)
     ,Id)
  M(n**2+1:2*n**2,1:n**2)=KRON(Id,h*butcher_a21*A(bTD*(2*
     i-1)+1,:,:))+KRON(h*butcher_a21*A(bTD*(2*i-1)+1,:,:)
     ,Id)
  M(n**2+1:2*n**2,n**2+1:2*n**2)=KRON(Id,h*butcher_a22*A(
     bTD*(2*i-1)+1,:,:)-Id/2)+KRON(h*butcher_a22*A(bTD
     *(2*i-1)+1,:,:)-Id/2,Id)

  KK=-REAL(MATMUL(MATINVERSE(CMPLX(M,Kind=Long)),FF))
  K1=reshape(KK(1:n**2),(/n,n/))
  K2=reshape(KK(n**2+1:2*n**2),(/n,n/))

  V(i+1,:,:)=V(i,:,:)+h*(butcher_b1*K1+butcher_b2*K2)
 end do
 covmat_RK4_implicit=V(Nt,:,:)

 if(present(Vfull))then
  Vfull=V
 end if

 !free memory
 deallocate(V)

 return
 end function covmat_RK4_implicit

!=============================================
 function covmat_euler(A,B,t_0,t_f,V_0,Nt,Vfull)
 !
 !   calculates the covariance matrix
 ! this subroutine uses euler method.
 !
 ! PARAMETERS:
```

```
!  input, A,B are the system matrices (may be Time
   dependent: must contain 2*(Nt-1) elements)
!  input, t_0 is the initial time
!  input, t_f is the final time
!  input, V_0 is the initial state
!  input, Nt, the number of data points used to solve
   the diff equation
!  output, (optional), Vfull to save the full dynamics
   of the covariance matrix (from time t=0, to time t_f)
!

implicit none

!declaration of input/output variables
   real(kind=long),dimension(:,:),intent(in)::V_0
real(kind=long),intent(in)::t_0,t_f
integer,intent(in)::Nt
real(kind=long),dimension(:,:,:),intent(in)::A,B
real(kind=long),dimension(:,:,:),intent(out),optional::
   Vfull

real(kind=long),dimension(1:size(V_0,dim=1),1:size(V_0,
   dim=1))::covmat_euler

   !local variables
   integer     ::n,i,bTD=0
   real(kind=Long)  ::h
real(kind=long),dimension(:,:,:),allocatable::V

   !cov mat size
   n=size(V_0,dim=1)

   !allocate memory
   allocate(V(1:Nt,1:n,1:n))

!check if A and B are time dependent
if(size(A,dim=1)>1)then
 bTD=1
end if

!time step
h=(t_f-t_0)/(Nt-1)

!initial state <==> t=0
V(1,:,:)=V_0

!V(t)=???
do i=1,Nt-1
```

```
  V(i+1,:,:)=V(i,:,:)+h*(MATMUL(A(i,:,:),V(i,:,:))+MATMUL
     (V(i,:,:),TRANSPOSE(A(i,:,:)))+B(i,:,:))
 end do
 covmat_euler=V(Nt,:,:)

 if(present(Vfull))then
  Vfull=V
 end if

 !free memory
 deallocate(V)

 return
 end function covmat_euler

!=============================================
 subroutine covmat_get_time(t_i,t_f,Nt,t)
 !
 ! calculates the intermediate times data points to be
    used by covmat
 !
 ! PARAMETERS :
 !  input, t_i, initial time
 !  input, t_f, final time
 !  input, Nt, number of  principal time data points in
    the interval [t_i,t_f]
 !  output, t, time array:  the calling routine must
    deallocate the memory used by t
 !
  implicit none

  !declaration of input/output variables
  real(Kind=Long),intent(in)::t_i,t_f
  integer,intent(in)::Nt
        real(Kind=Long),dimension(:),allocatable,intent(
           out)::t

  integer::i,NNt
  real(Kind=Long)::h

  NNt=covmat_get_data_size(Nt)
  allocate(t(1:NNt))

  h=(t_f-t_i)/(Nt-1)

  if(nCovmatMethod==COVMAT_SOLVER_EULER)then
   do i=1,NNt
    t(i)=(i-1)*h+t_i
```

```
   end do
  elseif(nCovmatMethod==COVMAT_SOLVER_RK4)then
   do i=1,NNt
    t(i)=(i-1)*h/2.0_Long+t_i
   end do
  elseif(nCovmatMethod==COVMAT_SOLVER_RK4_IMPLICIT)then
   do i=1,Nt-1
    t(2*i-1)=(i-1+butcher_c1)*h+t_i
    t(2*i)=(i-1+butcher_c2)*h+t_i
   end do
  end if

  return
 end subroutine covmat_get_time

!=============================================
 function gen_covmat(nID,n,sParam,vParam)
 !
 !   generates a covariance matrix described by nID of
    size dim1*dim2
 !
 ! PARAMETERS:
 !  input, nID, cov matrix identifier, see def.f90
 !  input, n, number of modes
 !  input (OPTIONAL), sParam, is scalar parameter
    relevant for some kinds of cov matrices (squeezing
    param for example)
 !  input (optional), vParam, is vector parameter
    relevant for some kinds of cov matrices (Omegas for
    example)
 !

  implicit none

  !declaration of input/output variables
  integer,intent(in)::nID,n
  real(kind=Long),intent(in),optional::sParam
  real(kind=Long),dimension(:),intent(in),optional::
     vParam
  real(kind=Long),dimension(1:2*n,1:2*n)::gen_covmat

  !local variables
        integer::i
        real(Kind=Long)::r,Nphon

     if (present(sParam)) then
      r=sParam
     else
```

```
     r=0.0_Long
    end if

  gen_covmat=0.0_Long
  if (nID==COVMAT_SQUEEZED) then      !vacuum/coherent (r
     =0) or squeezed state (r <> 0)
   do i=1,n
    gen_covmat(i,i)=exp(-2*ATANH(r))/2
    gen_covmat(n+i,n+i)=exp(2*ATANH(r))/2
   end do
  elseif(nID==COVMAT_SQUEEZED_VACUUMCAVITY) then !vacuum/
     coherent (r=0) or squeezed state (r <> 0) in the
     mechanical part, and vacuum state in the cavity
   do i=1,n-1
    gen_covmat(i,i)=exp(-2*ATANH(r))/2
    gen_covmat(n+i,n+i)=exp(2*ATANH(r))/2
   end do
   gen_covmat(n,n)=1.0_Long/2
   gen_covmat(2*n,2*n)=1.0_Long/2
  elseif(nID==COVMAT_THERMAL) then !thermal state
   do i=1,n
    if(sParam==0)then  !sParam=temperature
     Nphon=0.0_Long
    else
     Nphon=1/(exp(hbar*vParam(i)/Kb/sParam)-1) !vParam==
        Omegas
    end if
    gen_covmat(i,i)=Nphon+0.5_Long
    gen_covmat(n+i,n+i)=Nphon+0.5_Long
   end do
  elseif(nID==COVMAT_VACUUM_THERMAL) then !vacuum state
     for the cavity and thermal state for the mechanical
     modes
   do i=1,n-1
    if(sParam==0)then  !sParam=temperature
     Nphon=0.0_Long
    else
     Nphon=1/(exp(hbar*vParam(i)/Kb/sParam)-1) !vParam==
        Omegas
    end if
    gen_covmat(i,i)=Nphon+0.5_Long
    gen_covmat(n+i,n+i)=Nphon+0.5_Long
   end do
   gen_covmat(n,n)=1.0_Long/2
   gen_covmat(2*n,2*n)=1.0_Long/2
  end if

  return
```

```
 end function gen_covmat

!=============================================
 function covmat_fidelity(A1,A2)
 !
 ! calculates the distance between two covariance
    matrices using the fidelity measure
 !
 ! REFERENCES:
 !  Phys. Rev. A. 61. 022306
 !  J. Phys. A: Math. Theor. 46. 025304
 ! PARAMETERS:
 !  input, A1 and A2, two cov matrices
    !

  implicit none

  !declaration of input/output variables
        real(kind=long),dimension(:,:),intent(in)::A1,A2
        real(kind=Long)::covmat_fidelity

        complex(kind=long),dimension(1:size(A1,dim=1),1:
           size(A1,dim=1))::M1,M2,M3,M4,M5,M6,PHI1,B,
           PHI_B,J
        real(kind=long),dimension(1:size(A1,dim=1),1:size
           (A1,dim=1))::Id
        real(kind=long)::L
     integer::n,i

  !this definition is from J. Phys. A: Math. Theor. 46.
     025304
  !it is very fast compared to the other formula in Phys.
      Rev. A. 61. 022306
  !to use the other formula of Phys. Rev. A. 61. 022306,
     comment the following two lines

  covmat_fidelity=1/SQRT(DET(CMPLX(A1+A2,Kind=Long)))
  return

  !identity and J matrices
  J=0.0_Long
  Id=0.0_Long
  n=size(A1,dim=1)/2
  do i=1,n
   J(i,n+i)=1.0_Long
   J(n+i,i)=-1.0_Long

   Id(i,i)=1.0_Long
```

```
    Id(n+i,n+i)=1.0_Long
  end do

  !L=?
  L=1/real(DET(CMPLX(A1+A2,Kind=Long)))

  !PHI(A1)
  M1=MATINVERSE(MATMUL(J,2.0_Long*A1))
  M2=MATMUL(M1,M1)
  M3=MATSQRT(Id+M2)
  PHI1=MATMUL(2.0_Long*A1,Id+M3)

  !B=? and PHI(B) (here B is the matrix O 'Big O' in the
     reference paper)
  M1=PHI1-ii*J
  M2=PHI1+ii*J
  M3=2.0_Long*A2-ii*J
  M4=2.0_Long*A2+ii*J
  M5=MATINVERSE(PHI1+2.0_Long*A2)
  M6=MATINVERSE(PHI1+2.0_Long*A2-MATMUL(MATMUL(M3,M5),M4)
     )
  B=PHI1-MATMUL(MATMUL(M1,M6),M2)

  M1=MATINVERSE(MATMUL(J,B))
  M2=MATMUL(M1,M1)
  M3=MATSQRT(Id+M2)
  PHI_B=MATMUL(B,Id+M3)

  !fidelity
  covmat_fidelity=sqrt(L*REAL(DET(PHI_B)))

  return
 end function covmat_fidelity

end module covmat_module
```

Bibliography

[1] Manin, Y.: Computable and uncomputable. Sovetskoye Radio, Moscow (1980) 128

[2] Feynman, R.P.: Simulating physics with computers. Int. J. Theor. Phys. **21** (1982) 467–488

[3] Deutsch, D.: Quantum theory, the church-turing principle and the universal quantum computer. Proc. R. Soc. Lond. A **400(1818)** (1985) 97–117

[4] Poplavskii, R.: Thermodynamic models of information processes. Physics-Uspekhi **18**(3) (1975) 222–241

[5] Pomerance, C.: A tale of two sieves. Biscuits of Number Theory **85** (2008)

[6] Shor, P.W.: Algorithms for quantum computation: Discrete logarithms and factoring. In: Proceedings of the 35th Annual Symposium on Foundations of Computer Science, IEEE (1994) 124–134

[7] Grover, L.K.: A fast quantum mechanical algorithm for database search. In: Proceedings of the twenty-eighth annual ACM symposium on Theory of computing, ACM (1996) 212–219

[8] Grover, L.K.: Quantum mechanics helps in searching for a needle in a haystack. Phys. Rev. Lett. **79** (1997) 325

[9] Harrow, A.W., Hassidim, A., Lloyd, S.: Quantum algorithm for linear systems of equations. Phys. Rev. Lett. **103** (2009) 150502

[10] Lloyd, S.: Universal quantum simulators. Science **273**(5278) (1996) 1073

[11] Paar, C., Pelzl, J.: Understanding cryptography: a textbook for students and practitioners. Springer Science & Business Media (2009)

[12] Rivest, R.L., Shamir, A., Adleman, L.: A method for obtaining digital signatures and public-key cryptosystems. Communications of the ACM **21**(2) (1978) 120–126

[13] Kleinjung, T., Aoki, K., Franke, J., Lenstra, A.K., Thomé, E., Bos, J.W., Gaudry, P., Kruppa, A., Montgomery, P.L., Osvik, D.A., et al.: Factorization of a 768-bit rsa modulus. In: Advances in Cryptology–CRYPTO 2010. Springer (2010) 333–350

[14] Wikipedia: Integer factorization — wikipedia, the free encyclopedia (2015)

[15] Gisin, N., Ribordy, G., Tittel, W., Zbinden, H.: Quantum cryptography. Rev. Mod. Phys. **74**(1) (2002) 145

[16] Bruss, D., Erdélyi, G., Meyer, T., Riege, T., Rothe, J.: Quantum cryptography: A survey. ACM Computing Surveys (CSUR) **39**(2) (2007) 6

[17] Scarani, V., Bechmann-Pasquinucci, H., Cerf, N.J., Dušek, M., Lütkenhaus, N., Peev, M.: The security of practical quantum key distribution. Rev. Mod. Phys. **81**(3) (2009) 1301

[18] Moore, G.E.: Cramming more components onto integrated circuits. Electronics **38**(8) (1965)

[19] Markov, I.L.: Limits on fundamental limits to computation. Nature **512**(7513) (2014) 147–154

[20] Keyes, R.W.: Physical limits of silicon transistors and circuits. Rep. Prog. Phys. **68**(12) (2005) 2701

[21] Keyes, R.W.: Fundamental limits of silicon technology. Proc. IEEE **89**(3) (2001) 227–239

[22] Schulz, M.: The end of the road for silicon? Nature **399**(6738) (1999) 729–730

[23] Gottesman, D.: Fault-tolerant quantum computation with higher-dimensional systems. In: Quantum Computing and Quantum Communications. Springer (1999) 302–313

[24] Lloyd, S., Braunstein, S.L.: Quantum computation over continuous variables. In: Quantum Information with Continuous Variables. Springer (2003) 9–17

[25] Sanders, B.C., Bartlett, S.D., de Guise, H.: From qubits to continuous-variable quantum computation. arXiv preprint quant-ph/0208008 (2002)

[26] Deutsch, D.: Quantum computational networks. Proc. R. Soc. Lond. A **425(1868)** (1989) 73–90

[27] DiVincenzo, D.P.: The physical implementation of quantum computation. Fortschr. Phys. **48**(9-11) (2000) 771–783

[28] Raussendorf, R., Briegel, H.J.: A one-way quantum computer. Phys. Rev. Lett. **86**(22) (2001) 5188

[29] Farhi, E., Gutmann, S.: Quantum computation and decision trees. Phys. Rev. A **58**(2) (1998) 915

[30] Bernstein, E., Vazirani, U.: Quantum complexity theory. In: Proceedings of the twenty-fifth annual ACM symposium on Theory of computing, ACM (1993) 11–20

[31] Cirac, J.I., Zoller, P.: Quantum computations with cold trapped ions. Phys. Rev. Lett. **74**(20) (1995) 4091

[32] Gulde, S., Riebe, M., Lancaster, G.P., Becher, C., Eschner, J., Häffner, H., Schmidt-Kaler, F., Chuang, I.L., Blatt, R.: Implementation of the deutsch–jozsa algorithm on an ion-trap quantum computer. Nature **421**(6918) (2003) 48–50

[33] Garcia-Ripoll, J.J., Zoller, P., Cirac, J.I.: Speed optimized two-qubit gates with laser coherent control techniques for ion trap quantum computing. Phys. Rev. Lett. **91**(15) (2003) 157901

[34] Leibfried, D.: Ion-trap quantum computation. In: Frontiers of Engineering:: Reports on Leading-Edge Engineering from the 2002 NAE Symposium on Frontiers of Engineering, National Academies Press (2003) 97

[35] Kielpinski, D., Monroe, C., Wineland, D.J.: Architecture for a large-scale ion-trap quantum computer. Nature **417**(6890) (2002) 709–711

[36] Stolze, J., Suter, D.: Ion trap quantum computers. Quantum Computing: A Short Course from Theory to Experiment (2007) 173–188

[37] Vandersypen, L.M., Steffen, M., Breyta, G., Yannoni, C.S., Sherwood, M.H., Chuang, I.L.: Experimental realization of shor's quantum factoring algorithm using nuclear magnetic resonance. Nature **414**(6866) (2001) 883–887

[38] Jones, J.A., Vedral, V., Ekert, A., Castagnoli, G.: Geometric quantum computation using nuclear magnetic resonance. Nature **403**(6772) (2000) 869–871

[39] Kane, B.E.: A silicon-based nuclear spin quantum computer. Nature **393**(6681) (1998) 133–137

[40] Jones, J.A., Mosca, M.: Implementation of a quantum algorithm on a nuclear magnetic resonance quantum computer. J. Chem. Phys. **109**(5) (1998) 1648–1653

[41] Cory, D.G., Fahmy, A.F., Havel, T.F.: Ensemble quantum computing by nmr spectroscopy. Proc. Natl. Acad. Sci. U.S.A. **94**(5) (1997) 1634–1639

[42] Blais, A., Huang, R.S., Wallraff, A., Girvin, S., Schoelkopf, R.J.: Cavity quantum electrodynamics for superconducting electrical circuits: An architecture for quantum computation. Phys. Rev. A **69**(6) (2004) 062320

[43] Duan, L.M., Kimble, H.: Scalable photonic quantum computation through cavity-assisted interactions. Phys. Rev. Lett. **92**(12) (2004) 127902

[44] Pellizzari, T., Gardiner, S., Cirac, J., Zoller, P.: Decoherence, continuous observation, and quantum computing: A cavity qed model. Phys. Rev. Lett. **75**(21) (1995) 3788

[45] Nielsen, M.A., Chuang, I.L.: Quantum computation and quantum information. Cambridge university press (2010)

[46] Steane, A.: Quantum computing. Rep. Prog. Phys. **61**(2) (1998) 117

[47] Braunstein, S.L., Pati, A.K.: Quantum Information with Continuous Variables. first edn. Kluwer Academic, Dordrecht (2003)

[48] Lloyd, S., Braunstein, S.L.: Quantum computation over continuous variables. Phys. Rev. Lett. **82** (1999) 1784–1787

[49] Braunstein, S.L., Van Loock, P.: Quantum information with continuous variables. Rev. Mod. Phys. **77**(2) (2005) 513

[50] Carmichael, H.: An Open System Approach to Quantum Optics. first edn. Springer (1993)

[51] Gardiner, C.W., Zoller, P.: Quantum Noise. second edn. Springer, Berlin (2000)

[52] Breuer, H.P., Petruccione, F.: The Theory of Open Quantum Systems. first edn. Oxford University Press (2003)

[53] Ravazy, M.: Classical and Quantum Dissipative Systems. first edn. Imperial College Press, Canada (2005)

[54] Attal, S., Joye, A., Pillet, C.A.: Open Quantum Systems I. first edn. Springer (2006)

[55] Weiss, U.: Quantum Dissipative Systems. third edn. World Scientific (2008)

[56] Shor, P.W.: Scheme for reducing decoherence in quantum computer memory. Phys. Rev. A **52**(4) (1995) R2493

[57] Terhal, B.M.: Quantum error correction for quantum memories. Rev. Mod. Phys. **87**(2) (2015) 307

[58] Lu, Y., Kapit, E., Saskin, S., Leung, N., Earnest, N., Mckay, D., Koch, J., Schuster, D.: Autonomous quantum error correction with superconducting qubits. In: APS Meeting Abstracts. Volume 1. (2015) 37006

[59] Lidar, D.A., Brun, T.A.: Quantum error correction. Cambridge University Press (2013)

[60] Chiaverini, J., Leibfried, D., Schaetz, T., Barrett, M., Blakestad, R., Britton, J., Itano, W., Jost, J., Knill, E., Langer, C., et al.: Realization of quantum error correction. Nature **432**(7017) (2004) 602–605

[61] Knill, E., Laflamme, R., Viola, L.: Theory of quantum error correction for general noise. Phys. Rev. Lett. **84**(11) (2000) 2525

[62] Knill, E., Laflamme, R.: Theory of quantum error-correcting codes. Phys. Rev. A **55**(2) (1997) 900

[63] Calderbank, A.R., Rains, E.M., Shor, P.W., Sloane, N.J.: Quantum error correction and orthogonal geometry. Phys. Rev. Lett. **78**(3) (1997) 405

[64] Bennett, C.H., DiVincenzo, D.P., Smolin, J.A., Wootters, W.K.: Mixed-state entanglement and quantum error correction. Phys. Rev. A **54**(5) (1996) 3824

[65] Steane, A.: Multiple-particle interference and quantum error correction. In: Proc. R. Soc. A. Volume 452., The Royal Society (1996) 2551–2577

[66] Dong, D., Petersen, I.R.: Quantum control theory and applications: a survey. Control Theory & Applications, IET **4**(12) (2010) 2651–2671

[67] Caneva, T., Murphy, M., Calarco, T., Fazio, R., Montangero, S., Giovannetti, V., Santoro, G.E.: Optimal control at the quantum speed limit. Phys. Rev. Lett. **103**(24) (2009) 240501

[68] Werschnik, J., Gross, E.: Quantum optimal control theory. J. Phys. B At. Mol. Opt. Phys **40** (2007) R175

[69] Schulte-Herbrüggen, T., Spörl, A., Khaneja, N., Glaser, S.: Optimal control-based efficient synthesis of building blocks of quantum algorithms: A perspective from network complexity towards time complexity. Phys. Rev. A **72**(4) (2005) 042331

[70] Khaneja, N., Glaser, S.J., Brockett, R.: Sub-riemannian geometry and time optimal control of three spin systems: quantum gates and coherence transfer. arXiv preprint quant-ph/0106099 (2001)

[71] Peirce, A.P., Dahleh, M.A., Rabitz, H.: Optimal control of quantum-mechanical systems: Existence, numerical approximation, and applications. Phys. Rev. A **37**(12) (1988) 4950

[72] Makhlin, Y., Schön, G., Shnirman, A.: Quantum-state engineering with josephson-junction devices. Rev. Mod. Phys. **73**(2) (2001) 357

[73] Pastawski, F., Clemente, L., Cirac, J.I.: Quantum memories based on engineered dissipation. Phys. Rev. A **83**(1) (2011) 012304

[74] Verstraete, F., Wolf, M.M., Cirac, J.I.: Quantum computation and quantum-state engineering driven by dissipation. Nature physics **5**(9) (2009) 633–636

[75] Poyatos, J., Cirac, J., Zoller, P.: Quantum reservoir engineering with laser cooled trapped ions. Phys. Rev. Lett. **77**(23) (1996) 4728

[76] Carvalho, A., Milman, P., de Matos Filho, R., Davidovich, L.: Decoherence, pointer engineering and quantum state protection. In: Modern Challenges in Quantum Optics. Springer (2001) 65–79

[77] Plenio, M., Huelga, S.: Entangled light from white noise. Phys. Rev. Lett. **88**(19) (2002) 197901

[78] Diehl, S., Micheli, A., Kantian, A., Kraus, B., Büchler, H., Zoller, P.: Quantum states and phases in driven open quantum systems with cold atoms. Nature Physics **4**(11) (2008) 878–883

[79] Roy, A., Leghtas, Z., Stone, A.D., Devoret, M., Mirrahimi, M.: Continuous generation and stabilization of mesoscopic field superposition states in a quantum circuit. Phys. Rev. A **91**(1) (2015) 013810

[80] Kienzler, D., Lo, H.Y., Keitch, B., de Clercq, L., Leupold, F., Lindenfelser, F., Marinelli, M., Negnevitsky, V., Home, J.: Quantum harmonic oscillator state synthesis by reservoir engineering. Science **347**(6217) (2015) 53–56

[81] Houhou, O., Aissaoui, H., Ferraro, A.: Generation of cluster states in optomechanical quantum systems. Phys. Rev. A **92**(6) (2015) 063843

[82] Lidar, D.A., Chuang, I.L., Whaley, K.B.: Decoherence-free subspaces for quantum computation. Phys. Rev. Lett. **81**(12) (1998) 2594

[83] Gambetta, J., Houck, A., Blais, A.: Superconducting qubit with purcell protection and tunable coupling. Phys. Rev. Lett. **106**(3) (2011) 030502

[84] Plenio, M.B., Vedral, V., Knight, P.L.: Quantum error correction in the presence of spontaneous emission. Phys. Rev. A **55**(1) (1997) 67

[85] Blume-Kohout, R., Ng, H.K., Poulin, D., Viola, L.: Characterizing the structure of preserved information in quantum processes. Phys. Rev. Lett. **100**(3) (2008) 030501

[86] Shabani, A., Lidar, D.A.: Theory of initialization-free decoherence-free subspaces and subsystems. Phys. Rev. A **72**(4) (2005) 042303

[87] Bacon, D.: Decoherence, control, and symmetry in quantum computers, 2001. PhD thesis, University of California, Berkeley

[88] Meystre, P.: A short walk through quantum optomechanics. Ann. Phys. **525**(3) (2013) 215–233

[89] Rogers, B., Lo Gullo, N., De Chiara, G., Palma, G.M., Paternostro, M.: Hybrid optomechanics for quantum technologies. Quantum Measurements and Quantum Metrology **2**(1) (2014) 11–43

[90] Aspelmeyer, M., Kippenberg, T.J., Marquardt, F.: Cavity optomechanics. Rev. Mod. Phys. **86**(4) (2014) 1391

[91] Brooks, D.W., Botter, T., Schreppler, S., Purdy, T.P., Brahms, N., Stamper-Kurn, D.M.: Non-classical light generated by quantum-noise-driven cavity optomechanics. Nature **488**(7412) (2012) 476–480

[92] Purdy, T.P., Yu, P.L., Peterson, R.W., Kampel, N.S., Regal, C.A.: Strong optomechanical squeezing of light. Phys. Rev. X **3** (Sep 2013) 031012

[93] Safavi-Naeini, A.H., Gröblacher, S., Hill, J.T., Chan, J., Aspelmeyer, M., Painter, O.: Squeezed light from a silicon micromechanical resonator. Nature **500**(7461) (2013) 185–189

[94] Palomaki, T., Teufel, J., Simmonds, R., Lehnert, K.: Entangling mechanical motion with microwave fields. Science **342**(6159) (2013) 710–713

[95] Bhattacharya, M., Meystre, P.: Multiple membrane cavity optomechanics. Phys. Rev. A **78** (Oct 2008) 041801

[96] Hartmann, M.J., Plenio, M.B.: Steady state entanglement in the mechanical vibrations of two dielectric membranes. Phys. Rev. Lett. **101**(20) (2008) 200503

[97] Xuereb, A., Genes, C., Dantan, A.: Strong coupling and long-range collective interactions in optomechanical arrays. Phys. Rev. Lett. **109**(22) (2012) 223601

[98] Chang, D., Safavi-Naeini, A.H., Hafezi, M., Painter, O.: Slowing and stopping light using an optomechanical crystal array. New J. Phys. **13**(2) (2011) 023003

[99] Stannigel, K., Komar, P., Habraken, S., Bennett, S., Lukin, M.D., Zoller, P., Rabl, P.: Optomechanical quantum information processing with photons and phonons. Phys. Rev. Lett. **109**(1) (2012) 013603

[100] Schmidt, M., Ludwig, M., Marquardt, F.: Optomechanical circuits for nanomechanical continuous variable quantum state processing. New J. Phys. **14**(12) (2012) 125005

[101] Ludwig, M., Marquardt, F.: Quantum many-body dynamics in optomechanical arrays. Phys. Rev. Lett. **111**(7) (2013) 073603

[102] Seok, H., Buchmann, L., Wright, E., Meystre, P.: Multimode strong-coupling quantum optomechanics. Phys. Rev. A **88**(6) (2013) 063850

[103] Xuereb, A., Genes, C., Pupillo, G., Paternostro, M., Dantan, A.: Reconfigurable long-range phonon dynamics in optomechanical arrays. Phys. Rev. Lett. **112**(13) (2014) 133604

[104] Menicucci, N.C., van Loock, P., Gu, M., Weedbrook, C., Ralph, T.C., Nielsen, M.A.: Universal quantum computation with continuous-variable cluster states. Phys. Rev. Lett. **97**(11) (2006) 110501

[105] Ohliger, M., Kieling, K., Eisert, J.: Limitations of quantum computing with gaussian cluster states. Phys. Rev. A **82**(4) (2010) 042336

[106] Ohliger, M., Eisert, J.: Efficient measurement-based quantum computing with continuous-variable systems. Phys. Rev. A **85**(6) (2012) 062318

[107] Menicucci, N.C., Flammia, S.T., van Loock, P.: Graphical calculus for gaussian pure states. Phys. Rev. A **83**(4) (2011) 042335

[108] Menicucci, N.C.: Fault-tolerant measurement-based quantum computing with continuous-variable cluster states. Phys. Rev. Lett. **112**(12) (2014) 120504

[109] Chen, M., Menicucci, N.C., Pfister, O.: Experimental realization of multipartite entanglement of 60 modes of a quantum optical frequency comb. Phys. Rev. Lett. **112**(12) (2014) 120505

[110] Roslund, J., De Araujo, R.M., Jiang, S., Fabre, C., Treps, N.: Wavelength-multiplexed quantum networks with ultrafast frequency combs. Nature Photonics **8**(2) (2014) 109–112

[111] Li, G.x., Ke, S.s., Ficek, Z.: Generation of pure continuous-variable entangled cluster states of four separate atomic ensembles in a ring cavity. Phys. Rev. A **79**(3) (2009) 033827

[112] Koga, K., Yamamoto, N.: Dissipation-induced pure gaussian state. Phys. Rev. A **85**(2) (2012) 022103

[113] Ikeda, Y., Yamamoto, N.: Deterministic generation of gaussian pure states in a quasilocal dissipative system. Phys. Rev. A **87**(3) (2013) 033802

[114] Lebedew, P.: Untersuchungen über die druckkräfte des lichtes. Ann. Phys. **311**(11) (1901) 433–458

[115] Nichols, E.F., Hull, G.: A preliminary communication on the pressure of heat and light radiation. Physical Review (Series I) **13**(5) (1901) 307

[116] Einstein, A.: On the development of our views concerning the nature and constitution of radiation. Phys. Z **10** (1909) 817

[117] Frisch, O.: Experimental detection of the einstein recoil radiation. Z. Phys **86** (1933) 42–48

[118] Beth, R.A.: Mechanical detection and measurement of the angular momentum of light. Physical Review **50**(2) (1936) 115

[119] McDuff, D., Salamon, D.: Introduction to symplectic topology. Oxford University Press (1998)

[120] Guillemin, V., Sternberg, S.: Symplectic techniques in physics. Cambridge University Press (1990)

[121] Wigner, E.: On the quantum correction for thermodynamic equilibrium. Physical Review **40**(5) (1932) 749

[122] Surhone, L., Timpledon, M., Marseken, S.: Wigner Quasi-probability Distribution: Eugene Wigner, Quantum, Wave Function, Schrödinger Equation, Generating Function, Density Matrix, Weyl Quantization, Quantum Chemistry, Seismology, Negative Probability. Betascript Publishing (2010)

[123] Hudson, R.: When is the wigner quasi-probability density non-negative? Reports on Mathematical Physics **6**(2) (1974) 249–252

[124] Bojowald, M., Skirzewski, A.: Effective equations of motion for quantum systems. Reviews in Mathematical Physics **18**(07) (2006) 713–745

[125] Simon, R., Mukunda, N., Dutta, B.: Quantum-noise matrix for multimode systems: U (n) invariance, squeezing, and normal forms. Phys. Rev. A **49**(3) (1994) 1567

[126] Ferraro, A., Olivares, S., Paris, M.G.: Gaussian states in continuous variable quantum information. arXiv preprint quant-ph/0503237 (2005)

[127] Weedbrook, C., Pirandola, S., Garcia-Patron, R., Cerf, N.J., Ralph, T.C., Shapiro, J.H., Lloyd, S.: Gaussian quantum information. Rev. Mod. Phys. **84**(2) (2012) 621

[128] Adesso, G., Ragy, S., Lee, A.R.: Continuous variable quantum information: Gaussian states and beyond. Open Systems & Information Dynamics **21**(01n02) (2014) 1440001

[129] Bogolubov, N.: On the theory of superfluidity. Journal of Physics **11** (1966) 23–29

[130] Lvovsky, A.: Squeezed light. Photonics, Volume 1: Fundamentals of Photonics and Physics **1** (2015)

[131] Einstein, A., Podolsky, B., Rosen, N.: Can quantum-mechanical description of physical reality be considered complete? Physical review **47**(10) (1935) 777

[132] Bell, J.S., et al.: On the einstein-podolsky-rosen paradox. Physics **1**(3) (1964) 195–200

[133] Briegel, H.J., Raussendorf, R.: Persistent entanglement in arrays of interacting particles. Phys. Rev. Lett. **86**(5) (2001) 910

[134] Zhang, J., Braunstein, S.L.: Continuous-variable gaussian analog of cluster states. Phys. Rev. A **73**(3) (2006) 032318

[135] Yuen, H.P., Chan, V.W.: Noise in homodyne and heterodyne detection. Optics Letters **8**(3) (1983) 177–179

[136] Collett, M., Loudon, R., Gardiner, C.: Quantum theory of optical homodyne and heterodyne detection. Journal of Modern Optics **34**(6-7) (1987) 881–902

[137] Raussendorf, R., Browne, D.E., Briegel, H.J.: Measurement-based quantum computation on cluster states. Phys. Rev. A **68**(2) (2003) 022312

[138] Unruh, W.: Quantum non-demolition. In: Gravitational Radiation, Collapsed Objects and Exact Solutions. Springer (1980) 385–426

[139] Roch, J.F., Roger, G., Grangier, P., Courty, J.M., Reynaud, S.: Quantum non-demolition measurements in optics: a review and some recent experimental results. Applied Physics B **55**(3) (1992) 291–297

[140] Braginsky, V.B., Khalili, F.Y.: Quantum nondemolition measurements: the route from toys to tools. Rev. Mod. Phys. **68**(1) (1996) 1

[141] Nielsen, M.A., Chuang, I.L.: Quantum Computation and Quantum Information. first edn. Cambridge University Press, Cambridge (2000)

[142] Uhlmann, A.: The transition probability in the state space of a *-algebra. Rep. Math. Phys **9**(2) (1976) 273

[143] Jozsa, R.: Fidelity for mixed quantum states. Journal of modern optics **41**(12) (1994) 2315–2323

[144] Paraoanu, G.S., Scutaru, H.: Fidelity for multimode thermal squeezed states. Phys. Rev. A **61** (2000) 022306

[145] Spedalieri, G., Weedbrook, C., Pirandola, S.: A limit formula for the quantum fidelity. J. Phys. A: Math. Theor. **46** (2013) 025304

[146] Gordon, J.P., Zeiger, H.J., Townes, C.H.: The maser—new type of microwave amplifier, frequency standard, and spectrometer. Physical Review **99**(4) (1955) 1264

[147] Maiman, T.: Stimulated optical radiation in ruby. Nature **187** (1960) 493–494

[148] Hänsch, T.W., Schawlow, A.L.: Cooling of gases by laser radiation. Optics Communications **13**(1) (1975) 68–69

[149] Wineland, D., Dehmelt, H.: Proposed 1014 delta upsilon less than upsilon laser fluorescence spectroscopy on t1+ mono-ion oscillator iii. In: Bulletin of the American Physical Society. Volume 20. (1975) 637–637

[150] Wineland, D., Drullinger, R., Walls, F.: Radiation-pressure cooling of bound resonant absorbers. Phys. Rev. Lett. **40**(25) (1978) 1639

[151] Ashkin, A.: Trapping of atoms by resonance radiation pressure. Phys. Rev. Lett. **40**(12) (1978) 729

[152] Ashkin, A.: Optical trapping and manipulation of neutral particles using lasers. World Scientific (2006)

[153] Walls, D.F., Milburn, G.J.: Quantum optics. Springer Science & Business Media (2007)

[154] Hurwitz, A.: Ueber die bedingungen, unter welchen eine gleichung nur wurzeln mit negativen reellen theilen besitzt. Mathematische Annalen **46**(2) (1895) 273–284

[155] Scully, M.O., Zubairy, M.S.: Quantum optics. Cambridge university press (1997)

[156] van Loock, P., Weedbrook, C., Gu, M.: Building gaussian cluster states by linear optics. Phys. Rev. A **76**(3) (2007) 032321

[157] Furusawa, A., Van Loock, P.: Quantum teleportation and entanglement: a hybrid approach to optical quantum information processing. John Wiley & Sons (2011)

[158] Gu, M., Weedbrook, C., Menicucci, N.C., Ralph, T.C., van Loock, P.: Quantum computing with continuous-variable clusters. Phys. Rev. A **79**(6) (2009) 062318

[159] Eberle, T., Steinlechner, S., Bauchrowitz, J., Händchen, V., Vahlbruch, H., Mehmet, M., Müller-Ebhardt, H., Schnabel, R.: Quantum enhancement of the zero-area sagnac interferometer topology for gravitational wave detection. Phys. Rev. Lett. **104** (Jun 2010) 251102

[160] Monroe, C., Meekhof, D., King, B., Jefferts, S., Itano, W., Wineland, D., Gould, P.: Resolved-sideband raman cooling of a bound atom to the 3d zero-point energy. Phys. Rev. Lett. **75**(22) (1995) 4011

[161] Eschner, J., Morigi, G., Schmidt-Kaler, F., Blatt, R., et al.: Laser cooling of trapped ions. JOSA B **20**(5) (2003) 1003–1015

[162] Neuhauser, W., Hohenstatt, M., Toschek, P., Dehmelt, H.: Optical-sideband cooling of visible atom cloud confined in parabolic well. Phys. Rev. Lett. **41**(4) (1978) 233

[163] Diedrich, F., Bergquist, J., Itano, W.M., Wineland, D.: Laser cooling to the zero-point energy of motion. Phys. Rev. Lett. **62**(4) (1989) 403

[164] Hamann, S., Haycock, D., Klose, G., Pax, P., Deutsch, I., Jessen, P.: Resolved-sideband raman cooling to the ground state of an optical lattice. Phys. Rev. Lett. **80**(19) (1998) 4149

[165] Schliesser, A., Rivière, R., Anetsberger, G., Arcizet, O., Kippenberg, T.J.: Resolved-sideband cooling of a micromechanical oscillator. Nature Physics **4**(5) (2008) 415–419

[166] Routh, E.J.: A treatise on the stability of a given state of motion: particularly steady motion. Macmillan and Company (1877)

[167] Lin, Q., Rosenberg, J., Chang, D., Camacho, R., Eichenfield, M., Vahala, K.J., Painter, O.: Coherent mixing of mechanical excitations in nano-optomechanical structures. Nature Photonics **4**(4) (2010) 236–242

[168] Massel, F., Cho, S.U., Pirkkalainen, J.M., Hakonen, P.J., Heikkilä, T.T., Sillanpää, M.A.: Multimode circuit optomechanics near the quantum limit. Nature communications **3** (2012) 987

[169] Shkarin, A.B., Flowers-Jacobs, N.E., Hoch, S.W., Kashkanova, A.D., Deutsch, C., Reichel, J., Harris, J.G.E.: Optically mediated hybridization between two mechanical modes. Phys. Rev. Lett. **112** (Jan 2014) 013602

[170] Teufel, J., Donner, T., Li, D., Harlow, J., Allman, M., Cicak, K., Sirois, A., Whittaker, J.D., Lehnert, K., Simmonds, R.W.: Sideband cooling of micromechanical motion to the quantum ground state. Nature **475**(7356) (2011) 359–363

[171] Wollman, E., Lei, C., Weinstein, A., Suh, J., Kronwald, A., Marquardt, F., Clerk, A., Schwab, K.: Quantum squeezing of motion in a mechanical resonator. Science **349**(6251) (2015) 952–955

[172] Weinstein, A.J., Lei, C.U., Wollman, E.E., Suh, J., Metelmann, A., Clerk, A.A., Schwab, K.C.: Observation and interpretation of motional sideband asymmetry in a quantum electromechanical device. Phys. Rev. X **4** (2014) 041003

[173] Pirkkalainen, J.M., Damskägg, E., Brandt, M., Massel, F., Sillanpää, M.A.: Squeezing of quantum noise of motion in a micromechanical resonator. Phys. Rev. Lett. **115** (2015) 243601

[174] Vanner, M.R., Pikovski, I., Kim, M.: Towards optomechanical quantum state reconstruction of mechanical motion. Ann. Phys. **527**(1-2) (2015) 15–26

[175] Tufarelli, T., Ferraro, A., Kim, M., Bose, S.: Reconstructing the quantum state of oscillator networks with a single qubit. Phys. Rev. A **85**(3) (2012) 032334

[176] Moore, D., Paternostro, M., Ferraro, A. (unpublished)

[177] Higham, N.J.: Functions of matrices: theory and computation. Siam (2008)

Index

الحالات العنقودية ذات المتغيرات المستمرة في الأنظمة الميكانيكوضوئية

ملخص

تتناول هذه الأطروحة الجانبين النظري و التطبيقي لبعض موارد المعالجة الكمومية للمعلومات، حيث نعتبر الحالات العنقودية الكمية ممثلة في درجات الحرية الميكانيكية للأنظمة الميكانيكوضوئية، و نحاول أن نتغلب على المشاكل المتعلقة بتلاشي تناسق الحواسيب الكمومية و ذلك حتى نتمكن من إجراء حوسبة كمومية موثوقة النتائج. و نبين كيفية الحصول على الحالات العنقودية و ذلك بالأخذ بعين الاعتبار التبادلات الطاقوية للنظام المدروس مع محيطه، حيث نستخدم فكرة هندسة التبدد من أجل الحصول على حالات عنقودية لديها مناعة ضد آثار تلاشي التناسق. باستخدام البروتكول الموضح هنا نبين كيفية الحصول على حالات عنقودية ذات نسقين، أربعة و ثمانية أنساق و ذات أشكال هندسية و درجات انضغاط مختلفة، حيث نحصل عليها بموثوقية عالية رغم وجود بعض الاضطرابات و التأثيرات الخارجية غير المرغوب فيها بسبب تفاعل درجات الحرية الميكانيكية مع محيطها.

كلمات مفتاحية: الميكانيكوضوئية الكمومية بواسطة الفجوة الضوئية، الحالة العنقودية، المتغيرات المستمرة، تلاشي التناسق، التبديد، الحوسبة الكمومية، المعلوماتية الكمومية، الليزر .

Les Etats Du Cluster à Variables Continues dans un Système Optomécanique

Résumé

Cette thèse présente la théorie et l'implémentation du traitement de l'information de certaines ressources quantiques. Les états du cluster à variables continues sont étudiés dans le cadre des degrés de liberté mécaniques des systèmes opto-mécaniques. Nous avons essayé de surmonter les effets de la décohérence dans les ordinateurs quantiques afin que le traitement de l'information quantique soit fiable. Nous avons montré comment préparer par dissipation l'état du cluster dans les systèmes opto-mécaniques. Nous avons utilisé l'idée de dissipation pour obtenir des états de cluster stables et robustes contre les effets de la décohérence. En utilisant notre protocole, les états du cluster de deux, quatre et huit modes avec compression et avec des géométries différentes sont obtenus avec une grande fidélité et dans la présence de bruit mécanique.

Mot–clés: cavité opto-mécanique, état du cluster, variables continues, décohérence, dissipation, informatique quantique, information quantique, laser.

CONTINUOUS VARIABLE CLUSTER STATES IN OPTOMECHANICAL SYSTEMS

Abstract

This thesis presents theory and implementations of some quantum information processing resources. Continuous variable (CV) cluster states of the mechanical degrees of freedom in optomechanical systems are considered. We attempt to overcome the effects of decoherence in quantum computers so that quantum information processing becomes reliable. We show how to dissipatively prepare cluster states in optomechanical systems. We use the idea of dissipation engineering to obtain steady cluster states that are robust against the effects of decoherence. Using the scheme presented in this work, cluster states of two, four and eight modes with different squeezings and geometries are obtained with high fidelity and in the presence of mechanical noise.

Keywords: quantum cavity optomechanics, cluster state, continuous variables, decoherence, dissipation, quantum computation, quantum information, laser.